ANKARA YILDIRIM BEYAZIT UNIVERSITY

GRADUATE SCHOOL OF NATURAL AND APPLIED SCIENCES

PRODUCTION AND CHARACTERIZATION OF CERAMICS FOR MICROWAVE APPLICATIONS

M.Sc. Thesis by

Melike DÖNMEZ

Department of Materials Engineering

February 2023

ANKARA

PRODUCTION AND CHARACTERIZATION OF CERAMICS FOR MICROWAVE APPLICATIONS

A Thesis Submitted to

The Graduate School of Natural and Applied Sciences of

Ankara Yıldırım Beyazıt University

In Partial Fulfillment of the Requirements for the Degree of Master of Science in Materials Engineering, Department of Materials Engineering

by

Melike DÖNMEZ

February, 2023

ANKARA

M.Sc THESIS EXAMINATION RESULT FORM

We have read the thesis entitled "**PRODUCTION AND CHARACTERIZATION OF CERAMICS FOR MICROWAVE APPLICATIONS**" completed by **MELİKE DÖNMEZ** under supervision of **PROF. DR. CİHANGİR DURAN** and we certify that in our opinion it is fully adequate, in scope and in quality, as a thesis for the degree of Master of Science.

Prof. Dr. Cihangir DURAN

Supervisor

Assoc. Prof. Dr. Gülsüm TOPATEŞ

Jury Member

Prof. Dr. Abdullah ÖZTÜRK

Jury Member

Prof. Dr. Sadettin ORHAN

Director

Graduate School of Natural and Applied Science

ETHICAL DECLARATION

I hereby declare that, in this thesis which has been prepared in accordance with the Thesis Writing Manual of Graduate School of Natural and Applied Sciences,

- All data, information and documents are obtained in the framework of academic and ethical rules,
- All information, documents and assessments are presented in accordance with scientific ethics and morals,
- All the materials that have been utilized are fully cited and referenced,
- No change has been made on the utilized materials,
- All the works presented are original,

and in any contrary case of above statements, I accept to renounce all my legal rights.

Date: 0**8/02/2023** **Signature:**

Name & Surname: Melike DÖNMEZ

ACKNOWLEDGEMENTS

First and foremost, I would like to express my deepest gratitude to my supervisor Prof. Dr. Cihangir Duran who contributed in making this project possible with his valuable guidance, support and advice. I am thankful for his constructive comments and kind help.

I would like to thank to Oğuzhan Bilaç for his supports during my experiments, Bülent Alıcıoğlu for characterization at microwave frequencies and MEGAP Ltd. Şti. for financial support.

Finally, I would like to thank my family for their love, trust and support which helped me to complete this study.

2023, 08 February **Melike DÖNMEZ**

PRODUCTION AND CHARACTERIZATION OF CERAMICS FOR MICROWAVE APPLICATIONS

ABSTRACT

New research and developments on microwave communication result in a rising demand for dielectric resonators. Dielectric oxide ceramics are used as filters, oscillators in a variety of applications from mobile phones to global positioning systems. It has also played an important role in the microwave wireless communications industry by reducing the size and cost of the antenna components. In this study, dielectric ceramic compositions (i.e., CeO_2-Glass (5 wt.%, Al_2O_3-SiO_2-CaO based), $SrNb_2O_6$, $Ba_2Ti_9O_{20}$, $0.68CaTiO_3$-$0.32Ca(Zn_{1/3}Nb_{2/3})O_3$ and $Ba_{6-3x}(Nd_{1-y}Bi_y)_{8+2x}Ti_{18}O_{54}$ x=2/3 and y=0.07) with various dielectric constants between 20 and 100 were synthesized by solid state method and successfully fabricated by dry pressing. The ceramics were then characterized for densification, phase formation, microstructure evolution, dielectric and microwave properties. XRD proved the desired phase formation for all compositions. All sintered samples had a relative density ≥97.35%. Dielectric constants (losses) at 5 MHz at the best sintering conditions for each composition were 21.36 (0.0040) at 1150ºC for CeO_2-Glass, 28.87 (0.0047) at 1275ºC for $SrNb_2O_6$, 39.55 (0.0034) at 1300ºC for $Ba_2Ti_9O_{20}$, 89.98 (0.0035) at 1400ºC for $0.68CaTiO_3$-$0.32Ca(Zn_{1/3}Nb_{2/3})O_3$ and 92.04 (0.0053) at 1320ºC for $Ba_{6-3x}(Nd_{1-y}Bi_y)_{8+2x}Ti_{18}O_{54}$ x=2/3 y=0.07. The CeO_2-Glass (5 wt.%) composition was studied for the first time in literature.

Keywords: Dielectric ceramics, solid state phase formation, dry pressing, dielectric and microwave measurements, characterization.

MİKRODALGA UYGULAMALARI İÇİN SERAMİKLERİN ÜRETİMİ VE KARAKTERİZASYONU

ÖZ

Mikrodalga iletişimi konusundaki yeni araştırma ve gelişmeler dielektrik rezonatörlere olan talebin artmasına neden olmaktadır. Dielektrik oksit seramikler, cep telefonlarından küresel konumlandırma sistemlerine kadar çeşitli uygulamalarda filtreler, osilatörler olarak kullanılmaktadır. Anten bileşenlerinin boyutunu ve maliyetini azaltarak mikrodalga kablosuz iletişim endüstrisinde de önemli bir rol oynamaktadır. Bu çalışmada, 20 ile 100 arasında değişen dielektrik sabitlere sahip dielektrik seramik kompozisyonları (örn., CeO_2-Cam (ağ. %5, Al_2O_3-SiO_2-CaO esaslı), $SrNb_2O_6$, $Ba_2Ti_9O_{20}$, $0.68CaTiO_3$-$0.32Ca(Zn_{1/3}Nb_{2/3})O_3$ ve $Ba_{6-3x}(Nd_{1-y}Bi_y)_{8+2x}Ti_{18}O_{54}$ x=2/3 and y=0.07) katı hal yöntemiyle sentezlenmiş ve mikrodalga rezonatör uygulamaları için kuru presleme ile başarıyla üretilmişlerdir. Daha sonra, seramiklerin yoğunlaşma, faz oluşumu, mikroyapı gelişimi, dielektrik ve mikrodalga özellikleri açısından karakterizasyonları yapılmıştır. Tüm sinterlenen seramikler için göreceli yoğunluk ≥97.35% olarak ölçülmüştür. Kendi en iyi sinterleme koşullarında sinterlenen her bir kompozisyonun 5 MHz'deki dielektrik sabitleri (kayıpları) CeO_2-Cam için 1150ºC'de 21.36 (0.0040), $SrNb_2O_6$ için 1275ºC'de 28.87 (0.0047), $Ba_2Ti_9O_{20}$ için 1300ºC'de 39.55 (0.0034), $0,68CaTiO_3$-$0,32Ca(Zn_{1/3}Nb_{2/3})O_3$ için 1400ºC'de 89.98 (0.0035) ve $Ba_{6-3x}(Nd_{1-y}Bi_y)_{8+2x}Ti_{18}O_{54}$ x=2/3 y=0.07 için 1320ºC'de 92.04 (0.0053)'dir. CeO_2-Cam (ağ. %5) kompozisyonu literatürde ilk kez çalışılmıştır.

Anahtar Kelimeler: Dielektrik seramikler, katı hal faz oluşumu, kuru presleme, dielektrik ve mikrodalga ölçümler, karakterizasyon**.**

CONTENTS

NOMENCLATURE

Abbreviations

μm	Micrometer
GHz	Gigahertz
MHz	Megahertz
Pa	Pascal
MPa	Mega Pascal
GPa	Giga Pascal
μ	Poisson's ratio
°	Degree
h	Hour
2θ	Diffraction angle
Å	Angstrom
ppm	Part per million
vol%	Volume percent
wt.%	Weight percent
α	Thermal expansion coefficient
Ɛ	Permittivity
$Ɛ_r$	Relative permittivity
ρ	Density
tanδ	Loss tangent
$\tau_ε$	Temperature coefficient of dielectric constant
f_r	Resonant frequency
τ_f	Temperature coefficient of resonance frequency
Q.f	Quality factor of a resonator

λ_d	Wavelength in the dielectric
λ_0	Wavelength in air or vacuum
XRD	X-ray Diffraction
EDS	Energy Dispersive Spectrometry
SEM	Scanning Electron Microscopy

LIST OF TABLES

LIST OF FIGURES

CHAPTER 1

INTRODUCTION

Microwave dielectric materials play a significant role in modern life with a wide range of uses in satellite and terrestrial communication, including software radio, GPS (Global Position System), and DBS TV (Digital Broadcast Satellite), as well as environmental monitoring. Improved or novel microwave components based on new dielectric materials and designs are needed to meet the requirements of the existing and future systems. Recent advances in microwave telecommunications, intelligent transport systems and satellite broadcasting are critical for low dielectric loss dielectric resonators, which are mainly used in wireless communication devices [1, 2]. The dimensions of the microwave devices used are decreasing day by day and the frequency used is moving towards the GHz range. The region between 300 MHz and 300 GHz in the electromagnetic wave spectrum is called the microwave region. With the developing communication and wireless communication technologies, the desired properties of microwave dielectric ceramics are increasing, and therefore researchers continue to work on dielectric ceramics intensively [1].

Microwaves require special devices for transport and filtering due to cable response time and signal transport time. Conventional transistors, integrated circuits and cables cannot be used to carry microwaves. The inductive reactance of the cables is directly proportional to the frequency and is negligible at low frequencies. In other words, since the resistance of conventional cables is high at high frequencies, the transmitted signal is lost due to the resistance formed on the cable before it reaches the desired location [1, 3].

There are several reasons why microwave dielectric ceramics stand out over their competitors. Quartz resonators used in the transmission of radio waves are not preferred due to the high noise ratio in frequency multiplication at microwave frequencies [4, 5]. Another option is the metallic cavity resonator. However, this part is not preferred because it cannot be integrated into the Microwave Integrated Circuit (MIC) [2]. Microstrip resonators developed later are not preferred because their

dielectric coefficients are high, and their temperature stability is low. Ceramic dielectric resonators (DR) are the most preferred materials in this field, as they have almost all the above-mentioned properties [1, 6, 7].

Dielectric ceramics to be used in microwave circuit must meet certain criteria such as low dielectric loss and temperature stability. The high dielectric constant makes the component smaller because the dielectric constant is inversely proportional to the size of the part. Low dielectric loss (high quality factor) ensures low noise and low power loss in the signal. Temperature stability is important for the device to work at the same quality in all environmental conditions. Another factor that depends on the temperature stability is that the resonance frequency of the part is affected as little as possible by the temperature [8, 9].

Today, dielectric ceramics used in different working ranges have different dielectric constants. Ceramic materials with a dielectric constant less than 25 have applications in the high frequency band. Dielectric ceramics with a dielectric constant value between 25 and 50 are used in the field of satellite communication. Ceramic materials with a dielectric constant value greater than 50 find application in areas such as mobile communication where miniaturization is required [2].

1.1 Dielectric Properties of Materials

Dielectric materials are polarizable insulating materials that do not allow a charged part to pass; rather, electrostatic dipoles are present or formed under the influence of an electric field [10]. According to the band theory, since some of the electrons in the valence band in conductive materials are also in the conduction band, the two bands can be thought of as intertwined. As a result, electrons in the valence band can carry a charge. In semiconductors, there is some energy difference between the two bands. If the energy difference is closed by an external effect, electrical conductivity is also observed in semiconductor materials. In insulating materials, on the other hand, since the energy difference between the conduction band and the valence band is high, electrical conduction is not observed because the energy difference between the bands does not close under normal conditions (Figure 1.1). According to this theory, the valence band (VB), conduction band (CB), and forbidden band (FB) are the three

most significant energy bands in solids. The distance between the conduction band and the valence band of electrons is known as a band gap. Valance electrons in the VB are either fully or partially filled. Valance electrons are found in the atom's outer shell. The CB is vacant. The electrons can pass from the VB to the CB if they have enough energy. Electrons need to cross the energy gap for an electron to move from VB to CB. The transport of charged ions is the only cause of conductivity [11–14].

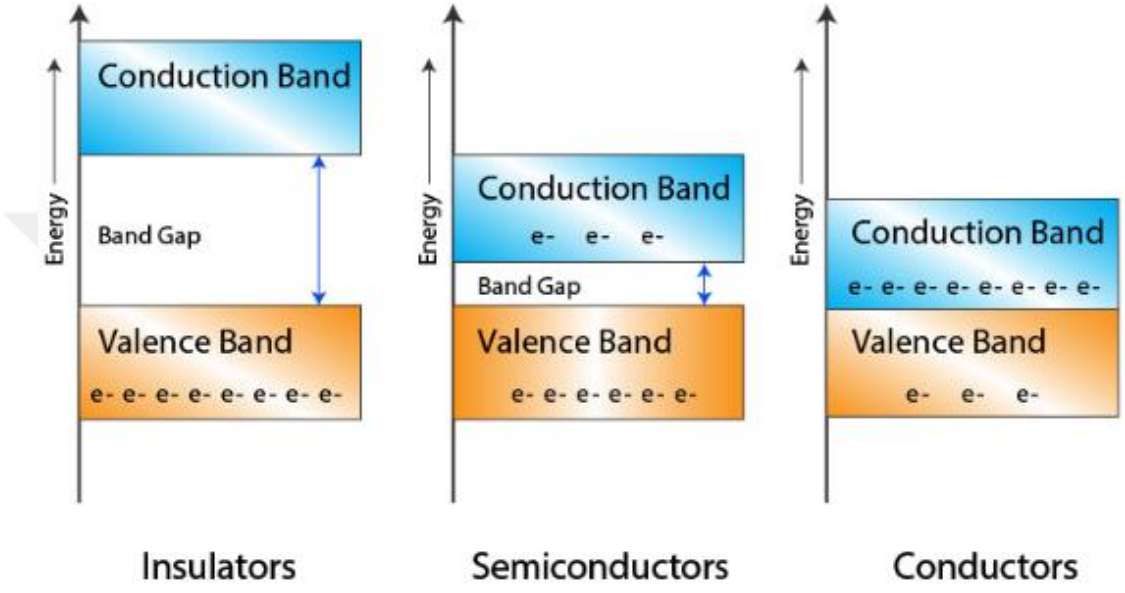

Figure 1.1 Band structure of materials [15]

The dielectrics are used in capacitors due to their ability to store energy under external electric field. Dielectrics, when placed between oppositely charged conductive plates, have interesting electrical properties such as increasing the capacitor's capacitance under a certain potential difference of the plates. Dielectric materials are an important part of the electronic circuits [16].

High frequency electronic circuits are built on dielectric materials and the operation of these circuits depends on the dielectric properties of the material such as electrical polarization, resonance, relaxation, and energy dissipation [17, 18].

In dielectric materials, anion and cation charges are in balance unless there is an external effect. As a result of the application of an electric field, this balance is disturbed in the direction of the electric field and dipole pairs are formed (Figure

1.2). In this dipole, one side is slightly positive and the other side is slightly negative [19]. Hence the electric charge centers shift and electrical polarization occurs. The resulting polarization weakens the electric field inside the dielectric. The consisting electric dipoles provide an accumulation of electric charge on the material. Although a perfect dielectric material has zero electrical conductivity, not all insulators are dielectrics [20, 21].

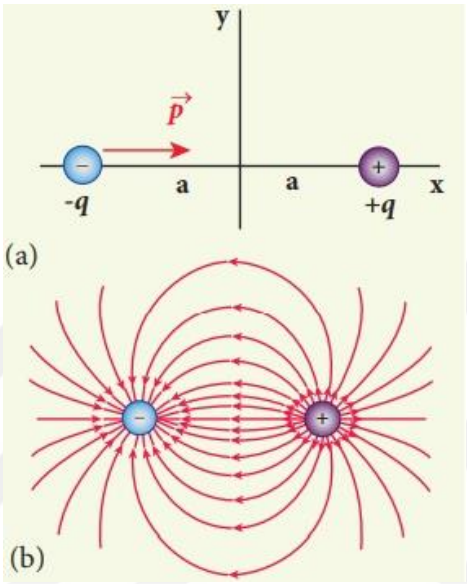

Figure 1.2 (a) Electric dipole (b) Electric field lines for electric dipole [22]

The dipoles formed after polarization have a dipole moment proportional to the distance between them [23].

$$\mu = qd \tag{1.1}$$

As a result of polarization, the dipole moment of a double dipole with a charge q depending on the distance d between them is denoted by μ. The total polarization that occurs in a material is expressed as the polarization intensity of the material and is denoted by P. The polarization intensity is the ratio of the total dipole moment of the material to the unit volume, V [23].

$$P = \frac{\Sigma\mu}{V} \tag{1.2}$$

1.2 Dielectric Polarization

A dielectric is an electrically insulating material that can be polarized under an external electric field, and this phenomenon is called dielectric polarization. There are four different polarization types in dielectric materials, which are; electronic, ionic, orientational (dipolar) and space charge (interfacial) polarizations [24].

1.2.1 Electronic Polarization

When a neutral atom is exposed to an electric field, the positive charges in its nucleus and the electrons in its orbit are pushed in opposite directions. The moment that occurs as a result of the displacement and rebalancing of the two load charge is called electronic polarization [24]. This creates an electrostatic dipole. Therefore, the interatomic dipole moment is shown as [25];

$$P_{elect} = \varepsilon_0 \alpha_{elect} E \tag{1.3}$$

E, ε_0 and α_{elect} are called external electrical field, the permittivity of vacuum and electronic polarizability, respectively. The polarization disappears when the electric field is removed. The variation of the electron cloud in the electric field is given in Figure 1.3 [26]. This polarization occurs in a short time interval at high frequencies (between 10^{13} Hz and 10^{15} Hz) due to the very small mass of the electron [27, 28]. This polarization can occur in all atoms and molecular structures. However, when compared with other polarization mechanisms, the dipole moment resulting from electronic polarization is quite small [26].

Figure 1.3 Electronic polarization; unpolarized (left) and polarized atom (right) [26]

1.2.2 Ionic (Atomic) Polarization

Ionic or atomic polarization causes the atoms or ions of a molecule to be displaced relative to each other by the external electric field. This is a disruption of the normal lattice vibration. For this reason, this polarization is sometimes called vibrational polarization [29]. This type of polarization, as in the electronic polarization, is a type of temporary polarization that occurs with the effect of external electric field. Ionic polarization only occurs in materials with ionic bonds such as NaCl and $BaTiO_3$. In ionic solids, each pair of neighboring cations and anions can form a dipole and has a dipole moment [26, 29]. The average location of positive and negative ions in ionic crystals changes when a field E is present. Assume that the ion is fully stiff at all times. The polar moment will change because the field's action will cause it to move by a quantity *l* with respect to a fixed mark centered in position [25];

$$P_{ion} = ql = \varepsilon_0 \alpha_{ion} E \tag{1.4}$$

where α_{ion} is the ionic polarizability. This is an induced ionic polarization and is proportional to the electric field E (elastic deformations). However, in the absence of an external electric field, the net dipole moment of the solid is zero. When an electric field is applied to an ionic solid, the cations and anions shift in opposite directions guided by the electric field. This shift causes unequal charge separations in adjacent dipoles. As a result of this change caused by the external electric field, ionic solids acquire a non-zero net dipole moment. The ionic polarization given in Figure 1.4 moves more slowly and occurs between 10^9 Hz and 10^{13} Hz [26, 28, 29].

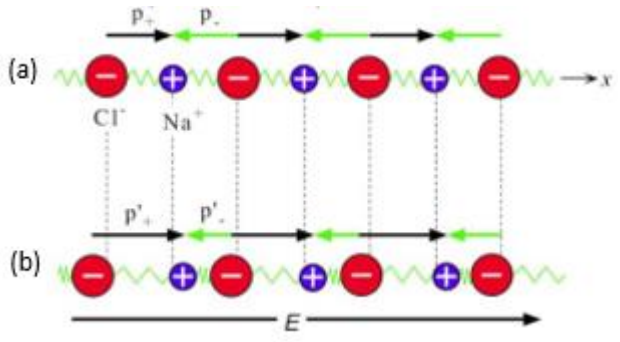

Figure 1.4 Ionic polarization; (a) unpolarized and (b) polarized atom [30]

1.2.3 Dipolar (Orientational) Polarization

Orientational polarization only occurs in polar dielectric materials, which are composed of molecules or particles with a permanent dipole moment. It is also called dipolar polarization. When an external electric field is applied, they are oriented in the direction of the applied field, as shown in Figure 1.5 [26]. Application of an electric field produces a polar component in the direction of the electric field for each molecule [25]:

$$P_{or} = \varepsilon_0 \alpha_{or} E \tag{1.5}$$

where α_{or} is the orientational polarizability. When the applied electric field is removed, the dipoles remain oriented, causing polarization. Compounds with asymmetric molecular structure have permanent dipoles. This type of polarization occurs not only in materials containing natural dipoles, but also in crystalline ceramic materials that contain defects in their structure. This polarization takes place in the radio frequency range of 10^3-10^9 Hz [26, 27, 31].

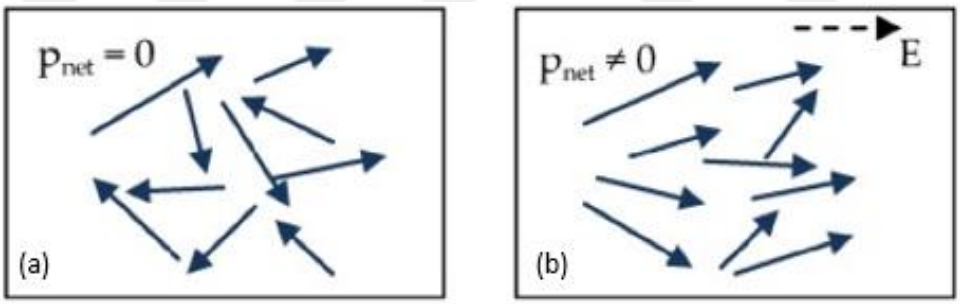

Figure 1.5 Dipolar polarization; (a) unpolarized and (b) polarized atom [26]

1.2.4 Interface (Space Charge) Polarization

Interface polarization is common in all materials containing the accumulation of charge carrier electrons in a physical barrier such as a grain boundary. Owing to the differences in electronic properties, charge accumulation is expected at interfaces between different regions/phases like grain boundaries in the polycrystalline materials, interfaces between amorphous and crystalline phases of semi-crystalline polymers, and at some structural defects and impurities. Electronic, atomic, and

directional polarization occur when charges are locally bonded to atoms or molecules. When a low frequency electric field is applied, charge carriers can be displaced within the material up to a certain distance. Interfacial or space charge polarization occurs when charge carriers move a certain distance along material interfaces under an electric field and the movement of these displaced charges is inhibited. It occurs as a result of the accumulation of charge carrier electrons in a physical barrier such as a grain boundary. Thus, charges can be trapped within the material's interfaces. This can also cause charge build-up and thus a higher capacitance. Interfacial polarization also occurs in the frequency range of 10^0-10^2 Hz. The interfacial polarization is given in Figure 1.6 [26, 29]. α_{inter} is called external electrical field, the permittivity of vacuum and interface polarizability.

$$P_{inter} = \varepsilon_0 \alpha_{inter} E \tag{1.6}$$

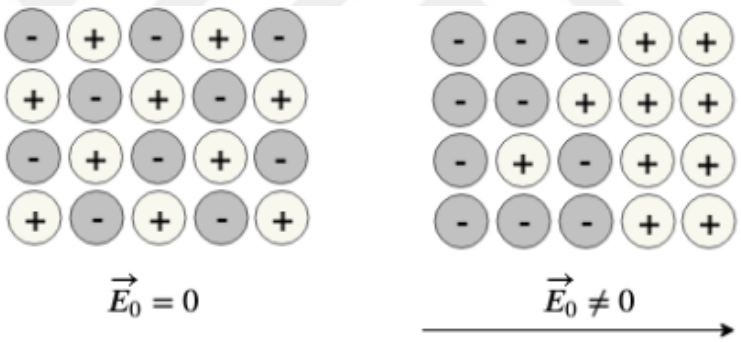

Figure 1.6 Interfacial polarization; unpolarized (left) and polarized atom (right) [26]

1.2.5 Frequency and Temperature Dependence of Dielectric Polarization

The dielectric performance of materials is attributed to at least one of the four polarization mechanisms mentioned above. When an alternating electric field is applied across the material, polarization occurs as a function of time. The polarization as a function of time t is indicated by [24, 32, 33];

$$P(t) = P\left[1 - e^{\left(-\frac{t}{tr}\right)}\right] \tag{1.7}$$

where P is the maximum polarization produced by an applied electrostatic field over a long period of time, tr is the relaxation time [33].

Each polarization effect has a resonance or relaxation frequency characteristic. In general, electronic and ionic polarization have resonance effects, while orientation polarization has a relaxation effect. That is, dielectric relaxation is associated with directional polarization [26, 32, 34, 35]. Figure 1.7 shows the variation of polarization with frequency for a hypothetical material showing all four polarization mechanisms [36]. This process takes a finite amount of time, which varies for each polarization mechanism. At relaxation frequencies, the dipoles can nearly reorient to the applied electric field. At this frequency, dielectrics are lossy, and energy is lost in the form of heat. Dielectric losses are maximized when the frequency of the external field matches the relaxation frequency of a particular polarization mechanism. At frequencies above the relaxation frequency, the dipole can no longer respond to applied field changes and the contributing polarization mechanisms are effectively frozen and become non-contributing [24]. At optical frequencies (10^{15} Hz), only electronic polarization exists. In the 10^{13}-10^{15} Hz range, ionic polarization occurs in addition to electronic polarization. In the range 10^{6}–10^{9} Hz there is an additional contribution from orientational polarization, and in the 10^{0}-10^{2} Hz range space charge polarization also contributes. Note that at low frequencies all four types of polarization contribute and thus the total polarization is very high. The total polarization decreases with increasing frequency and reaches a minimum in the optical frequency range [33]. Electronic polarization is the fastest polarization and is completed the moment the electric field is applied. This is because electrons are lighter particles than ions. Therefore, even if very high frequencies (optical range) are applied, electronic polarization occurs during each cycle of the applied field. Ionic polarization is slightly slower than electronic polarization. Ions are heavier than the electron cloud, so they take longer to shift. Furthermore, the frequency of the applied electric field used to displace the ions is equal to the frequency of lattice vibrations (10^{13} Hz). If the frequency of the applied electric field is less than 10^{13} Hz, the ions have sufficient time to react during each cycle of the applied electric field. Directional polarization is even slower than ionic polarization. This type of polarization only occurs in the electrical frequency range (10^{6} Hz). Space-charge

polarization is the slowest, as it must diffuse over a few atomic distances. This process occurs at a very low frequency (10^2 Hz) [33, 37].

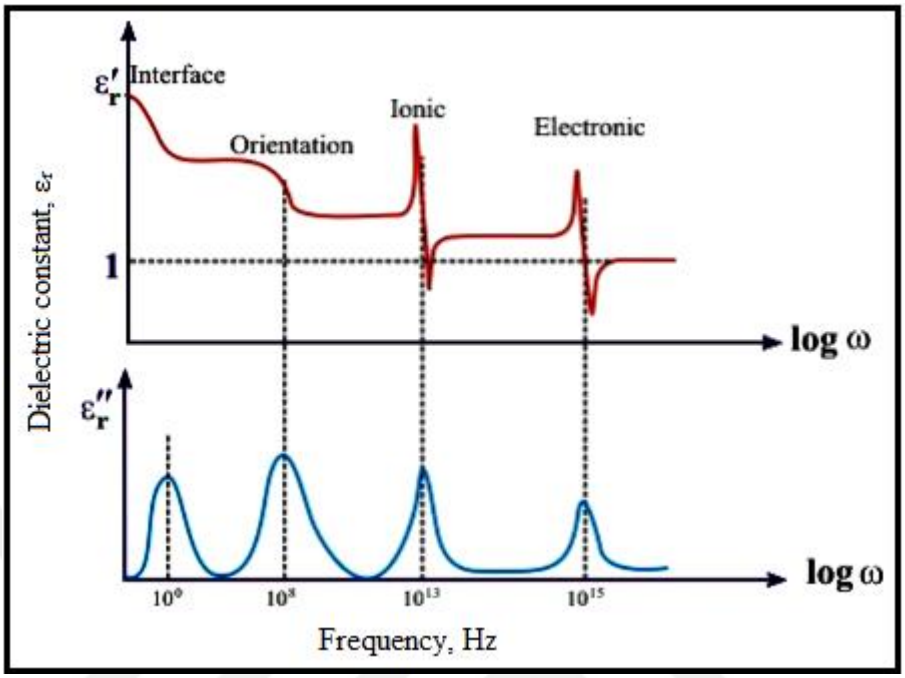

Figure 1.7 The frequency regions corresponding to the polarization mechanisms; ε_r' the real part of the dielectric constant, and ε_r'' the imaginary part of the dielectric constant [38]

If the dielectric material is exposed to elevated temperature, the electronic distribution of the molecular components is unaffected. Therefore, there is no effect of temperature on the polarization mechanism of electrons and ions. Therefore, the electronic and ionic polarizations are virtually independent of temperature. Increasing the temperature introduces a high degree of randomness in the molecular orientation of the material. This affects the tendency of permanent dipoles to align along the direction of the electric field. Therefore, orientation polarization decreases with increasing temperature. However, in space charge polarization, increasing temperature supports ion movement by diffusion. As a result, the polarization increases. Therefore, both the orientation and space-charge polarization mechanisms are highly dependent on temperature [28, 33].

Thus, the total polarization of a material is given as [24];

$$P_t = P_{elect} + P_{ion} + P_{or} + P_{inter} \tag{1.8}$$

where, P_e, P_i, P_d, and P_s denote electronic, ionic, orientational (dipolar) and space charge (interfacial) polarizations, respectively. Also, examples of variety materials corresponding to the polarization mechanisms are shown in Table 1.1.

Table 1.1 Examples of polarization mechanisms [39]

Example	Polarization	Static ε_r	Comment
Ar gas	Electronic	1.0005	Small N in gases: $\varepsilon_r \approx 1$
Ar liquid (T<87.3K)	Electronic	1.53	Van der Waals bonding
Si crystal	Electronic polarization due to valence electrons	11.9	Covalent solid; Electronic bond polarization
NaCl crystal	Ionic	5.90	Ionic crystalline solid
CsCl crystal	Ionic	7.20	Ionic crystalline solid
Water	Orientational	80	Dipolar liquid
Nitromethane (27°C)	Orientational	34	Dipolar liquid
PVC (Polyvinly chloride)	Orientational	7	Dipole orientations partly hindered in the solid

1.3 Dielectric Constant

The dielectric constant (ε_r) of the material indicates its energy storage capacity when a potential is applied. It is related to macroscopic properties such as polarization or capacitance [25, 40]. It is expressed as the ratio of the permittivity (ε_r) of the material to the vacuum permittivity (ε_0) as given in Equation 1.9 [41].

$$\varepsilon_r = \frac{\varepsilon}{\varepsilon_0} \tag{1.9}$$

Vacuum permeability (ε_0) is a constant value of 8.854×10^{-12} Fm^{-1} [26]. The dielectric constant is usually expressed as the relative permittivity (ε_r) in terms of ease of use. The relative permittivity describes the effect of the material on the electric field. In other words, it is an amount that reduces the electrostatic force between two electrical charges and is also a measure of the power to separate opposite charges

[19, 31, 41]. Figure 1.8 shows that two plates are separated by a certain distance d (thickness) between them. The insulator between the plates is air. When a potential difference V is applied to the two plates, one of the plates will have a positive charge and the other will have a negative charge [31].

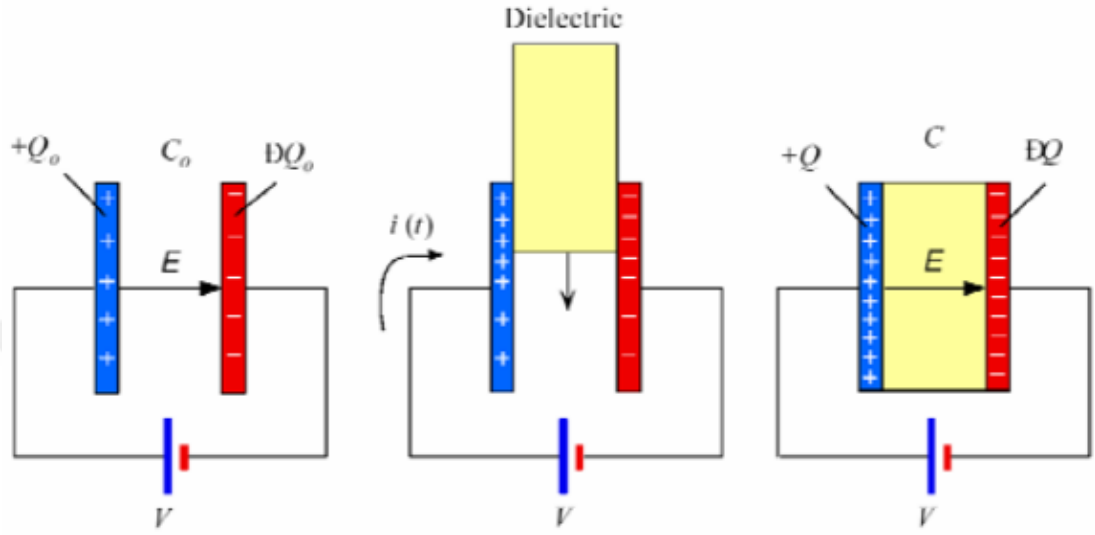

Figure 1.8 Parallel plate method [30]

In this case, the capacitance, C, is defined as the ratio of the total charge (Q) to the potential difference (V) as shown in Equation 1.10 [26, 31].

$$C = \frac{Q}{V} = \varepsilon_0 \varepsilon_r \frac{A}{d} \tag{1.10}$$

d (m) and A (m^2) are called the distance between electrodes and the area of an electrode, respectively. When a dielectric material is placed between the plates, the capacitance of material (C) will increase compared to the first (same capacitor without dielectric material, C_0 of the capacitance in air). The ratio of the capacitance that will occur in the case of the dielectric material to that in the first case gives the relative permittivity of the material (Equation 1.11). The polarization of dielectric materials can occur under both direct current and alternating current [19, 42].

$$\varepsilon_r = \frac{C}{C_0} \tag{1.11}$$

In polarizations under the influence of alternating current (AC), the dielectric constant is expressed as a complex number as in Equation 1.12 [41].

$$\mathcal{E}_r = \mathcal{E}' - j\mathcal{E}'' \tag{1.12}$$

In the equation, $\mathcal{E}_r$ represents the relative permittivity, $\mathcal{E}'$ the real part of the dielectric constant, and $\mathcal{E}''$ the imaginary part of the dielectric constant. The expression $\mathcal{E}'$ is an indication of the polarization ability of the material. The imaginary part of the dielectric constant represents the absorption and scattering of electromagnetic energy and the conversion of energy into heat. In other words, it expresses the dielectric losses of the material [41, 43]. Also, porosity in the sintered ceramics has an impact on the $\mathcal{E}_r$. Therefore, the measured $\mathcal{E}_r$ needs to be adjusted for porosity to obtain the material's real permittivity [40];

$$\mathcal{E}^{\iota} = \mathcal{E}_m\left(1 - \frac{3P(\mathcal{E}_m - 1)}{2\mathcal{E}_m + 1}\right) \tag{1.13}$$

where $\mathcal{E}^{l}$ is the permittivity obtained experimentally, $\mathcal{E}_m$ is the material's permittivity adjusted for porosity. The dielectric constant ($\mathcal{E}_r$) affects the wavelength (λ) in resonator applications and is expressed as [44];

$$\lambda_d = \frac{\lambda_0}{\sqrt{\mathcal{E}_r}} \tag{1.14}$$

Here, λ_d is the wavelength in the dielectric, and λ_0 is the wavelength in air or vacuum. The material with high dielectric constant in the microwave region is generally used for circuit miniaturization because the wavelength in the dielectric resonator is inversely proportional to the square root of the dielectric constant. At millimeter wavelengths, the dielectric constant is expected to be small, since miniaturization is not required. The size of the dielectric sample must be an exact multiple of the dielectric half wavelength for it to resonate in the simplest fundamental mode [45]. If this wavelength is reduced, the physical dimensions of the resonator must also be reduced because it is known that as $\mathcal{E}_r$ increases, the resonance frequency decreases and as the dimensions of the sample decrease, the resonance frequency increases. The dielectric constant of a material determines the behavior of

an electrical signal in that material. A low ε_r will result in a high signal propagation rate. Figure 1.9 shows how microwaves behave when passing through a dielectric material. It shows that when microwave enters a dielectric material, its wavelength decreases by the same amount and its frequency is affected [40].

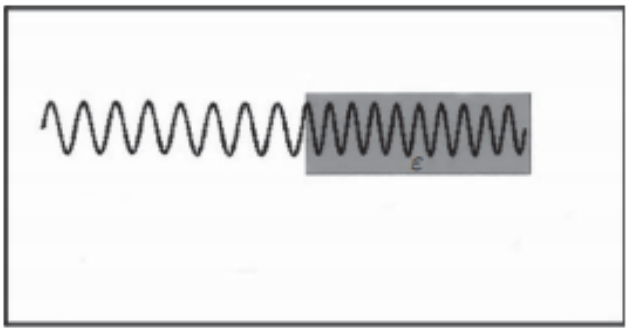

Figure 1.9 The decreased wavelength by a factor of √ε, when the microwave dielectric reaches the ceramic [40]

The dielectric constant is also a factor in the time delay phenomenon expressed by T_{PD}. Time delay is a desirable property to improve the speed of the signal and is expressed by the following equation [9].

$$T_{PD} = \frac{\sqrt{\varepsilon_r}}{c} \tag{1.15}$$

where √ε and c are square root of the dielectric constant and the speed of light, respectively. Since the dielectric constant is frequency dependent, it is very rare that the square of the refractive index measured at optical frequencies is the same as the dielectric constant measured in microwaves [46];

$$\varepsilon_r = n^2 \tag{1.16}$$

Figure 1.7 shows the relationship of polarization processes with frequency. The same polarization processes are excited by optical, microwave and radio frequencies, and this is usually only true for basic solid materials such as diamond (n^2 = 5.85, ε_r = 5.68) or germanium (n^2 = 16.73, ε_r = 16) [46]. In other materials, this rule does not apply as dipolar polarization processes that happen at lower frequencies generally do not happen at higher optical frequencies. As shown in Figure 1.7, ionic and

electronic polarization mechanisms at microwave frequencies predominantly conduce to net dipole moments and dielectric constant.

1.4 Dielectric Loss

A certain amount of energy is absorbed and emitted as heat when a dielectric material is exposed to an alternating electric field. Dielectric loss is the name given to this energy loss. It is the tangent of the dielectric loss angle between current and voltage in a material (see Figure 1.10). It is a measure of the heat production capacity of the ceramic when operated. This is a direct measurement and usually occurs under the same conditions as capacity measurement. The dielectric loss generally depends on the applied voltage, frequency, humidity and temperature, and the loss increases with the increase of these factors [47].

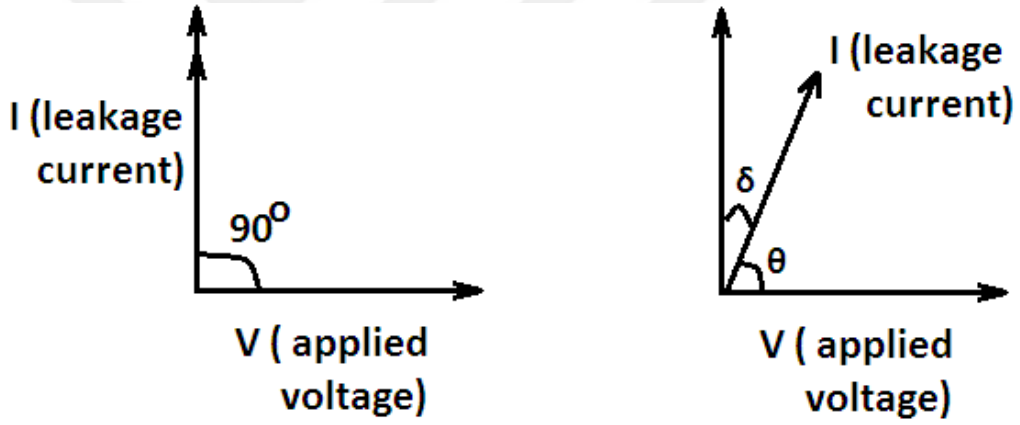

Figure 1.10 The dielectric loss; ideal (left) and commercial (right); I: current, and V: voltage [48]

Commercial insulators do not always lead the applied voltage by exactly 90° when it comes to leakage current (a current that passes through the insulator and flows to earth). The phase angle is never equal than 90°. The dielectric loss angle is defined as the complementary angle δ= 90°-θ. The dielectric's power loss P for an insulator with capacitance C and a voltage V applied to it at a frequency (f, Hz) can be computed as follows [48]:

$$P = V^2 2\pi f C tan\delta \tag{1.17}$$

where tanδ is power loss of the dielectric. In other words, the dielectric loss factor of materials (tanδ) is expressed by the ratio of the imaginary part (Ɛ′′) of the complex number expressing the dielectric constant to the real part (Ɛ′) and is given by;

$$tan\delta = \frac{\mathcal{E}''}{\mathcal{E}'} \tag{1.18}$$

Also, the formula for dielectric loss and porosity is given Equation 1.19 [49].

$$tan\delta = (1-P)tan\delta_0 + A'P\left(\frac{P}{1-P}\right)^{2/3} \tag{1.19}$$

where $tan\delta_0$ is the loss tangent of pore-free bulk material, P is the porosity fraction and A' is an empirical fit parameter.

A microwave system's quality factor, or Q, measures its power loss. It is also referred to as 1/tanδ in the literature [50]. Quality factor is a unitless term often used with microwave resonators and expresses the ratio of the energy stored on the dielectric material per unit time of a microwave system to the energy lost per unit time (Equation 1.20) [43].

$$Q = 2\pi \frac{maximum\ energy\ stored\ per\ cycle}{Average\ energy\ dissipated\ per\ cycle} \tag{1.20}$$

Since the quality factor of the materials is directly proportional to the frequency, the measurement is given by multiplying with the frequency. For this reason, it is shown as Q.f and its unit is GHz. Dielectric losses generally tend to increase with increasing applied frequency [50, 51]. This factor depends on grain size, porosity, internal stress, structure, phase development and conductivity. The dielectric loss tangent (tanδ) of a material absorbs the electrical energy of the material exposed to an alternating electric field, causing heat dissipation throughout the material [40]. Electrical conduction refers to the quantitative distribution of electrical energy due to different physical processes such as dielectric relaxation, dielectric resonance [52]. The delay between the electric field and the electrical displacement vectors is a contributing factor in the dielectric loss. [53]. Dielectric losses depend on crystal

structure, frequency and temperature. To ensure maximum signal identification, the dielectric loss should be less than 10^{-3} [54].

There are two main reasons for the occurrence of dielectric losses [40]. The first one arises due to the composition of the material and are called internal losses. The interactions between the phonon system and the alternating current electric field can explain the losses in perfect crystals, which depend on the crystal structure [55, 56]. The loss due to composition in microwave dielectric ceramics arises when the applied electric field interacts with the optical phonons in the material. The interacting optical phonons produce thermal phonons, and the resulting heat dampens the optical phonon vibrations, causing dielectric loss. For this reason, there is a linear relationship between frequency and increase in dielectric loss [50, 55–58]. The intrinsic dielectric losses depend on alternating current field frequency, crystal symmetry and temperature [40]. These intrinsic losses result in lower dielectric losses in defect-free single crystals or ideally pure materials. The other reason is called external losses and they occur due to the microstructure of the material. It is correlated to crystal lattice imperfections such impurities, microstructural imperfections, grain boundaries, porosity, microcracks, disorder, random crystal orientation, dislocations, atomic vacancies, and doping atoms. Since the emergence of external losses occurs during the production phase, they can theoretically be reduced to a minimum during production. Grain boundaries can form poles in dielectric materials. For this reason, grain growth is a factor that increases the loss factor in these materials. Since dielectric losses cause scattering of electromagnetic waves by heat, losses at high frequency or high voltage act as a thermal source. For this reason, dielectric materials can cause a decrease in their performance. In material selection, the dielectric loss factor is an important parameter both to prevent power loss and to preserve the properties of the material under operating conditions [40, 55, 58].

Microwave resonators are more frequently associated with the phrase "quality factor". There are four different types of losses that can occur in a microwave resonator: dielectric, conduction, radiation, and external [43]. The quality factors for dielectric Q_d, conduction Q_c, and radiation Q_r are provided by Equation 1.21.

$$Q_d = 2\pi \frac{W_1}{P_d T} = \frac{\omega_0 W_1}{P_d}, \qquad Q_c = \frac{\omega_0 W_1}{P_c}, Q_r = \frac{\omega_0 W_1}{P_r} \tag{1.21}$$

where W_1 is the resonator's total electrical energy storage, P_r, P_d and P_c, and represent the the radiation, dielectric, and conductor of power dissipated, respectively. Q_u (unloaded quality factor) is connected to additional Q-factors via [40].

$$\frac{1}{Q_u} = \frac{1}{Q_d} + \frac{1}{Q_c} + \frac{1}{Q_r} \tag{1.22}$$

In practice, the electromagnetic coupling of metal shielding box leads to external losses ($1/Q_{ext}$). Probes for conducting microwaves are brought up close to the resonator (usually within millimeters of one another) in order to introduce an electromagnetic field into it; the greater the resonator's ε_r, the closer the probe must be. They are related because the dielectric ceramic causes electromagnetic fields in response to the electromagnetic fields around them; nevertheless, the presence of conducting probes in the resonator's electromagnetic field lines causes further loss. The definition of the total or loaded Q-factor Q_L is given Equation 1.23 [45, 50].

$$\frac{1}{Q_L} = \frac{1}{Q_d} + \frac{1}{Q_c} + \frac{1}{Q_r} + \frac{1}{Q_{ext}} \tag{1.23}$$

Figure 1.11 shows the resonance peak and its associated parameters, and the Q_L is determined experimentally. The relationship between the Q_L and Q_u depends on the coupling coefficients. The Q_L (total loss in the system) refers to a resonator connected with an external circuit. At the resonant frequency, the transmitted signal's amplitude reaches a peak with a finite width. The breadth of the resonance curve at 50% power values is known as the -3 dB bandwidth (BG). Q_L is equal to the peak frequency (resonant frequency), f, divided by the width of -3 dB. The measured resonant frequency f and the half-power (-3 dB) bandwidth f of the TE_{011} mode resonance are used to calculate the loaded Q_L and expressed mathematically in Equation 1.24 [40, 50].

$$Q_L = \frac{f}{\Delta f} \tag{1.24}$$

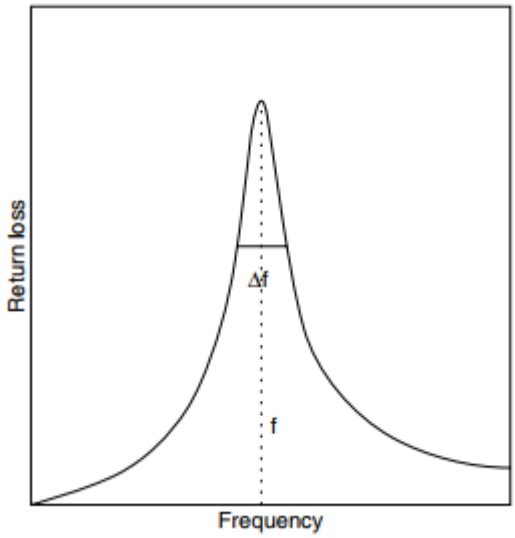

Figure 1.11 Resonance peak and related parameters [40]

The resonator bandwidth is inversely proportional to the Q factor. Therefore, high Q resonators have narrow BG. If the coupling is low (coupling coefficients<<1), the unloaded Q factor is approximately equal to the loaded Q factor. In practice, resonators are often used with tunable couplings that allow such an approximation without the need to measure coupling coefficients. If conduction, radiation and external losses are negligible, then $Q_L = 1/\tan\delta$. When we measure the dielectric loss at a given frequency, we get the total loss tangent, and we cannot distinguish the contributing factors [40].

1.5 Temperature Coefficient of Resonance Frequency

The frequency stability is determined by temperature coefficient of resonance frequency (τ_f), which is described as [50].

$$\tau_f = \frac{1}{f_r} x \frac{\Delta f}{\Delta T} \tag{1.25}$$

where Δf is the variation in resonance frequency from room temperature for a change in temperature ΔT and f_r is the resonant frequency at room temperature.

With the effect of temperature, the resonance frequency in dielectric ceramic materials changes for two reasons; linear thermal expansion and variation of

dielectric constant with temperature [59]. The terms expressing the variation of the dielectric constant with temperature are the temperature coefficient of dielectric constant (τ_ε) and the temperature coefficient of resonance frequency (τ_f). The τ_ε shows the change in the dielectric property of the material with temperature and is calculated by Equation 1.26 [45, 50, 60].

$$\tau_\varepsilon = \frac{\varepsilon_{T_2} - \varepsilon_{T_1}}{\varepsilon_{T_1}(T_2 - T_1)} \tag{1.26}$$

In the equation, T_1 and T_2 represent two different temperatures, and ε_{T1} and ε_{T2} represent the dielectric constants at these temperatures. τ_f indicates the trend of the resonant frequency with changing temperature. Microwave resonators require τ_f values as close to zero as possible. As the temperature coefficient value moves away from the ideal, the operation of the circuit on cold and hot days will be different from each other. The dielectric resonators to be used in applications are expected to operate between -40°C and 100°C. For this reason, the temperature coefficient value should be -10 and +10 ppm°C^{-1} [50]. The resonator frequency of the resonator depends on the resonator environment, dielectric constant and sample sizes. The linear thermal expansion coefficient α_L and temperature coefficient of dielectric constant τ_ε are related with the resonator dimensions and the dielectric constant change with temperature [43]. Therefore, τ_f is related to thermal expansion and dielectric constant and its mathematical representation is given in Equation 1.27.

$$\tau_f = -\alpha_L - \frac{\tau_\varepsilon}{2} \tag{1.27}$$

where τ_ε is the temperature coefficient of permeability. It is valid for 100% electrical energy storage in the sample and the thermal expansion of the metal cavity surrounding the dielectric resonator can be neglected. Therefore, from Equation 1.27 for zero τ_f, τ_ε must have twice the value of α_L and be negative [40].

Experimentally, τ_f is measured by monitoring the deviation in the resonance peak frequency as the temperature slowly changes. To measure τ_f, the dielectric resonator is kept short between two copper plates in the Courtney setup. This is then kept in a temperature-controlled oven. The E-field probe is held near the dielectric resonator

to achieve resonance. The TE_{011} mode is defined and then the installation is gradually heated in the temperature range of 25–80°C at a heating rate of about 1°C/min. The heat probe is kept just inside the furnace so that it does not disturb the resonance frequency. The shift of the resonance frequency as a result of heating in the reflection mode is noted using the network analyzer when the temperature is constant. The variation of the resonant frequency is plotted as a function of temperature. This τ_f (ppm^oC^{-1}) is calculated from the slope of the curve using Equation 1.28 [40].

$$\tau_f = \frac{f_{80} - f_{25}}{f_{25}(80 - 25)} = \frac{1}{f}\frac{\Delta f}{\Delta T} \tag{1.28}$$

τ_f can also be measured by the gap method used to measure the quality factor. The thermal expansion of the cavity during heating limits the accuracy of the method [40]. However, the precision can be increased by using a hollow constructed invar. If the sample's dielectric constant is high and it is placed far from any cavity walls, the thermal expansion of the cavity for a $TE_{01\delta}$ mode resonant structure is extremely tiny. τ_ε is very for the dielectric substrates. This can be obtained by heating the sample and utilizing the parallel plate capacitor approach with an LCR (inductor-capacitor-resistor) meter operating at a low frequency (for example, 1 MHz). The τ_ε can be determined from the ε_r noted at various temperatures. In the microwave range, one can get τ_ε based on the values of τ_f and α_L and using Equation 1.27 [40].

1.6 Dielectric Breakdown

A system dielectric breakdown is a simple material puncture or the damage of all (or a portion) of the material. Dielectric degradation in solids is a limiting factor in the design of microcircuit components, cables, capacitors and other electronic components. Understanding the dielectric breakdown mechanism is important to ensure that the part to be designed is isolated. In general, dielectric decay is studied in two classes such as thermal and electrical breakdown mechanisms [61, 62].

Thermal dielectric degradation occurs when the electrical conductivity increases by heating the dielectric material. In a material where thermal degradation occurs,

effects such as burning, crack formation or separation into components can be seen. Materials with a high dielectric constant temperature coefficient also increase the possibility of thermal dielectric degradation. When the dielectric material is polarized under the influence of an electric field, a certain strain occurs as a result of the displacement or polarization of the electric charge inside the material. An atom tries to keep its electrons bound to itself by being charged in the opposite direction of the applied electric field under the influence of an electric field. Free electrons arise when the applied electric field is above the limit of countercharge that the atom can exert. The electron released under a sufficiently large electric field ionizes other atoms in the material, creating new free electrons and starting a chain reaction. Thus, the free electrons grow like an avalanche and allow the electric current to be carried through the material. This phenomenon is called electronic decay. With this deterioration, irreversible damages occur in the material [63]. Factors affecting dielectric strength; density, impurities, temperature, humidity and frequency of applied voltage [61, 62]. Since it is controlled by more than one factor, a theory that explains the dielectric strength to cover all factors has not yet been developed [64]. The purpose of conducting a test determines the type of test that should be used because the physical stresses that dielectric materials are subject to do not, by themselves, cause these materials to fail or prematurely age [64].

1.7 Microwave Dielectric Ceramics

With the development of communication technology, the importance of dielectric ceramic materials in microwave devices is constantly increasing and resulting in an increased demand for dielectric resonators used in wireless communication devices. Microwave dielectric materials are used in mobile phones, global positioning systems, military radars and satellite communication systems. It is revolutionized the microwave wireless communications industry by reducing the size and cost of antenna components. Applications and electromagnetic spectrum are shown in Figure 1.12. Microwave region falls in the spectrum between 300 MHz and 300 GHz or wavelengths ranging from 1 mm to 1 m. Microwaves have higher frequency and lower wavelength than radio waves. As a result of its huge bandwidth capacity in

comparison to radio waves, their information carrying capabilities are high [1, 65, 66]. Microwave dielectric ceramic resonators examples are given in Figure 1.13.

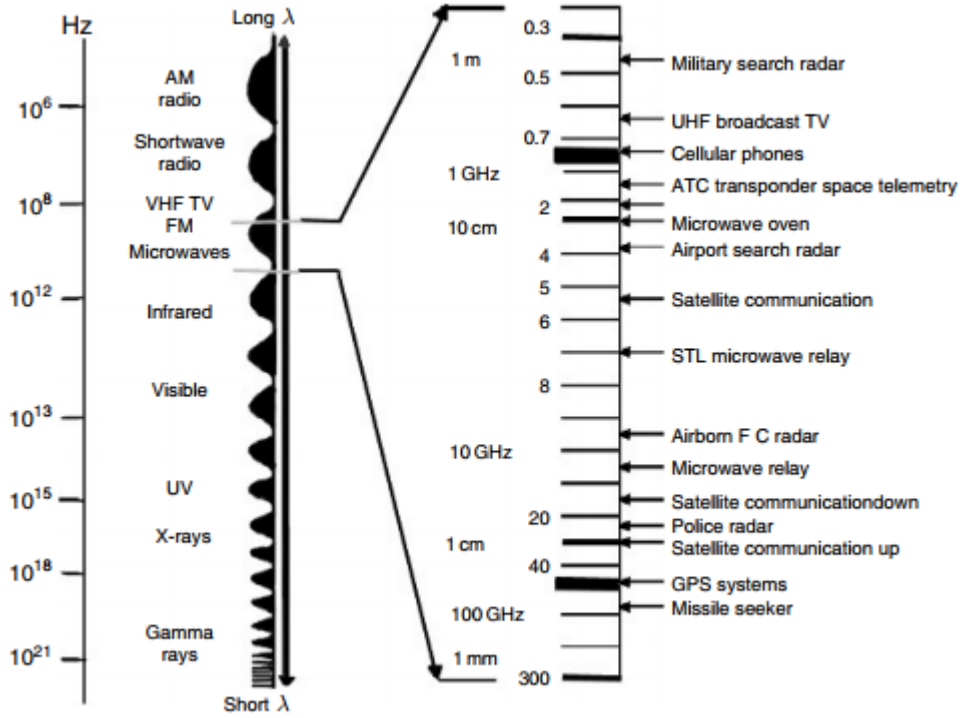

Figure 1.12 Electromagnetic spectrum and some microwave applications [1]

Figure 1.13 Microwave dielectric ceramic resonators [67]

A dielectric resonator is an electromagnetic component that exhibits resonance for a narrow frequency range with useful properties [68]. It generally consists of a ceramic material with a high dielectric constant and a low loss factor. The material's overall physical parameters, the dielectric constant of the material and its immediate surroundings dictate the resonant frequency. The main characteristics for a dielectric resonator have high quality factor (Q), high dielectric constant (ε_r), and near-zero temperature coefficient of resonance frequency (τ_f) [69]. Microwave applications require special devices for transport and filtering due to cable response time and transport time. Conventional transistors, integrated circuits and cables cannot be used to carry these waves. Due to the high resistance that occurs in conventional circuits at high frequencies, the signal is lost before reaching to the desired location. For this reason, ceramic materials find use in microwave circuits due to their dielectric properties. It provides a constant impetus for the discovery and development of materials to perform the same or improved function with less size and weight. The ceramic resonators have superior features with ground gain and signal selectivity [68]. The ceramics used in this field are used in the production of parts such as resonators and oscillators [58]. The dielectric resonator filters used in mobile phone base stations are employed in microwave communications to distinguish between desired and undesirable signal frequencies from the received and broadcast signals. To keep a high signal-to-noise ratio, the desired frequency is extracted from the signal and identified. It is crucial for clarity that seasonal temperature changes have no impact on the desired signal frequency [70].

In the literature, it has been revealed that there are many dielectric ceramics with dielectric constants ranging from 3.9 to 838, but the number of suitable ones for use is very few. The dielectric ceramic materials in the literature are generally classified in three classes, as shown in Figure 1.14 [71, 72].

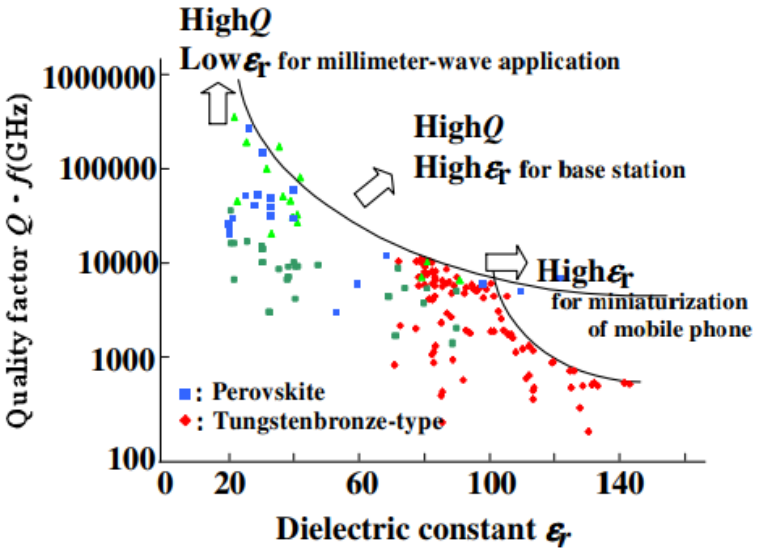

Figure 1.14 Development and grouping of microwave dielectric ceramics [72]

The first group, ceramics with high dielectric constant ($\varepsilon_r \geq 50$), are used in areas where miniaturization is at the forefront. The most important member of this group is $Ba_{6-3x}R_{8+2x}Ti_{18}O_{54}$ (R=Pr, Sm, La) dielectric ceramics. They are used in microwave devices that require miniaturization, such as mobile phones, with dielectric constants between 70-100 and low resonance temperature coefficient values [-10 and +10 ppm$^oC^{-1}$] [71, 73, 74]. In addition, Bi_2O_3-ZnO-Nb_2O_5 system ceramics have become one of the remarkable material groups in recent years, thanks to their microwave dielectric properties. In Table 1.2, microwave ceramics belonging to this group and their dielectric properties are given together.

Table 1.2 Microwave ceramic examples in $\varepsilon_r \geq 50$

Composition	ε_r	Q.f	τ_f	Reference
$Ba_{6-3x}Nd_{8+2x}Ti_{18}O_{54}$ (x=0.08)	92.3	6460	10	[75]
Bi_3NbO_7	91	730	-	[76]
(1-x)$CaTiO_3$-xCa$(Zn_{1/3}Nb_{2/3})O_3$ (x=0.4)	76	7560	164	[77]
$Ba_4Sm_{9.33}Ti_{18}O_{54}$	80	10700	-15	[78]

The second group, dielectric ceramics with dielectric constants between 25 and 50, also has low dielectric loss factor [10^{-3}]. It is used to improve signal-to-noise ratios in satellite communications and cell phone base stations. $BaMg_{1/3}Ta_{2/3}O_3$ and $BaZn_{1/3}Ta_{2/3}O_3$ are prominent members of this group. Microwave ceramics from this group and their dielectric characteristics are listed together in Table 1.3 [71, 74].

Table 1.3 Microwave ceramic examples in ε_r = 25-50

Composition	**ε_r**	**Q.f**	**τ_f**	**Reference**
$Ca(Zn_{1/3}Nb_{2/3})O_3$	35	16000	-43	[79]
$Ba_2Ti_9O_{20}$	38.8	43200	+4	[80]
$Ba_5Nb_4O_{15}$	39	23700	78	[81]
$(1-x)CaTiO_3$-$xCa(Zn_{1/3}Nb_{2/3})O_3$ (x=0.8)	42	13030	-28	[77]

In the third group, there are ceramics with dielectric constants less than 25 and high-quality factors. Ceramics in this group are used as antenna circuit elements at high frequencies. The dielectric constants are very low because they have very strong covalent bonds. For this reason, both the number of electrical dipoles that can occur in the material and the movement capacity of the formed dipoles are limited [71]. It generally consists of aluminates and silicates such as $MgSi_2O_4$, $MgAl_2O_4$ and $ZnAl_2O_4$ [71]. Table 1.4 shows the microwave ceramics belonging to this group.

Table 1.4 Microwave ceramic examples in $\varepsilon_r \leq 25$

Composition	**ε_r**	**Q.f**	**τ_f**	**Reference**
$MgSi_2O_4$	6.8	270000	-67	[82]
$MgAl_2O_4$	8.5	175000	-63	[83]
$ZnAl_2O_4$	8.5	56000	-79	[84]
$MgNb_2O_6$	21.4	93800	-70	[85]
$SrNb_2O_6$	21.7	16900	-	[86]

1.8 Literature Review

The term "dielectric resonator" initially originated, that Richtmeyer demonstrated that correctly formed dielectric component can serve as a microwave resonator in 1939 [87]. However, it took more than 20 years for the knowledge to be tested empirically. Superhigh permittivity materials and their use as capacitors at relatively low radio frequencies were reported by Schlicke [88] in 1953.

After that, Okaya and Barash [89] brought the dielectric resonator system back during their studies on rutile single crystals in the early 1960s [65]. They measured the dielectric constant and Q factor values of single crystal TiO_2 ceramics at room temperature using the commensurate/transmission line technique [65]. The high resonance frequency temperature coefficient of TiO_2 ceramics (+450 ppm°C^{-1}) limits the use of this material group in industrial applications [1]. In the early 1970s, barium tetratitanate ($BaTi_4O_9$) with desired temperature stability values and low dielectric losses was produced for the first time developed by Masse et al [90]. Then, barium nonatitanate ($Ba_2Ti_9O_{20}$) developed by Bell Laboratories was reported [91]. The next important development in microwave applications was the development of $(Zr,Sn)TiO_4$ dielectric oxide ceramics by the Japanese company Murata Manufacturing [92, 93]. Various compositions have been developed by the Murata Manufacturing company, thanks to which the resonance frequency temperature coefficients of these materials can be adjusted between +10 and 10 ppm°C^{-1} [93]. After these developments, many researchers studied dielectric constant (ε_r), quality factor (Q) and resonance frequency (τ_f) values [1, 68, 71].

The ceramic dielectric resonators are reduced in size and have a higher Q compared to the conventional microwave materials. In the majority of microwave and millimeter wave applications, dielectric resonators have replaced the use of cavity resonators due to cost, size, mass, efficiency, durability, stability, robustness and ease of use. Also, the temperature variation of the resonant frequency of dielectric resonators can be designed to a desired value to meet the circuit designer's requirements (see Figure 1.15) and commercial dielectric resonators are given in

Figure 1.16 [1]. The objectives set for the development of microwave dielectric ceramics are listed below [68]:

a) The Dielectric Constant (ε_r) should be as high as possible because the size of a resonator is inversely related to the square root of the dielectric constant (see Equation 1.14). The dielectric material spectrum is practically limited to about $20< \varepsilon_r <100$.

b) To ensure maximum signal identification, the dielectric loss ($\tan\delta$) should be less than 10^{-3} [54]. This is closely related to the quality factor (i.e., $Q=1/\tan\delta$), which should generally be maximized. Nowadays, $Q>30{,}000$ at 1 GHz is required for many practical applications.

c) Especially in the communication systems, in order to ensure a certain temperature balance, the resonator's temperature coefficient of resonance frequency (τ_f) must be around $\sim \pm 2$ ppm°C^{-1} so that the signal does not shift during operation [50, 68].

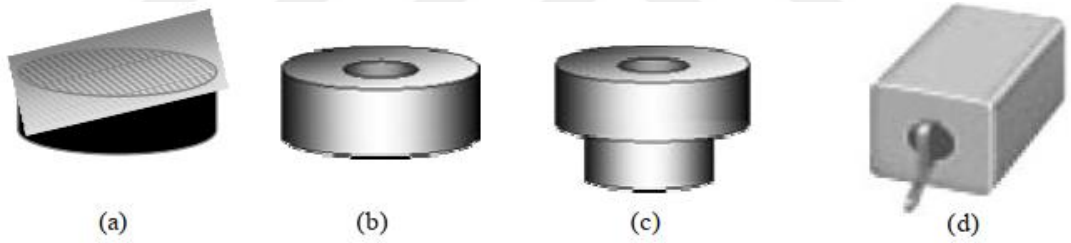

Figure 1.15 Images of dielectric resonators in different shapes; (a) disc, (b) coaxial cylinder, (c) supported coaxial cylinder, (d) TEM mode dielectric resonator [50]

Figure 1.16 Commercial dielectric resonators [94]

System performance is closely related to material properties because grain size, grain boundaries, crystal structure and point defects affect ceramic physical properties [68]. In terms of ceramic processes, the purity of the starting materials, calcination temperature and time, forming method, sintering temperature and time, density are the parameters that affect the system performance. Figure 1.17 shows the effect of calcination and sintering temperature on the density and microwave dielectric properties of ceramic dielectric resonators. For optimum properties (low τ_f, high Q.f and ε_r) a high density is required [71].

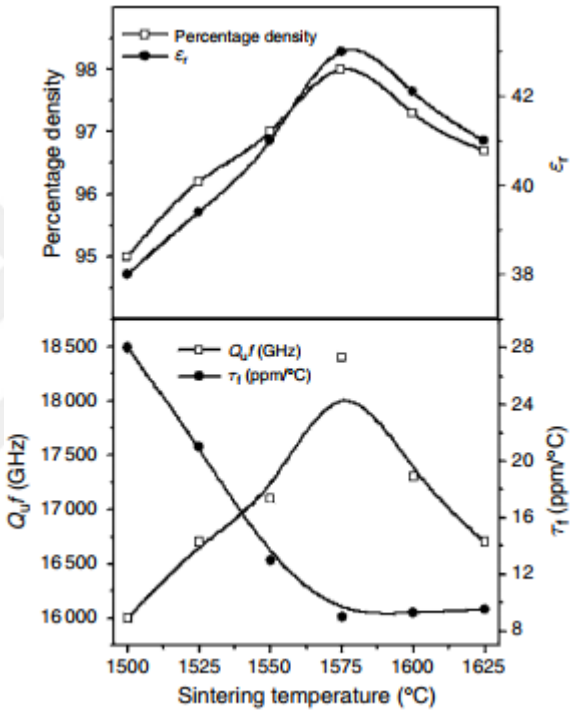

Figure 1.17 The alteration of ε_r, Q.f, τ_f and the relative density of $Ba(Sm_{1/2}Nb_{1/2})O_3$ ceramic versus the sintering temperature [1]

Microwave ceramics are generally optimized for densification where ε_r and Q.f are best. Powders prepared by solid-state methods require a higher sintering temperature than those prepared by chemical methods [1]. A high Q.f value can only be achieved in ceramics with fine grain and/or homogeneous microstructures. Low densification is mainly due to rapid and abnormal grain growth. Therefore, pores are entrapped inside the grains, which eventually decreases dielectric constant and mechanical properties. The additives can be used to promote densification. Additives (dopants)

allow densification to occur in shorter times and at lower temperatures. In addition, it prevents grain growth and allows the elimination of pores [40]. Additives added to aid sintering affect the dielectric properties of ceramics by changing the density, microstructure, defect chemistry and crystal structure. A higher relative density results in higher ε_r. The selection of suitable additives, their optimum amount and optimum processing conditions are effective in increasing the quality factor [1].

1.9 Objective

Dielectric ceramics used at various applications have different dielectric properties. Dielectric ceramic materials with $\varepsilon_r \leq 25$ are used for microwave circuit elements in substrate material and missile tracking systems. ε_r=25-50 are used to improve signal-to-noise ratios in satellite communications and cell phone base stations. $\varepsilon_r \geq 50$ are used for miniaturization such as mobile phones. The aims of this thesis are to synthesize dielectric ceramic compositions in three wavelength ranges (i.e., $\varepsilon_r \leq 25$: CeO_2-Glass, ε_r=25-50: $SrNb_2O_6$ and $Ba_2Ti_9O_{20}$, $\varepsilon_r \geq 50$: $0.68CaTiO_3$-$0.32Ca(Zn_{1/3}Nb_{2/3})O_3$ and $Ba_{6-3x}(Nd_{1-y}Bi_y)_{8+2x}Ti_{18}O_{54}$ x=2/3 y=0.07) by solid state calcination method, to fabricate them by dry pressing at desired dimensions and then to investigate densification, phase formation, microstructure evolution, dielectric and microwave properties. Especially, the CeO_2-Glass composition was investigated in this study for the first time. The suitability of the ceramics was compared with the literature values.

CHAPTER 2

EXPERIMENTAL METHODS

CeO_2-Glass (5 wt.%), $SrNb_2O_6$, $Ba_2Ti_9O_{20}$, $0.68CaTiO_3$-$0.32Ca(Zn_{1/3}Nb_{2/3})O_3$, and $Ba_{6-3x}(Nd_{1-y}Bi_y)_{8+2x}Ti_{18}O_{54}$ x=2/3 y=0.07 powders were synthesized by solid state method. Dry pressing was used as the shaping method in all ceramic compositions. The steps followed in the experimental studies are given in Figure 2.1. Also, the materials used for ceramic compositions are tabulated with their trade names and properties in Table 2.1.

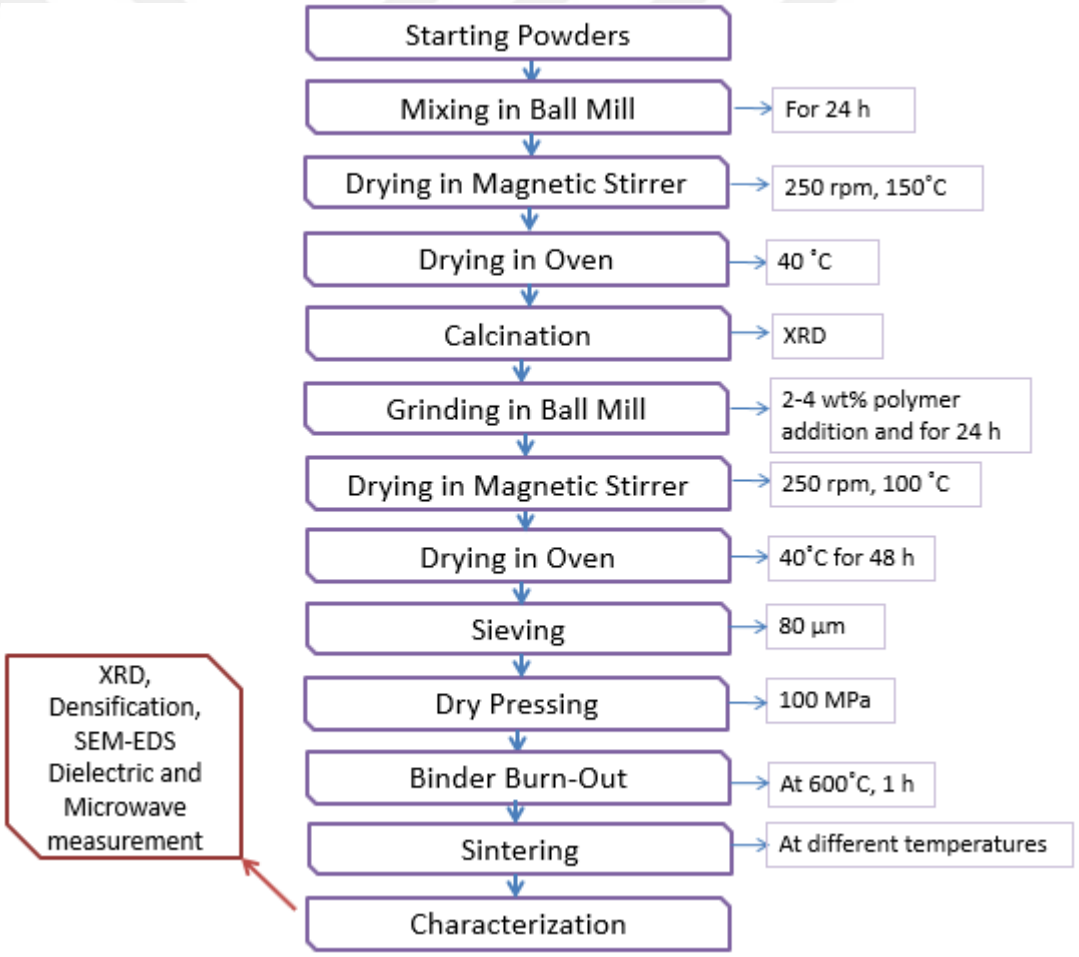

Figure 2.1 Flowchart of the sample preparation steps

Table 2.2 summarizes the starting components and calcination conditions. The mixed powders were weighed at stoichiometric ratios and ball milled in ethanol for 24 h at 185 rpm using 0.5 cm diameter yttria stabilized zirconia balls. The mixtures were dried on a hot plate at 150°C at 250 rpm, and then oven dried at 40°C for 48 h. Commercial $CaTiO_3$ powders were used as-received. Glass frits were first ground into a fine powder using an agate mortar and pestle and then ball milled for 48 h in ethanol using yttria-stabilized zirconium balls.

Table 2.1 The ceramic materials used in compositions

Powders	**Trade name**	**Property**
CeO_2	Inframant, England	99.5% purity
Glass	Akcoat, Türkiye	CaO-Al_2O_3-SiO_2 based
$SrCO_3$	Sigma-Aldrich, Germany	≥98% purity
$BaCO_3$	Sigma-Aldrich, Germany	≥99% purity
TiO_2	Aeroxide, Germany	P25 (20 nm, Specific surface area 35-62 m^2g^{-1})
CaO	Nanografi, Türkiye	99.9% purity
ZnO	Nanografi, Türkiye	99.99% purity
Nb_2O_5	Sigma-Aldrich, Germany	99.9% purity
$CaTiO_3$	Function Material Group Co., Ltd, China	99.5% purity, 325 mesh
Bi_2O_3	Nanografi, Türkiye	99.99% purity
Nd_2O_5	Function Material Group Co., Ltd, China	99.99% purity, 20-500 mesh

Table 2.2 The calcination conditions of $SrNb_2O_6$, $Ca(Zn_{1/3}Nb_{2/3})O_3$, $Ba_2Ti_9O_{20}$ and $Ba_4(Nd_{0.93}Bi_{0.07})_{28/3}Ti_{18}O_{54}$ ceramics

Starting Components	**Final Components**	**Calcination Conditions**
$SrCO_3 + Nb_2O_5$	$SrNb_2O_6$	1050°C- 5 h [95]
$CaO + 1/3ZnO + 1/3Nb_2O_5$	$Ca(Zn_{1/3}Nb_{2/3})O_3$	1300°C- 3 h [79]
$2BaCO_3 + 9TiO_2$	$Ba_2Ti_9O_{20}$	1250°C- 3 h [80]
$4BaCO_3 + 4.34Nd_2O_5 + 0.326Bi_2O_3 + 18TiO_2$	$Ba_4(Nd_{0.93}Bi_{0.07})_{28/3}Ti_{18}O_{54}$	1100°C- 3 h [75]

Before shaping, 4 wt.% vinyl–based binder solution (MSE Teknoloji, Türkiye) was added as a binder to the calcined powders given in Table 2.2 together with $0.68CaTiO_3$-$0.32Ca(Zn_{1/3}Nb_{2/3})O_3$ and CeO_2-Glass powder mixtures. The slurries were dried on a hot plate at 100°C at 250 rpm with continuous stirring. Ethanol was fully evaporated in the drying oven at 40°C for 24 h. The dried powders were first ground with a mortar and then passed through an 80-µm sieve. The sieved powders were compacted at 100 MPa to disc shapes. The pellets were burned-out at 600°C for 1 h with a heating rate of 0.5°C/min (as shown in Figure 2.2).

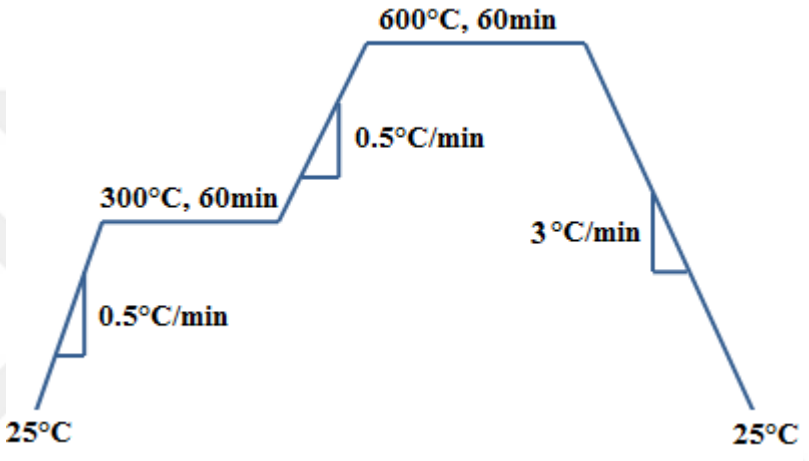

Figure 2.2 The temperature-time profile for burnout process

The green ceramics were sintered at different temperatures in the range of 950°C–1350°C for 1 h for CeO_2-Glass, 1200°C–1325°C [86] for 1 h for $SrNb_2O_6$, 1250°C–1350°C [80] for 3 h for $Ba_2Ti_9O_{20}$, 1350°C–1450°C [77] for 4 h for $0.68CaTiO_3$-$0.32Ca(Zn_{1/3}Nb_{2/3})O_3$ and 1280°C–1350°C [75] for 3 h for $Ba_{6-3x}(Nd_{1-y}Bi_y)_{8+2x}Ti_{18}O_{54}$ x=2/3 y=0.07 in air with a heating and cooling rate of 5°C/min. The sintering temperature range of all compositions except CeO_2-Glass were determined from the literature. It was determined cover the glass sphere temperature of 958°C and glass melting temperature of 1180°C [96] for the CeO_2-Glass composition.

The bulk density was measured using the Archimedes' method. The bulk density, apparent porosity and water absorption were calculated according to Equation 2.1, Equation 2.2, and Equation 2.3, respectively [97].

$$\text{Bulk Density} = \left[\frac{W_d}{W_w - W_s}\right] \text{x } d_{water} \quad (2.1)$$

$$\text{Apparent Porosity} = \left[\frac{W_w - W_d}{W_w - W_s}\right] \text{x } 100 \quad (2.2)$$

$$\text{Water Absorption} = \left[\frac{W_w - W_d}{W_d}\right] \text{x } 100 \quad (2.3)$$

W_d: dried weight (g)

W_s: weight of sample suspended in liquid (g)

W_w: weight of sample impregnated with water (g)

d_{water}: density of water (g/cm^3)

Phase formation of the calcined powders and sintered samples were checked by X-ray diffraction (XRD), (Miniflex600, Rigaku) with a scan rate was 2°C/min and a step interval of 0.02°C. Parallel (Equation 2.5), series (Equation 2.4) and logarithmic mixing (Equation 2.6) models [98] were used to estimate the bulk density and dielectric constant of the CeO_2-Glass powder mixtures:

$$A = A_1 . V_1 + A_2 . V_2 \quad (2.4)$$

$$A = {V_1}/{A_1} + {V_2}/{A_2} \quad (2.5)$$

$$A = V_1 . log A_1 + V_2 . log A_2 \quad (2.6)$$

In these formulae, A is the physical property of the mixture (e.g., dielectric constant or theoretical density), A_1 and A_2 are the respective physical property, and V_1 and V_2 are the respective volume fraction in the powder mixtures.

The samples surfaces were first cleaned with ethanol. Then, the parallel surfaces of the samples were coated with an air-dry silver ink and dried on a hot plate at 50°C for 10 min. to measure dielectric properties. Dielectric properties were measured at 5 MHz at room temperature using an impedance analyzer (HIOKI IM3570 and

AGILENT 4294A). The dielectric constant was calculated from the capacitance measurements according to Equation 2.7 [99].

$$\varepsilon_r = \frac{Cxd}{\varepsilon_0 xA} \tag{2.7}$$

where ε_r is dielectric constant, C is capacitance (F), d is thickness of specimen (m), ε_0 is permittivity of vacuum (F/m) and A is electroded area of the specimen (m^2). The microstructures and elemental analysis from fractured surfaces were examined by a Scanning Electron Microscopy (SEM) and Energy Dispersive Spectroscopy (EDS) (Hitachi, SU5000 Plus), respectively. The microwave properties were measured by a Vector Network Analyzer (Anritsu, MS4644B, 40 GHz).

CHAPTER 3

RESULTS AND DISCUSSION

The dielectric ceramic materials in the literature are generally classified in three classes. The dielectric ceramics have dielectric constant less than 25 for the microwave circuit components, between 25-50 for enhancing signal-to-noise ratios in the satellite communications and cell phone base stations, higher than 50 for the miniaturization such as in mobile phones. Table 3.1 shows the compositions of the compositions investigated in this study. All ceramics were fabricated by dry pressing method. The ball milling was applied to mix powders and to reduce particle size. Anorthite-based glass was added to decrease sintering temperature by means of liquid phase sintering and adjust the dielectric constant less than 25 for CeO_2. This glass composition was selected based on previous studies [96, 100].

Table 3.1 The compositions of the samples

CeO_2-Glass (5 wt.%)
$SrNb_2O_6$
$Ba_2Ti_9O_{20}$
(1-x) $CaTiO_3$-x $Ca(Zn_{1/3}Nb_{2/3})O_3$ x=0.32
$Ba_{6-3x}(Nd_{1-y}Bi_y)_{8+2x}Ti_{18}O_{54}$ x=2/3 y=0.07

3.1. Powder Characterization

The glass powder was first ball milled in ethanol for 48 h with ZrO_2 balls. Figure 3.1 shows the chemical analysis, SEM image, and particle size analysis. The EDS

spectrum is displayed in Figure 3.1(a). Au plating caused the Au peaks, while carbon tape caused the C peaks. As a result, they were not taken into account while calculating composition. The predicted stable oxide composition was then calculated as listed in Table 3.2. The glass powder primarily consisted of SiO_2, Al_2O_3, and CaO, and hence anorthite phase crystallization ($CaO.Al_2O_3.2SiO_2$ or $(Ca,Na)(Si_2Al)_4O_8$) (PDF Card No: 00-041-1481) was anticipated. SiO_2 served as the network former, while Al_2O_3 served as intermediate and CaO, Na_2O, and K_2O as modifiers [101]. The SEM picture of the angular-shaped particles is depicted in Figure 3.1(b). XRD pattern shows in Figure 3.1(c) that the glass powder was amorphous in nature and had a minor peak corresponding to the quartz phase (Card number: 00-009 0466). After milling, a unimodal particle size distribution with d_{50}=2.13 µm, d_{90}=3.91 µm, (Figure 3.1(d)) and SSA = 1.89 m^2/g was obtained [96, 100].

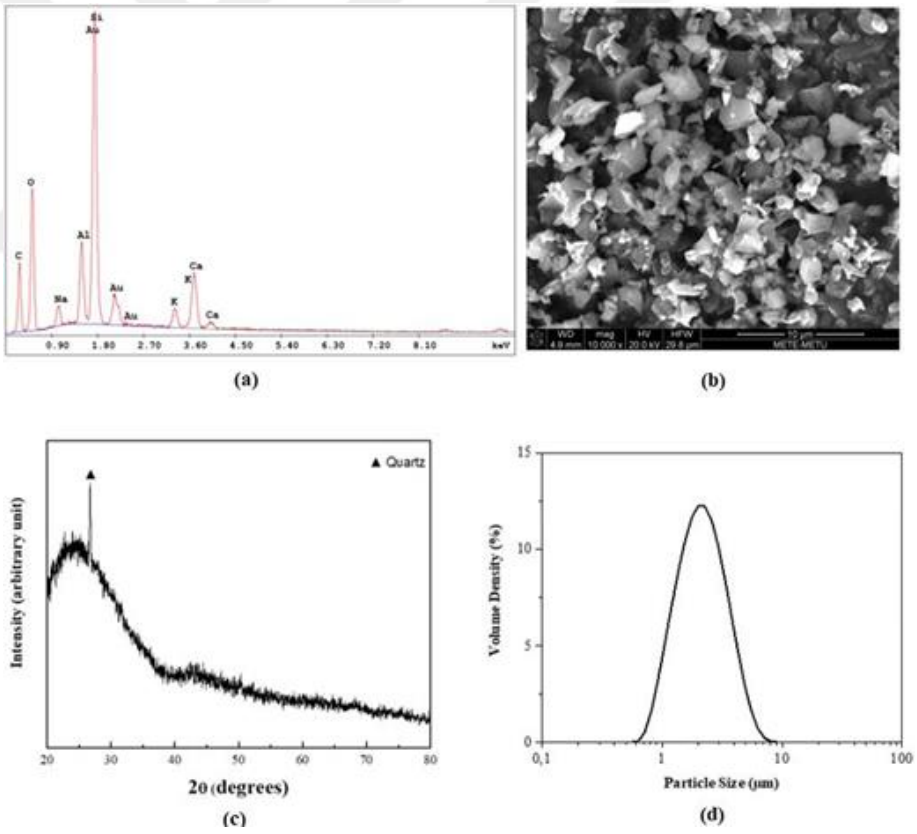

Figure 3.1 (a) EDS; (b) SEM image; (c) XRD; (d) Particle size after 48 h of ball milling [96]

Table 3.2 The stable oxide composition of glass powder

Phases	SiO_2	Al_2O_3	CaO	Na_2O	K_2O
wt.%	65.8	15.1	11.7	4.0	3.4

The heat microscopy result of the glass is shown in Figure 3.2. The temperatures for sintering, softening, sphere, and melting were found to be 726°C, 852°C, 958°C and 1180°C, respectively. The glass pellets heated to 750°C and 825°C exhibited similar behavior with the heat microscope results [96, 100].

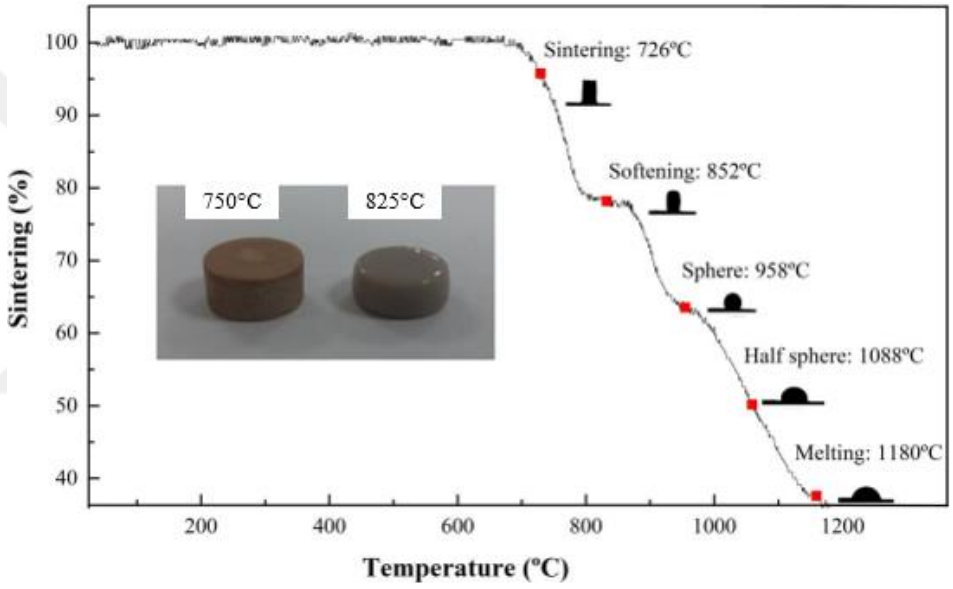

Figure 3.2 Heat microscope result of glass powder [96]

3.2. Phase Formation

The phase formation of the calcined powders was investigated by XRD.

3.2.1 $SrNb_2O_6$ Powder

Figure 3.3 shows the XRD pattern of the $SrCO_3$+Nb_2O_5 powder mixture calcined at 1050°C for 5 h [95]. A pure orthorhombic $SrNb_2O_6$ phase (PDF Card No: 00-028-1243) was formed after calcination.

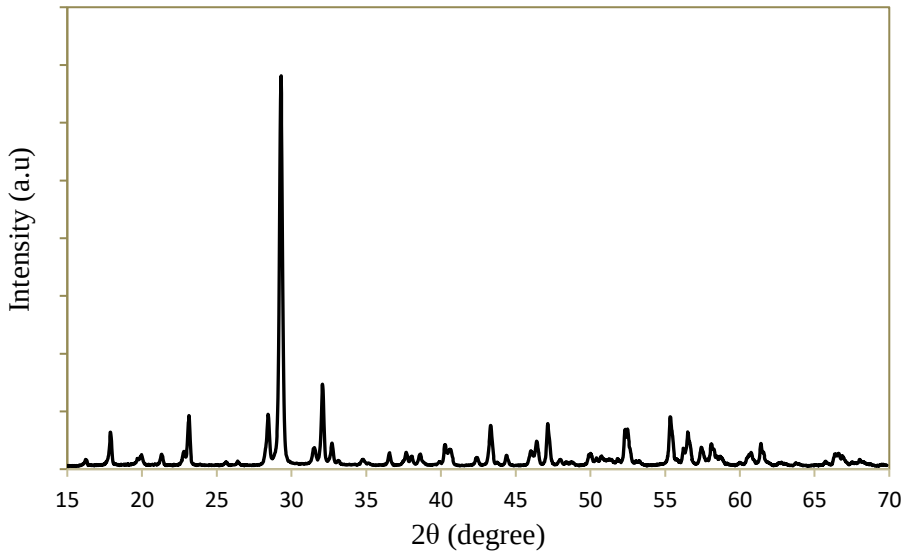

Figure 3.3 XRD pattern of $SrNb_2O_6$ powder calcined at 1050°C for 5 h

3.2.2 $Ca(Zn_{1/3}Nb_{2/3})O_3$ Powder

Figure 3.4 gives the XRD pattern of $CaO+ZnO+Nb_2O_5$ powder mixture calcined at 1300°C for 3 h [79]. A pure perovskite $Ca(Zn_{1/3}Nb_{2/3})O_3$ phase was formed after calcination according to Chen at al. [79] study.

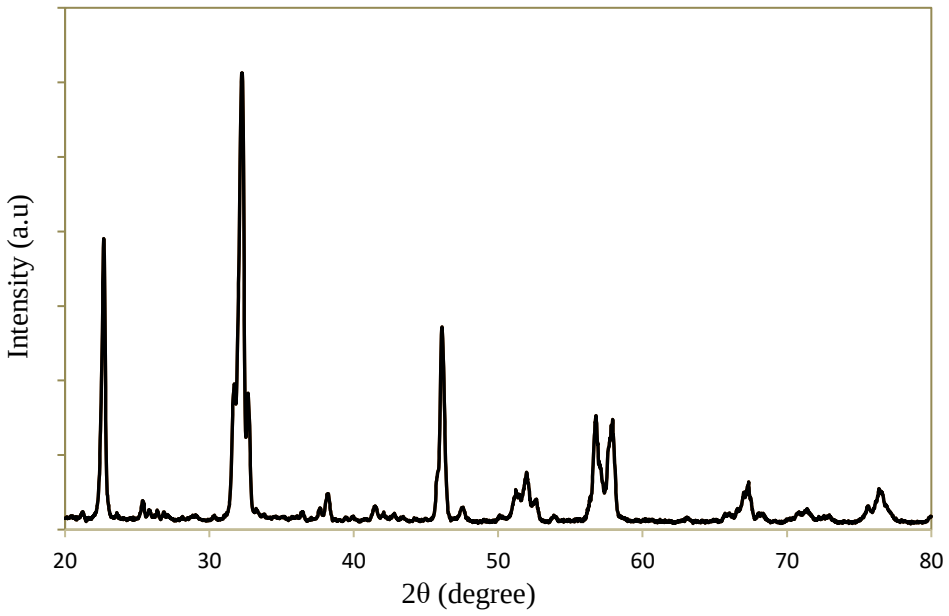

Figure 3.4 XRD pattern of $Ca(Zn_{1/3}Nb_{2/3})O_3$ powder calcined at 1300°C for 3 h

3.2.3 $Ba_2Ti_9O_{20}$ Powder

Figure 3.5 shows the XRD pattern of the $BaCO_3$ + TiO_2 powder mixture calcined at 1250°C for 3 h [80]. A pure triclinic $Ba_2Ti_9O_{20}$ phase (PDF Card No: 01-076-1424) was formed after calcination.

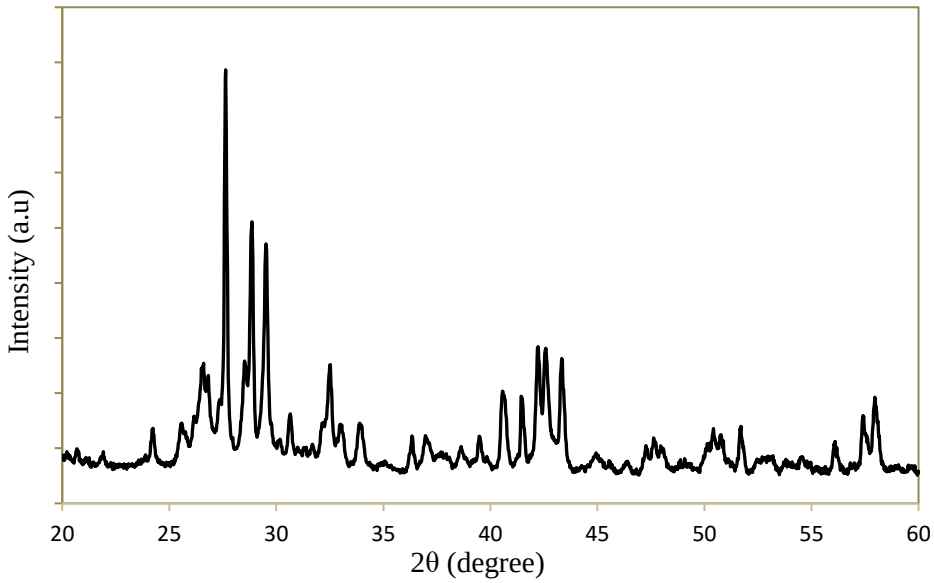

Figure 3.5 XRD pattern of $Ba_2Ti_9O_{20}$ powder calcined at 1250°C for 3 h

3.2.4 $Ba_4(Nd_{0.93}Bi_{0.07})_{28/3}Ti_{18}O_{54}$ Powder

Figure 3.6 indicates the XRD pattern of $BaCO_3$ + Nd_2O_5 + Bi_2O_3 + TiO_2 powder mixture calcined at 1100°C for 3 h [75]. A pure tungsten bronze type solid solution $Ba_4(Nd_{0.93}Bi_{0.07})_{28/3}Ti_{18}O_{54}$ phase formed according to Chen at al. [75] study.

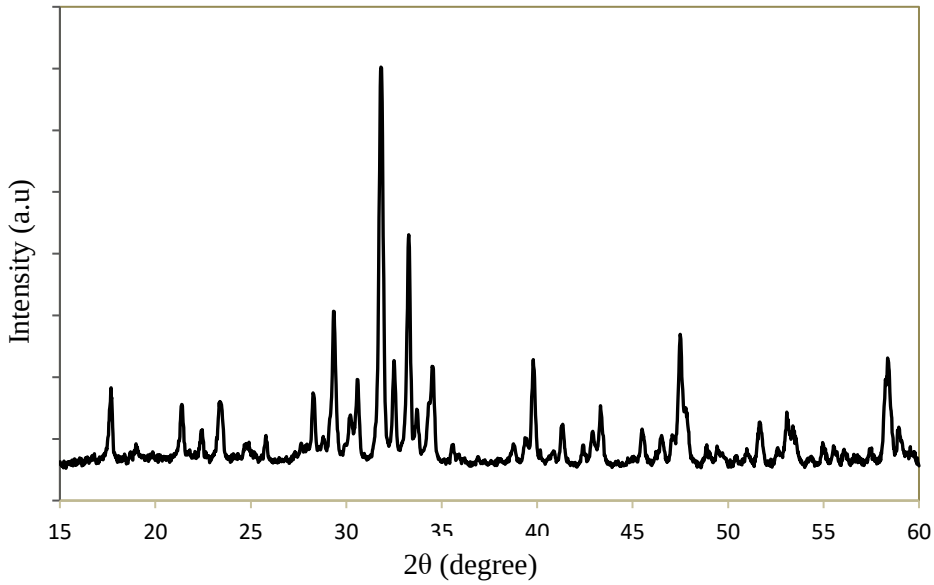

Figure 3.6 XRD pattern of $Ba_4(Nd_{0.93}Bi_{0.07})_{28/3}Ti_{18}O_{54}$ powder calcined at 1100°C for 3 h

3.3. Densification and Phase Analysis

3.3.1 CeO_2-Glass Ceramics

For CeO_2 ceramic powder, 5 wt.% glass (CaO-Al_2O_3-SiO_2 based) was used to lower very high sintering temperature of CeO_2 (e.g., 1675°C) [102] by means of liquid phase sintering and to adjust the dielectric constant less than 25. The dielectric modeling will be given in Section 3.5. The glass composition was selected based on previous studies [96, 100]. The sintering temperature range for the CeO_2-Glass (5 wt.%) composition was determined between 950°C and 1350°C to cover the glass sphere temperature of 958°C and glass melting temperature of 1180°C.

The bulk density and apparent porosity of the CeO_2-Glass ceramics sintered between 950°C and 1350°C are shown in Figure 3.7. Equations 2.4, 2.5 and 2.6 were used for the theoretical density (ρ) calculation in series, parallel and logarithmic models, respectively. The modeled bulk densities were 6.9 g/cm^3 for the series model, 5.860 g/cm^3 for the parallel model and 6.499 g/cm^3 for the logarithmic model (see Appendix A.1). It was seen that the logarithmic model gave the closest values to the measured bulk densities. Averaged relative density (apparent porosity) values were

calculated as 72.35% (27.42%) at 950°C, 98.64% (0.13%) at 1050°C, 100% (0.00%) at 1100°C, 98.50% (0.06%) at 1150°C, 96.76% (0.27%) at 1200°C, 93.73% (0.57%) at 1250°C, 91.14% (3.02%) at 1300°C and 90.20% (1.09%) at 1350°C. It was aimed to induce a liquid phase between the CeO_2 grains in such way to enhance diffusion of solid or mass transport through the liquid depending on the solid solubility in the liquid. The ability of a solid to dissolve in a liquid is dependent on wetting of the solid by the liquid, which induces capillary forces. It is very well known that rearrangement of the solid grains immediately after a liquid formation provides faster densification through more efficient packing of the grains [103, 104]. Therefore, very high sintering temperature of CeO_2 (e.g., a relative density of 94% after sintering at 1675°C for 2 h [102]) was successfully reduced to 1050°C-1150°C range (e.g., relative density ≥98.5% and apparent porosity ≤0.13%) by means of liquid phase sintering caused by the addition of 5 wt.% glass. It is also evident that maximum densification obtained at 1100°C (or, 1050°C-1150°C range) is lower than the glass melting temperature of 1180°C, which possibly indicates that CeO_2 changed the thermal behavior of the glass phase and solid solubility in liquid (or, in glass) started at lower temperatures. Figure 3.7 also shows that de-densification started after 1150°C with increasing apparent porosity. The green and sintered samples are shown in Figure 3.8. Some slight shape distortion on the surface of the sintered samples was observed after 1200°C. The averaged thickness (diameter) shrinkage values were 16.26% (15.8%) at 950°C, 24.76% (24.88%) at 1050°C, 24.7% (24.7%) at 1100°C, 25% (24.75%) at 1150°C, 24.55% (24.73%) at 1200°C, 23.26% (23.96%) at 1250°C, 24.09% (23.63%) at 1300°C and 23.69% (23.81%) at 1350°C. The maximum shrinkage was reached at maximum densification temperature range. A high bulk density required for the optimum dielectric effect for the microwave dielectric ceramics was successfully satisfied [68].

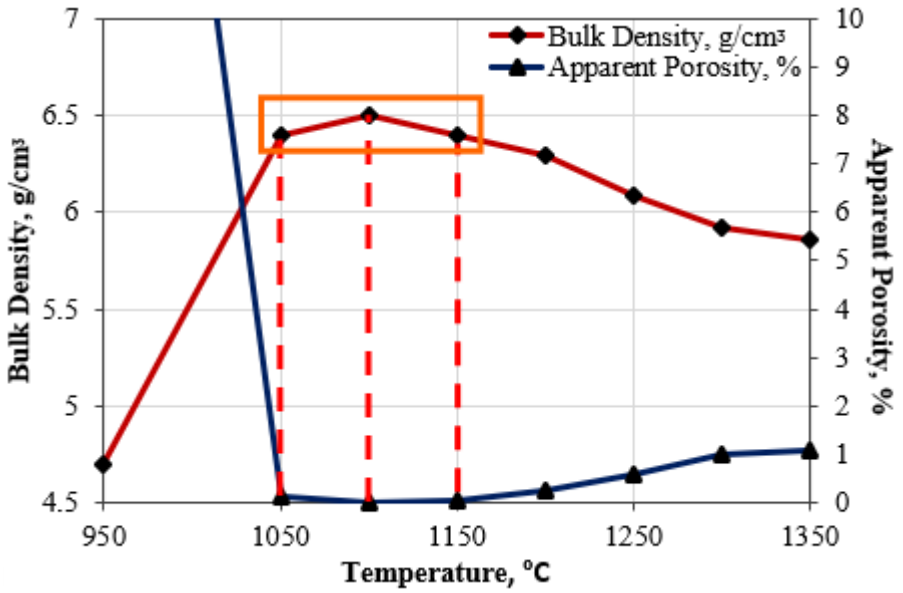

Figure 3.7 Bulk densities and apparent porosities of the sintered CeO_2-Glass samples

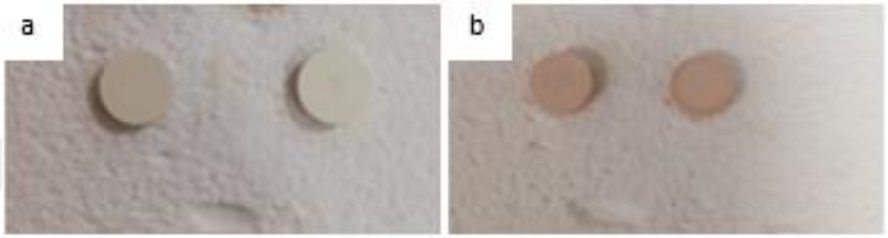

Figure 3.8 The sintering process of CeO_2-Glass (a) green samples before sintering, (b) samples after sintering

Figure 3.9 and Figure 3.10 present XRD patterns and lattice parameters of the ceramics sintered from 950°C to 1350°C for 1 h, respectively. XRD patterns were fully compatible with cubic CeO_2 phase (PDF Card No: 01-081-0792) without any other phases formed, except for peak splitting after $2\theta=75°$ due to $K\alpha 2$. The CeO_2 powder was also given as a reference in Figure 3.9. Note that the lattice parameters calculated from CeO_2 powder and pdf card were 5.4197 Å and 5.4120 Å, respectively. The patterns indicate that there is a shift of all peaks with respect to the CeO_2 reference peak, and a systematic shift among the sintered ceramics based on the sintering temperature. Figure 3.10 shows the lattice parameter variation calculated based on the cubic unit cell as a function of sintering temperature. The lattice parameter first increased at 1050°C and then sharply decreased up to 1150-

1200°C, and finally slightly increased and stabilized. Figures 3.9 and 3.10 clearly reveal that CeO_2-glass interaction (or, solubility in the glass) started at much lower temperatures because the lattice parameter increased from 5.4197 (powder) to 5.4758 at 950 °C and to 5.5301 at 1050°C, which can be attributed to the increased unit cell dimensions due to incorporation of cations from glass composition (see Table 3.2) into the CeO_2 unit cell. However, decrement of the lattice parameter to 5.4525 at 1200°C can be due to the removal of incorporated cations by means of evaporation of particularly bigger cations such as K^+ and Na^+. The weight losses increased with the sintering temperature and were recorded as 2.02% at 950°C, 2.15% at 1050°C, 2.23% at 1100°C, 2.31% at 1150°C, 4.06% at 1200°C, 4.29% at 1250°C, 4.34% at 1300°C and 4.44% at 1350°C. In literature, TG analysis of Al_2O_3/20 wt.% glass composite (note that the same glass composition was used) showed that the weight loss was 0.93% at 1150°C, 1.27% at 1200°C, 2.53% at 1300°C, and 3.22% at 1350°C, which was attributed to Na_2O and K_2O evaporation [96]. Higher weight losses observed in our study may be due to the lowered viscosity of the liquid phase caused by CeO_2-glass interaction started at lower temperatures. Note that some slight shape distortion on the surface of the sintered samples started after 1200°C, which may cause slight increase of the lattice parameter. SEM-EDS analysis of the glass phase and CeO_2 grains will be given in Section 3.4.1, and phase analysis will be discussed further.

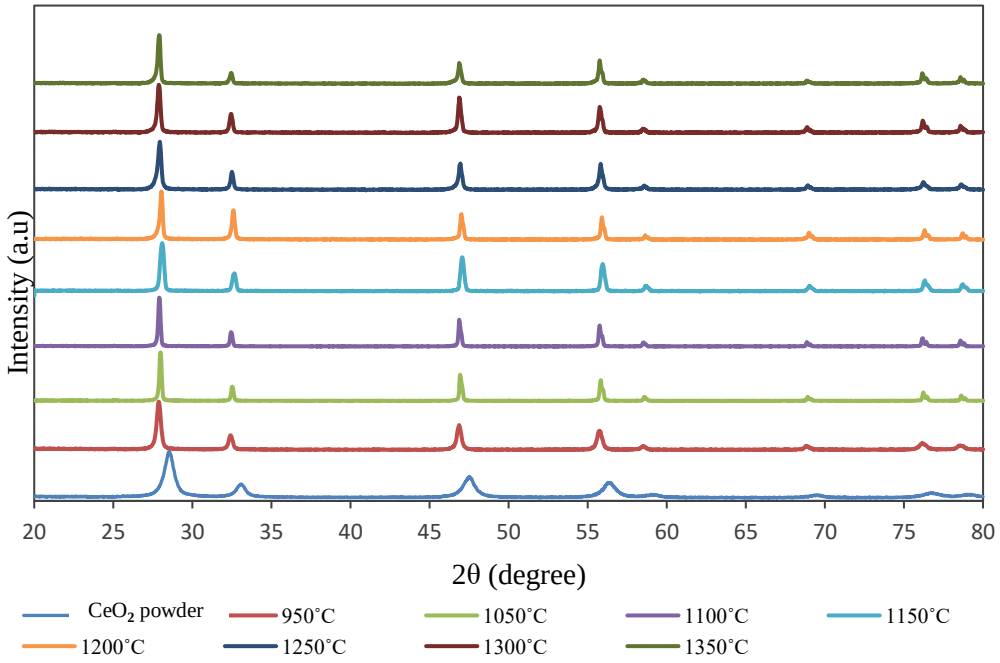

Figure 3.9 XRD patterns of CeO_2-Glass ceramics sintered from 950 to 1350°C

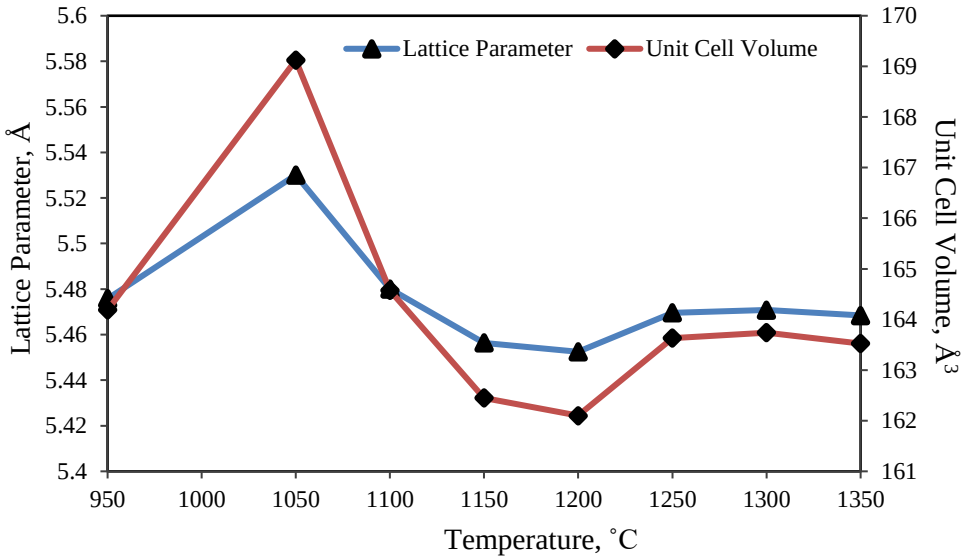

Figure 3.10 Lattice parameters and unit cell volume of sintered CeO_2-Glass ceramics versus temperature

3.3.2 $SrNb_2O_6$ Ceramics

The bulk density and apparent porosity of $SrNb_2O_6$ ceramics sintered between 1200°C and 1325°C as a function of temperature are given in Figure 3.11. Theoretical density of $SrNb_2O_6$ is 5.16 g/cm^3 (PDF Card No: 00-028-1243). Averaged relative density (apparent porosity) values were calculated as 97.64% (1.76%) at 1200°C, 98.14% (0.94%) at 1275°C, and 93.58% (3.27%) at 1325°C. Densities obtained at the maximum temperature range of 1200°C-1275°C are much higher than the one reported in literature (e.g., 94.6% at 1300°C [86]). De-densification happened in samples sintered at 1325°C with higher apparent porosity. Also, its mechanical strength was very low and it was easily broken by hand. Figure 3.12 shows the green and sintered samples. Figure 3.13 gives the XRD pattern of the $SrNb_2O_6$ ceramic sintered at 1275°C for 1 h. A pure orthorhombic $SrNb_2O_6$ phase (PDF Card No: 00-028-1243) was formed after sintering. The averaged thickness (diameter) shrinkage values were 20.25% (18.81%) at 1200°C, 20.41% (18.9%) at 1275°C, and 18.7% (17.96%) at 1325°C. With increasing temperature and densification, the shrinkage values relatively increased and attained maximum value at 1275°C. A high bulk density required for the optimum dielectric effect for the microwave dielectric ceramics was successfully satisfied [68].

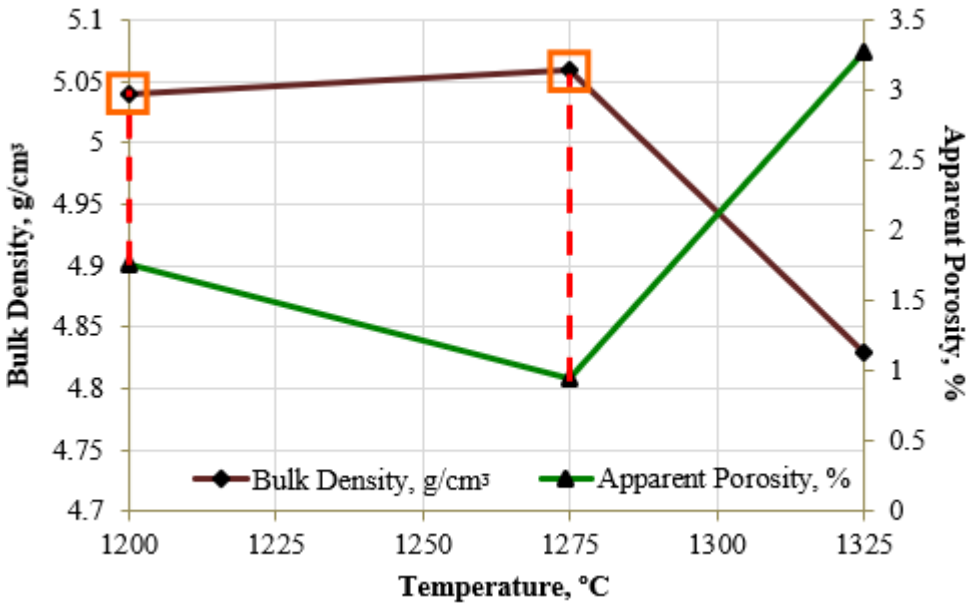

Figure 3.11 Bulk densities and apparent porosities of the sintered $SrNb_2O_6$ samples

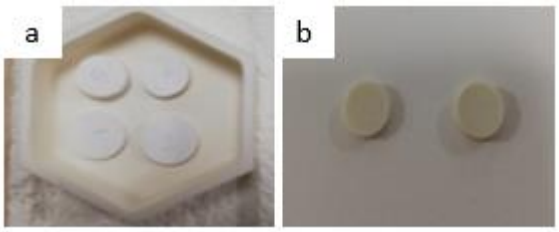

Figure 3.12 The sintering process of $SrNb_2O_6$ (a) green samples before sintering, (b) samples after sintering

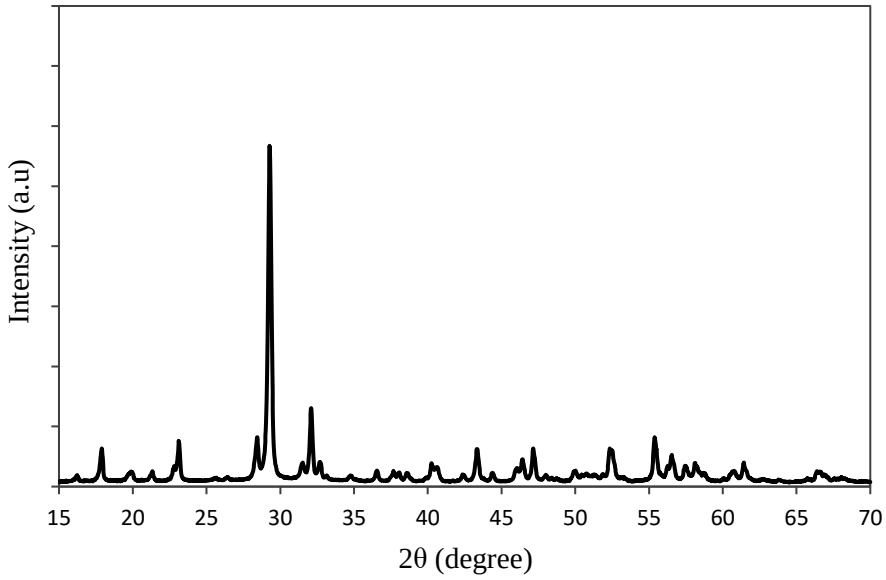

Figure 3.13 XRD pattern of $SrNb_2O_6$ ceramic sintered at 1275°C

3.3.3 $Ba_2Ti_9O_{20}$ Ceramics

The calculated bulk density and apparent porosity of the $Ba_2Ti_9O_{20}$ ceramics sintered between 1250°C and 1350°C are shown in Figure 3.14. Theoretical density of $Ba_2Ti_9O_{20}$ is 4.615 g/cm^3 (PDF Card No: 01-076-1424). The maximum densification temperature range was determined as 1250°C-1300°C with a relative density ≥97.5% and apparent porosity ≤0.05%. However, Huang [80] reported that the $Ba_2Ti_9O_{20}$ samples sintered at 1380°C had a bulk density of 4.42 g/cm^3 and a relative density of 95.8%. In fact, the bulk densities of all samples were recorded between 4.45 and 4.52 g/cm^3, which ensured relative densities >96.6% and apparent porosities <0.09%. Figure 3.15 shows the green and sintered samples. Figure 3.16 gives the XRD pattern

of the $Ba_2Ti_9O_{20}$ ceramic sintered at 1300°C for 3 h. A pure triclinic $Ba_2Ti_9O_{20}$ phase (PDF Card No: 01-076-1424) was formed after sintering. The averaged thickness (diameter) shrinkage values of $Ba_2Ti_9O_{20}$ ceramics were 18.82% (18.75%) at 1250°C, 19.72% (19.05%) at 1300°C and 20.6% (19%) at 1350°C. A high bulk density required for the optimum dielectric effect for the microwave dielectric ceramics was successfully satisfied [68].

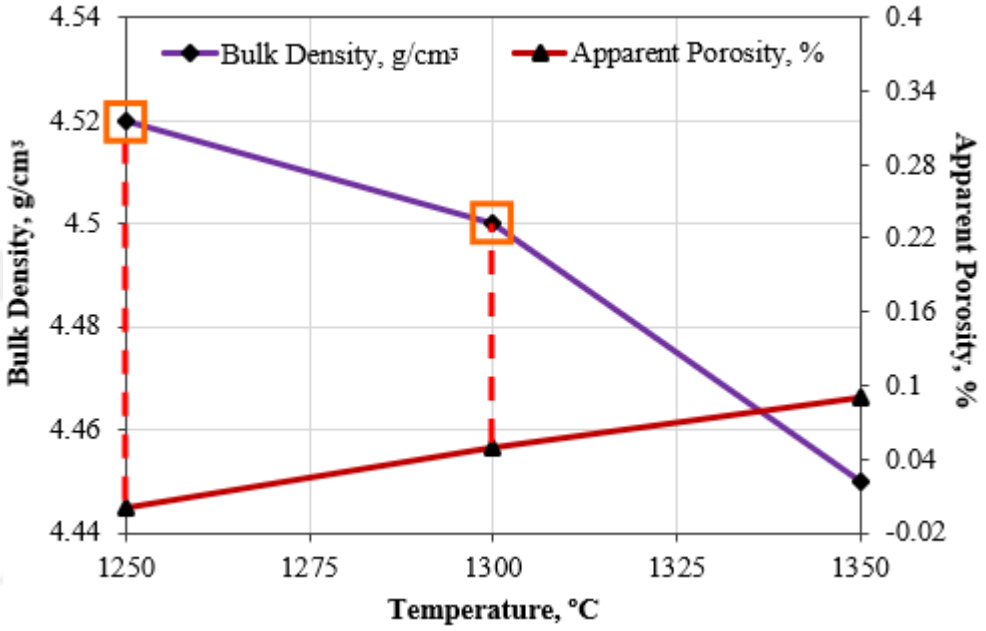

Figure 3.14 Bulk densities and apparent porosities of the sintered $Ba_2Ti_9O_{20}$ samples

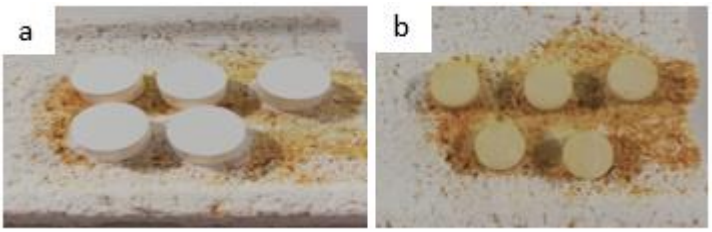

Figure 3.15 The sintering process of $Ba_2Ti_9O_{20}$ (a) green samples before sintering, (b) samples after sintering

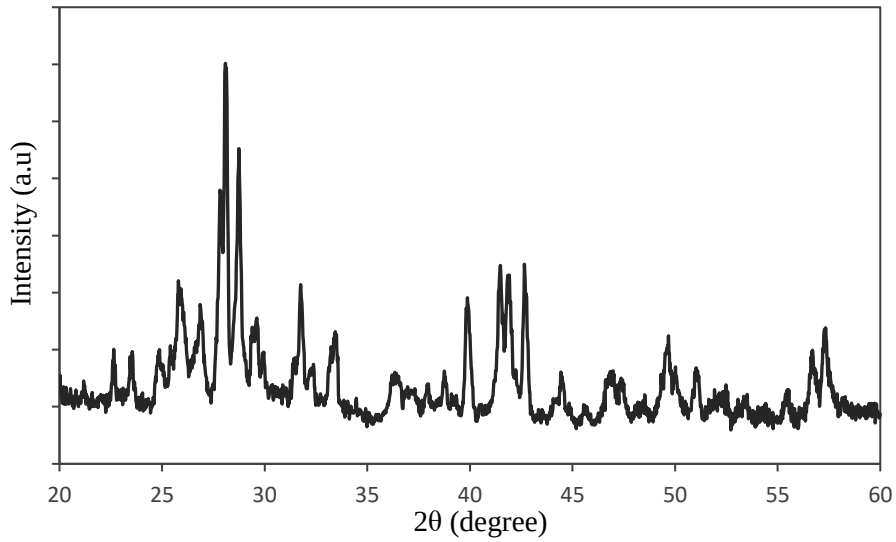

Figure 3.16 XRD pattern of $Ba_2Ti_9O_{20}$ powder sintered at 1300°C

3.3.4 $0.68CaTiO_3$-$0.32Ca(Zn_{1/3}Nb_{2/3})O_3$ Ceramics

The bulk densities and apparent porosity of $0.68CaTiO_3$-$0.32Ca(Zn_{1/3}Nb_{2/3})O_3$ ceramics sintered between 1350°C and 1400°C as a function of temperature are given in Figure 3.17. The densities were compared with a theoretical density of 4.28 g/cm^3 [77]. The densities were found to be 4.73 g/cm^3 for $Ca(Zn_{1/3}Nb_{2/3})O_3$ [77] and 4.036 g/cm^3 for $CaTiO_3$ (PDF Card No: 01-089-6949). The apparent porosity values of all samples were obtained less than 0.05%. Sintered samples had similar densification levels with relative densities >97%. Therefore, the maximum temperature range was determined as 1350°C-1400°C-1450°C for 4 h due to the nearly zero apparent porosity values. Figure 3.18 shows the green and sintered samples. Figure 3.19 gives the XRD pattern of $0.68CaTiO_3$-$0.32Ca(Zn_{1/3}Nb_{2/3})O_3$ ceramic sintered at 1400°C for 4 h [77]. A pure orthorhombic perovskite $0.68CaTiO_3$-$0.32Ca(Zn_{1/3}Nb_{2/3})O_3$ phase according to Liu at al. [77] was formed after sintering. The averaged thickness (diameter) shrinkage values of $0.68CaTiO_3$-$0.32Ca(Zn_{1/3}Nb_{2/3})O_3$ ceramics had 17.07% (17.36%) at 1350°C, 18% (17.36%) at 1400°C and 17.49% (17.36%) at 1450°C. Close shrinkage values were found at all temperatures. A high bulk density required for the optimum dielectric effect for the microwave dielectric ceramics was successfully satisfied [68].

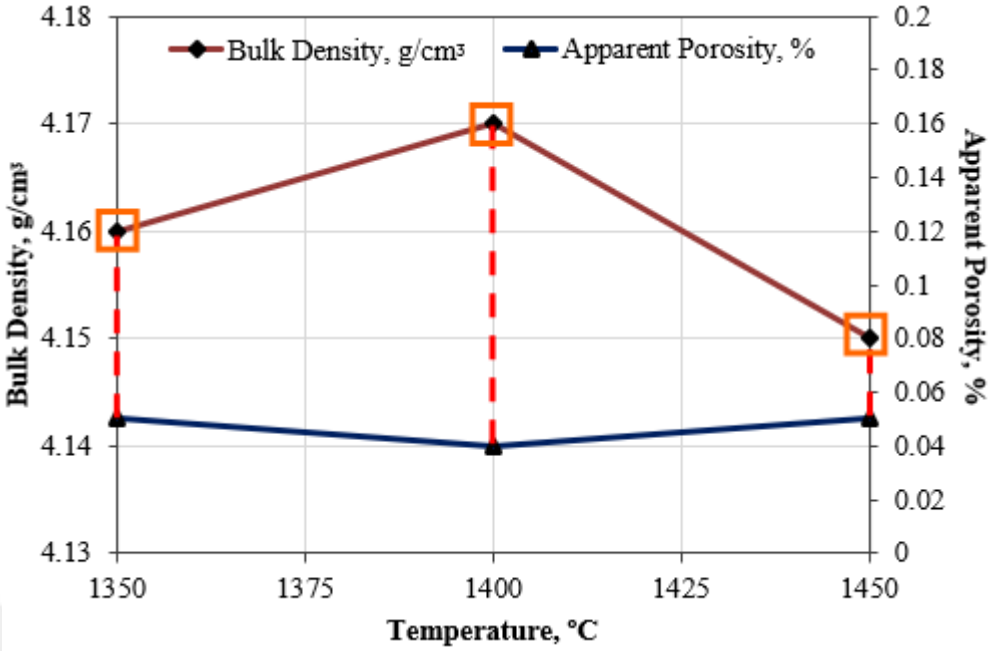

Figure 3.17 Bulk densities and apparent porosities of the sintered $0.68CaTiO_3$-$0.32Ca(Zn_{1/3}Nb_{2/3})O_3$ samples

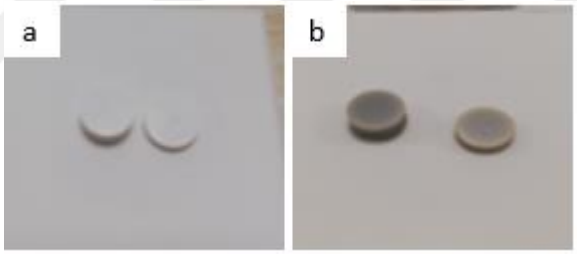

Figure 3.18 The sintering process of $0.68CaTiO_3$-$0.32Ca(Zn_{1/3}Nb_{2/3})O_3$ (a) green samples before sintering, (b) samples after sintering

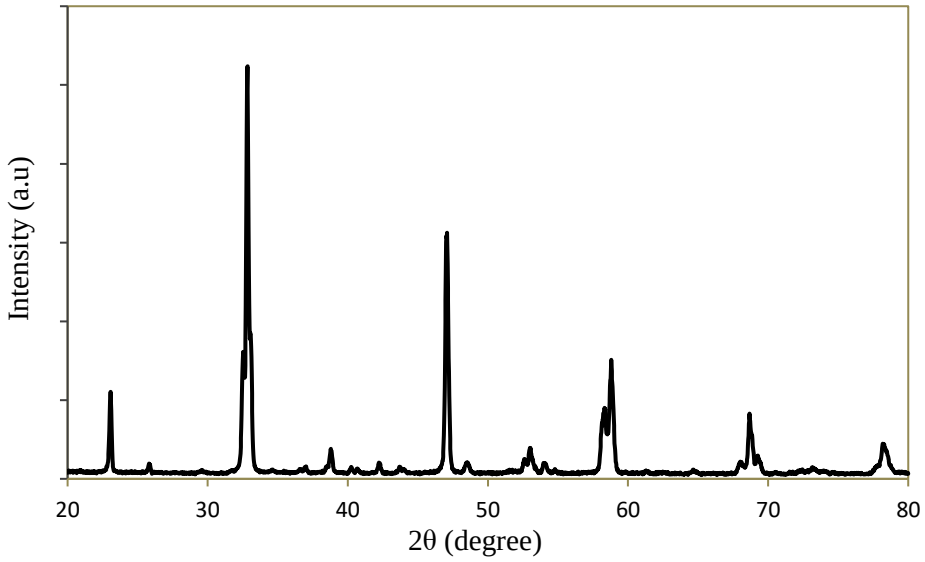

Figure 3.19 XRD pattern of $0.68CaTiO_3$-$0.32Ca(Zn_{1/3}Nb_{2/3})O_3$ ceramic sintered at 1400°C

3.3.5 $Ba_4(Nd_{0.93}Bi_{0.07})_{28/3}Ti_{18}O_{54}$ Ceramics

The calculated bulk densities and apparent porosities of $Ba_{6-3x}(Nd_{1-y}Bi_y)_{8+2x}Ti_{18}O_{54}$ x=2/3 y=0.07 ceramics sintered between 1280°C and 1320°C as a function of temperature are shown in Figure 3.20. The bulk densities of all samples were close to the theoretical density of 5.80-5.90 g/cm^3 [75]. Averaged bulk density values were recorded as 5.75 g/cm^3 at 1280°C, 5.77 g/cm^3 at 1320°C and 5.75 g/cm^3 at 1350°C, which ensured relative densities >98.2%. Hence, the maximum temperature range was determined as 1280°C-1320°C-1350°C for 3 h. The apparent porosity values are less than 0.24%. Figure 3.21 shows the green and sintered samples. Figure 3.22 indicates the XRD pattern of $Ba_4(Nd_{0.93}Bi_{0.07})_{28/3}Ti_{18}O_{54}$ ceramic sintered at 1320°C for 3 h. A pure tungsten bronze type solid solution $Ba_4(Nd_{0.93}Bi_{0.07})_{28/3}Ti_{18}O_{54}$ phase according to Chen at al. [75] was formed after sintering. The averaged thickness (diameter) shrinkage values of the ceramics were 16.23% (15.84%) at 1280°C, 18.7% (16.77%) at 1320°C and 17.35% (16.57%) at 1350°C. With increasing temperature and densification, the shrinkage values relatively increased and attained maximum value at 1320°C. A high bulk density required for the optimum dielectric effect for the microwave dielectric ceramics was successfully satisfied [68].

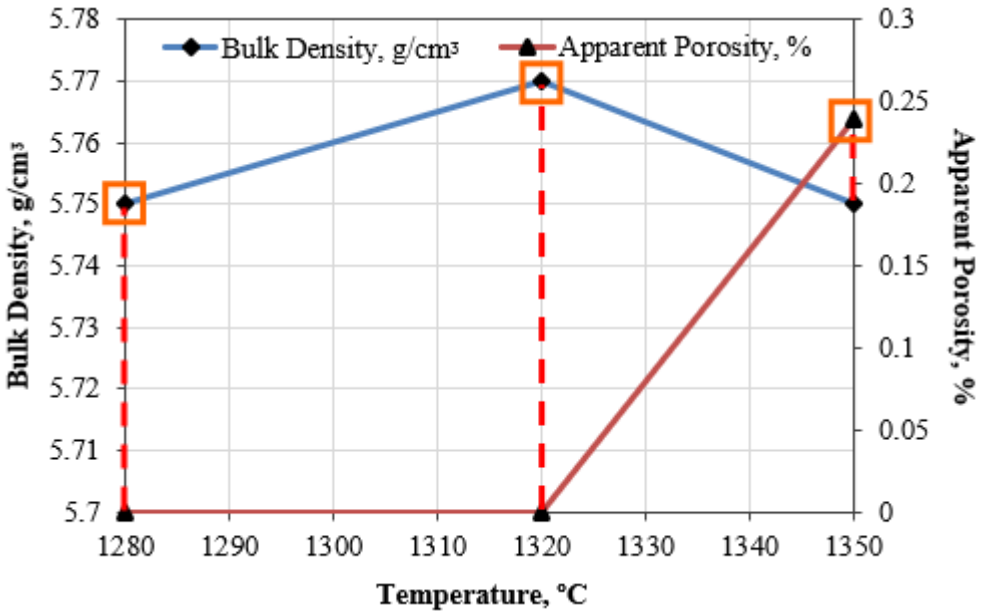

Figure 3.20 Bulk densities and apparent porosities of the sintered $Ba_4(Nd_{0.93}Bi_{0.07})_{28/3}Ti_{18}O_{54}$ samples

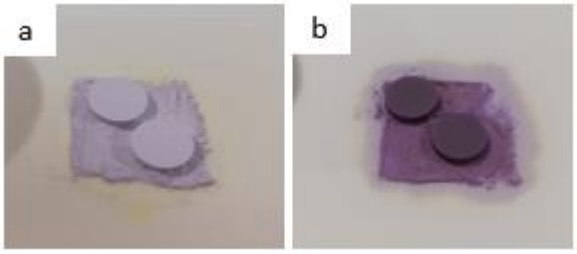

Figure 3.21 The sintering process of $Ba_4(Nd_{0.93}Bi_{0.07})_{28/3}Ti_{18}O_{54}$ (a) green samples before sintering, (b) samples after sintering

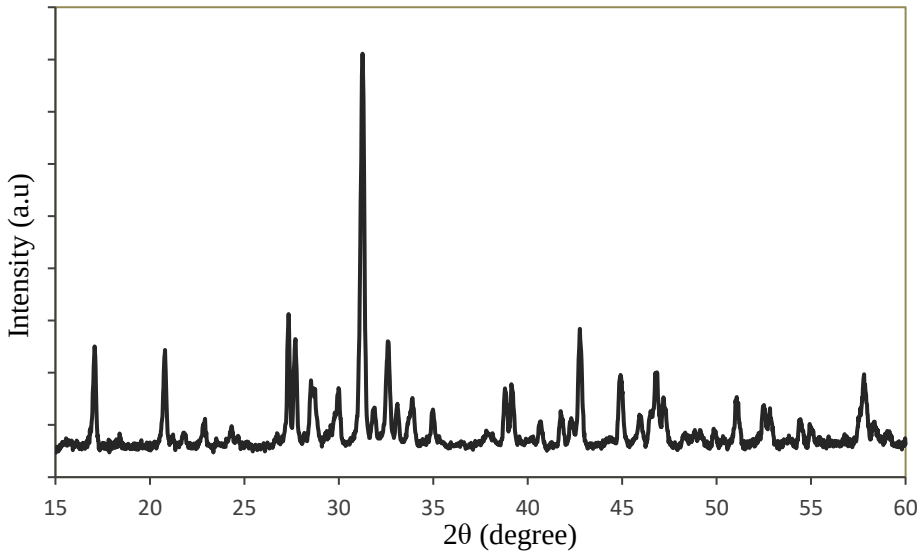

Figure 3.22 XRD pattern of $Ba_4(Nd_{0.93}Bi_{0.07})_{28/3}Ti_{18}O_{54}$ ceramic sintered at 1320°C.

3.4 Microstructure Analysis

3.4.1 CeO_2-Glass Ceramics

Figure 3.23 shows backscattered SEM images of the fractured surfaces of CeO_2-Glass ceramics sintered between 950°C and 1350°C. The fracture type was intra-granular for all samples. As specified by EDS, lighter colored regions are CeO_2 grains and continuous darker colored regions are the glass phase. The non-melting of the glass phase and the presence of visible irregular large pores indicate that densification was not completed at 950°C. However, rapid densification was achieved right after sintering at 1050°C, which is lower than the glass melting temperature of 1180°C. In other words, CeO_2 changed the thermal behavior of the glass phase and solid solubility in liquid (or, in glass) started at lower temperatures. CeO_2 grains become rounded and embedded within the glass matrix, revealing a liquid phase sintering. Transport of dissolved solid through a liquid leaded to further densification. It is also evident that CeO_2 grains were uniformly packed, glass phase was homogeneously distributed, and microstructures exhibited normal grain growth behavior with increasing sintering temperature. In other words, homogeneous packing of the particulate solid, homogeneous distribution of the liquid phase between the grains, and fairly fine particle size resulted in maximum densification at

the temperature range between 1050°C and 1150°C. Figure 3.7 shows that de-densification started after 1150°C together with increased apparent porosity due to evaporation of Na_2O and K_2O from the glass phase, resulting in appearance of some visible pores within the glass matrix as-marked on the microstructures.

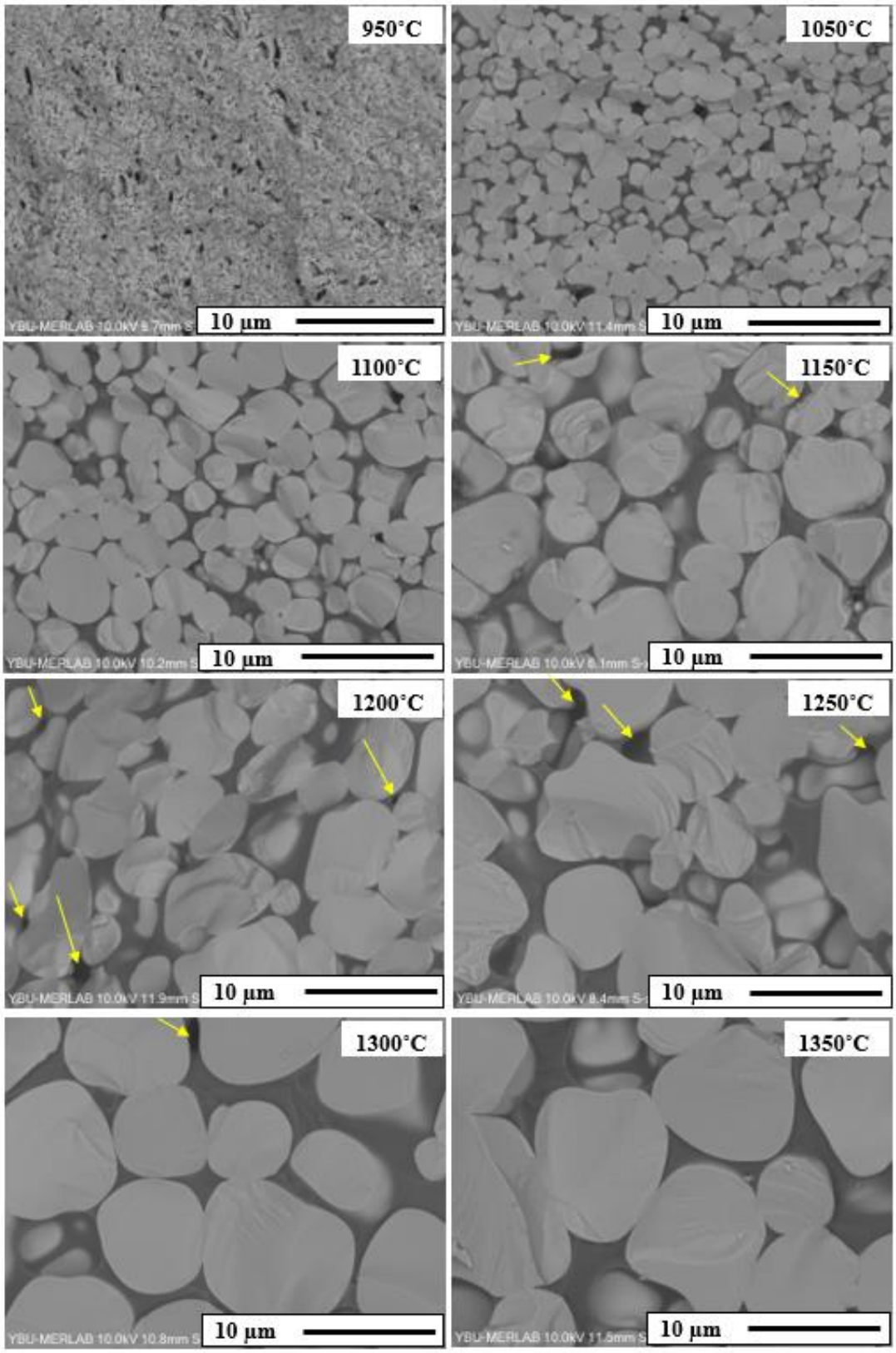

Figure 3.23 Backscattered SEM images of CeO_2-Glass ceramics

Figure 3.24 shows SEM-EDS analysis of the CeO_2-Glass ceramic sintered at 1150°C for 1 h. The marked grains were subjected to a qualitative elemental analysis within the EDS resolution limit. Table 3.3 lists the anlaysis of the glass composition as determined by the EDS analysis. Table 3.4 tabulates the elemental analysis from the glass phase excluding Ce and O. The analysis from the CeO_2 grains (marked as C, D and E) proves little incorporation of mainly Si, Al and Ca cations together with K from the glass phase, revealing a low liquid solubility in the solid. On the other hand, the analysis from the glass phase (marked as A, B, F and G) proves a significant amount of Ce incorporation, revealing a high solid solubility in liquid (or, glass). In fact, low liquid solubility in solid and vice versa is an ideal situation for the liquid phase sintering, facilitating rapid solution-reprecipitation mechanism to reach maximum densification at lower temperatures. Some variations in the elemental ratios from the glass phase can be attributed to a high acceleration voltage used to receive signals (i.e., a 10 kV can collect signals from surface as well as sub-surface) and proximity of the EDS point to the neighboring grains (i.e., smaller grains have higher solubility and can easily saturate its surrounding glass composition as compared to bigger grains). Therefore, Table 3.4 indicates in general that glass phase is deficient in K^+ and Na^+ due to evaporation of Na_2O and K_2O during sintering (total weight loss of 2.31%). The EDS results are also consisted with the phase analysis such that CeO_2 grains has cation incorporation from the glass phase, changing the composition and lattice parameters (see Figures 3.9 and 3.10). In other words, the increase in lattice parameters from 950ºC to 1050ºC is due to the incorporation of cations from the glass into the CeO_2 and the decrease after 1050ºC is due to the volatility of Na_2O and K_2O.

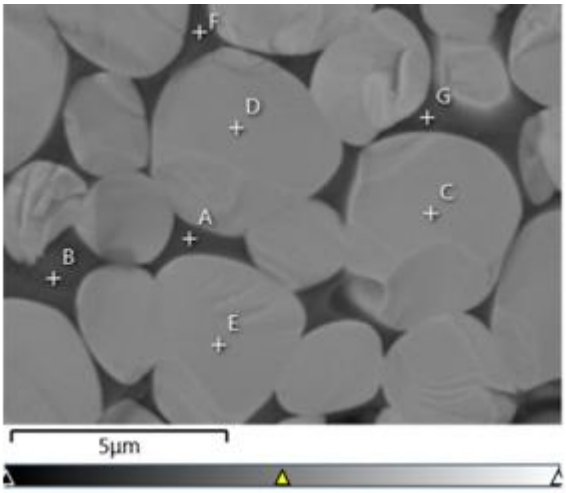

NO	Ce (wt.%)	Si (wt.%)	Al (wt.%)	Ca (wt.%)	Na (wt.%)	K (wt.%)	O (wt.%)
A	74.4	3.5	1.9	2.9	0.1	0.6	16.6
B	55.1	10.9	3.5	2.5	1	0.6	26.5
C	83	1.1	0.8	0.3	0	0	14.8
D	83.5	0.8	0.8	0.4	0	0.2	14.3
E	83.5	1.2	1	0.2	0	0.2	14
F	57.3	11	3.5	2.8	0.8	0.7	23.9
G	71.3	5.9	2.2	1.3	0.4	0.3	18.6

Figure 3.24 SEM-EDS analysis of CeO_2-Glass ceramic sintered at 1150°C for 1 h

Table 3.3 The elemental analysis of glass powder [96]

Elements	O	Si	Ca	Al	Na	K
wt.%	45.8	31.5	7.9	8.5	3.6	2.7

Table 3.4 The elemental analysis of glass phase excluding Ce and O

Elements, wt.%	Si	Al	Ca	Na	K
Glass Phase	**58.12**	**15.68**	**14.58**	**6.64**	**4.98**
A Point	38.89	21.11	32.22	1.11	6.67
B Point	58.92	18.92	13.51	5.41	3.24
F Point	58.51	18.62	14.89	4.26	3.72
G Point	58.42	21.78	12.87	3.96	2.97

3.4.2 $SrNb_2O_6$ Ceramics

Figure 3.25 shows the backscattered SEM images of the fractured surfaces of $SrNb_2O_6$ ceramic sintered at maximum densification temperature of 1275ºC at various magnifications. The fracture type was inter-granular. The grain size was uniform without any abnormal grain growth and it was roughly in the range between 2 and 4 μm.

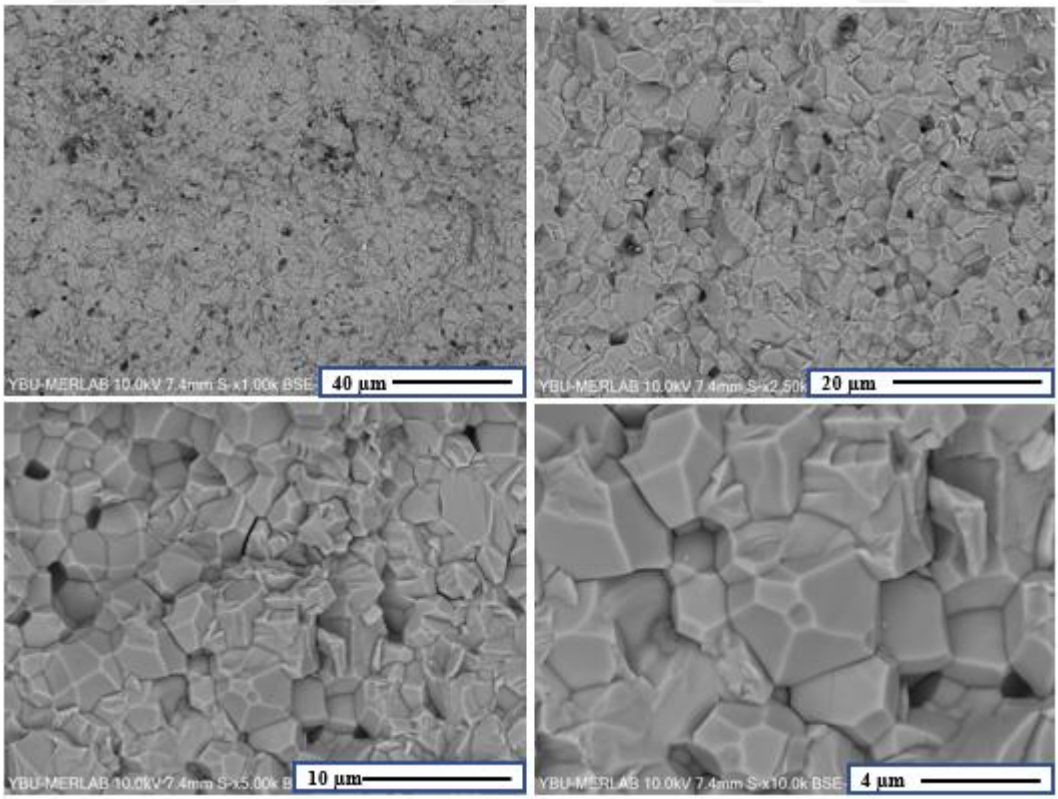

Figure 3.25 Backscattered SEM images of $SrNb_2O_6$ ceramic at 1275ºC

3.4.3 $Ba_2Ti_9O_{20}$ Ceramics

Figure 3.26 represents the backscattered SEM images of the fractured surfaces of $Ba_2Ti_9O_{20}$ ceramic sintered at maximum densification temperature of 1300ºC at various magnifications. The fracture type was intragranular.

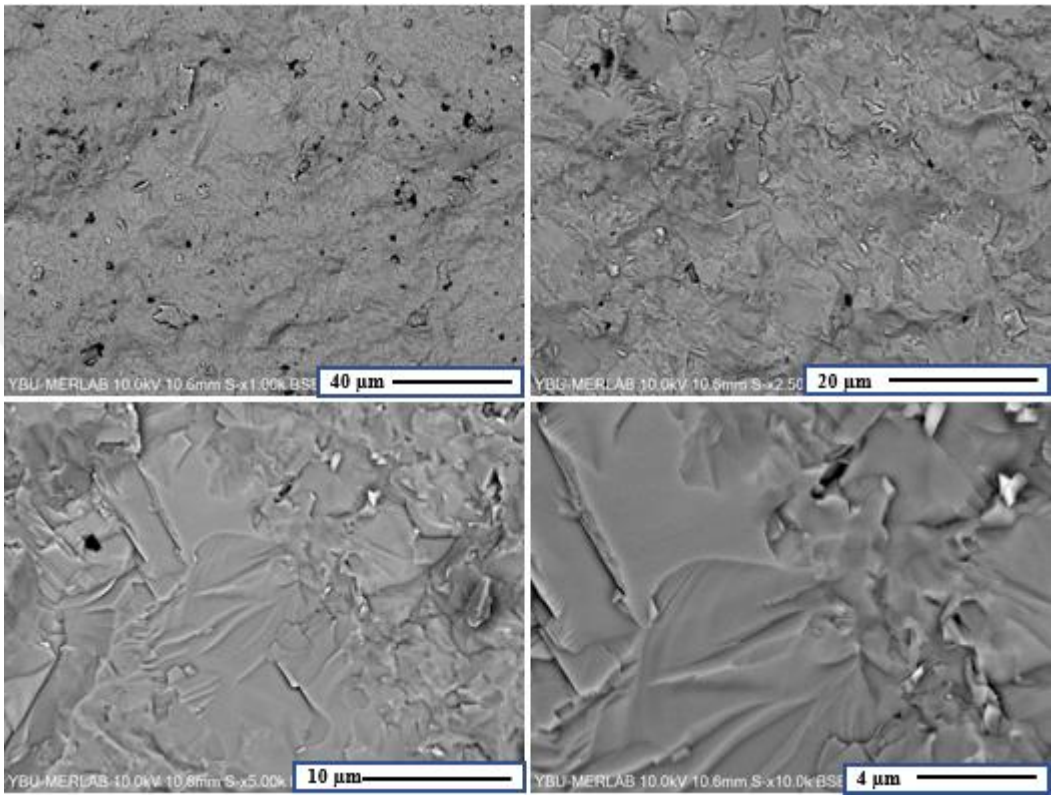

Figure 3.26 Backscattered SEM images of $Ba_2Ti_9O_{20}$ ceramic at 1300ºC

Figure 3.27 shows SEM-EDS analysis of $Ba_2Ti_9O_{20}$ ceramic sintered at 1300ºC for 3 h. Elemental analysis was performed in the regions marked on the micrograph and the results together with the stoichiometric $Ba_2Ti_9O_{20}$ is given in Table 3.5. The points A, B and C had very close Ba/Ti ratios but lower than the original $Ba_2Ti_9O_{20}$, which may be attributed to the qualitative EDS analysis method.

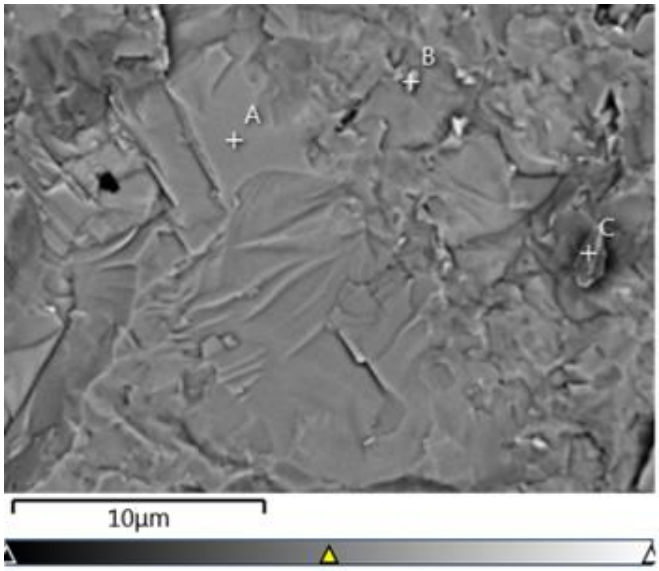

Figure 3.27 SEM-EDS analysis of $Ba_2Ti_9O_{20}$ ceramic sintered at 1300ºC for 3 h

Table 3.5 The elemental analysis of Ba, Ti, O and Ba/Ti ratios.

Elements, wt.%	Ba	Ti	O	Ba/Ti
$Ba_2Ti_9O_{20}$	**26.78**	**42.01**	**31.21**	**0.63**
A Point	22.6	42.5	34.9	**0.54**
B Point	23.2	44.9	31.9	**0.52**
C Point	24.5	47.3	28.2	**0.52**

3.4.4 $0.68CaTiO_3$-$0.32Ca(Zn_{1/3}Nb_{2/3})O_3$ Ceramics

Figure 3.28 shows the backscattered SEM images of fractured surfaces of $0.68CaTiO_3$-$0.32Ca(Zn_{1/3}Nb_{2/3})O_3$ ceramic sintered at maximum densification temperature of 1400ºC at various magnifications. According to the microstructure, both intergranular and intragranular fractures were observed. The grain size was uniform without any abnormal grain growth and it was roughly in the range between 3 and 5 µm.

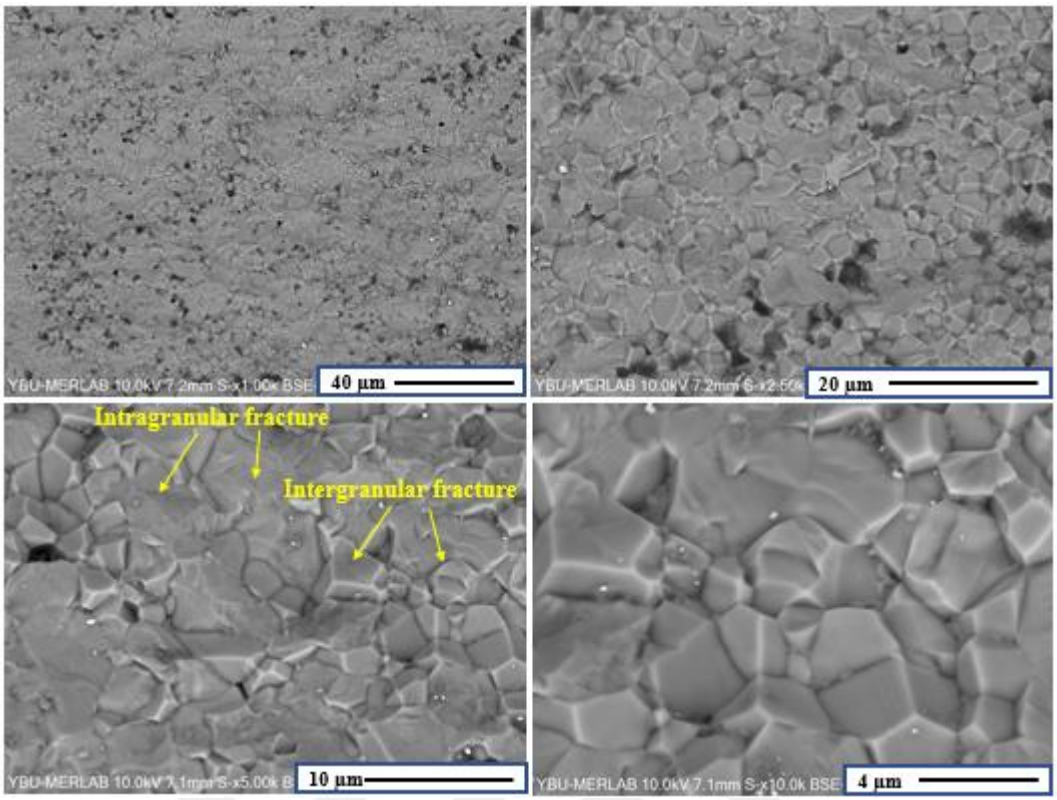

Figure 3.28 Backscattered SEM images of $0.68CaTiO_3$-$0.32Ca(Zn_{1/3}Nb_{2/3})O_3$ ceramic at 1400ºC

3.4.5 $Ba_4(Nd_{0.93}Bi_{0.07})_{28/3}Ti_{18}O_{54}$ Ceramics

Figure 3.29 shows the backscattered SEM images of the fractured surfaces of $Ba_4(Nd_{0.93}Bi_{0.07})_{28/3}Ti_{18}O_{54}$ ceramic sintered at maximum densification temperature of 1320ºC at various magnifications. Mostly intragranular fractures were observed. The grain size was uniform without any abnormal grain growth and it was roughly in the range between 2 and 5 µm.

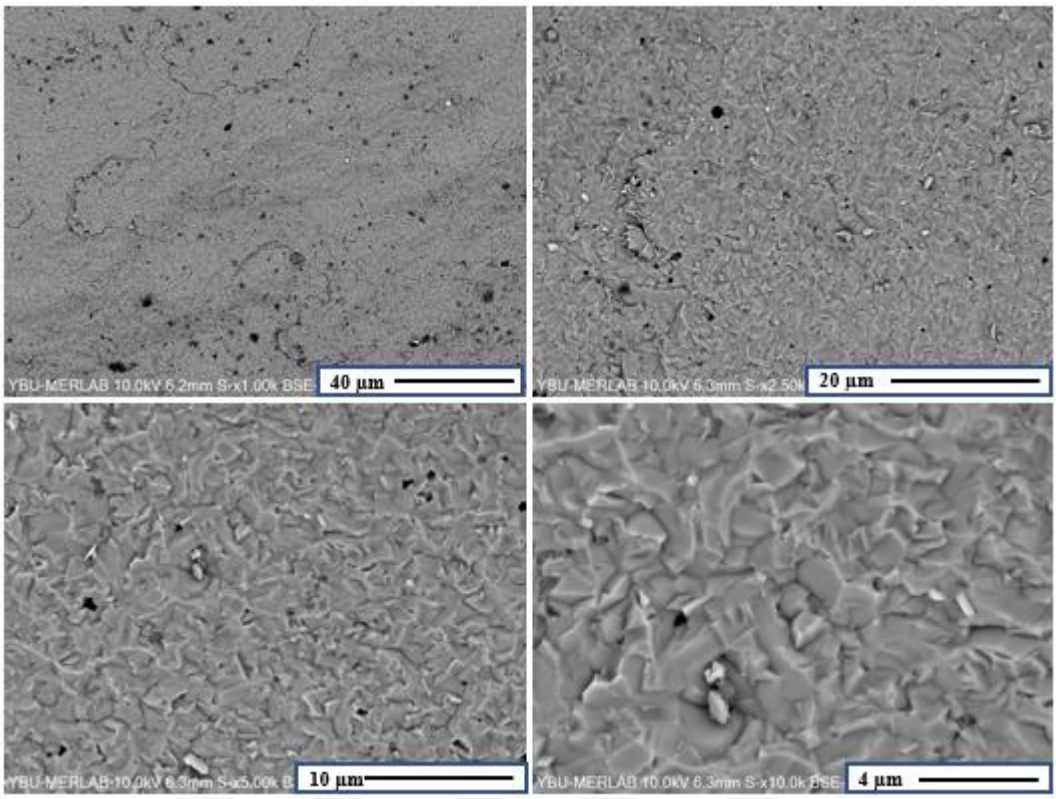

Figure 3.29 Backscattered SEM images of $Ba_4(Nd_{0.93}Bi_{0.07})_{28/3}Ti_{18}O_{54}$ ceramic at 1320ºC

3.5 Dielectric Properties

The dielectric properties were measured at 1-5 MHz for each composition at room temperature using impedance analyzers HIOKI IM3570 and AGILENT 4294A. The dielectric constant was calculated from the capacitance measurement at room temperature according to Equation 2.7. Temperature coefficient of the dielectric constant were calculated at 1-5 MHz for 20ºC and 80ºC according to Equation 1.26 using HIOKI IM3570. The Ag coated samples are shown in Figure 3.30.

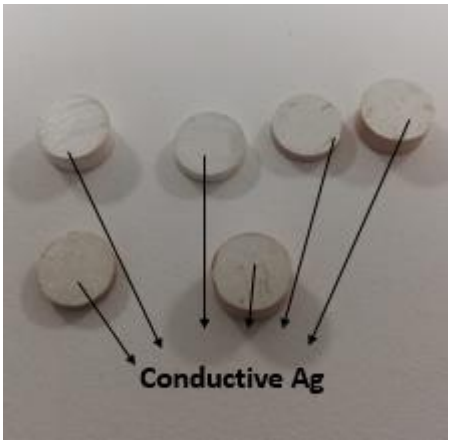

Figure 3.30 Dry-on silver coating on parallel surfaces to achieve conductivity

3.5.1 CeO_2-Glass Ceramics

Table 3.6 summarizes dielectric properties of the CeO_2-5 wt.% glass ceramics sintered between 950°C and 1350°C. Equations 2.4, 2.5 and 2.6 were used to estimate dielectric constant (ε_r) using series, parallel and logarithmic models, respectively (see Appendix B.1). Note that these mixture models are based on the assumption that a solid solution does not form. However, EDS analysis proved considerable CeO_2 dissolution into the glass matrix and little glass incorporation into the CeO_2 grains (see Figure 3.24), although cubic crystal structure was retained after sintering for all temperatures (see Figure 3.9). The modeled dielectric constants as a function of glass content are drawn in Figure 3.31. The dielectric constant of CeO_2 is 23 at 6 GHz [102] and glass is 6.37 at 5 MHz [100]. The modeled dielectric constants were 20.64 for the series model, 16.78 for the parallel model and 19.16 for the logarithmic model at 5 wt.% glass content. It is seen that the series model yields the closest value to the dielectric constants measured using Equation 2.7 because averaged dielectric constants at 5 MHz and maximum densification temperature range are 21.12 at 1050°C, 21.35 at 1100°C, and 21.36 at 1150°C. Correspondingly, the dielectric losses (tanδ) were minimum at the same temperature range because dielectric properties are optimized (i.e., highest ε_r with lowest tanδ) when the maximum densification is attained in the ceramics. In other words, dielectric properties are closely related with the densification as given in Figure 3.32 such that ε_r follows the densification path and tanδ follows the apparent porosity path. In this

regard, ceramic sintered at 1150°C have the best dielectric properties among the ceramics densified between the temperature range of 1050°C-1150°C. Lower ε_r and higher tanδ observed out of this temperature range are due to the porosity effect (or, lower densification) because it decreases ε_r and increases tanδ (i.e., ε_r=1 and tanδ=0 for air [105]). It was also observed that the ε_r slightly decreased and tanδ increased with increasing frequency from 1 MHz to 5 MHz, which is expected for dielectric materials due to dielectric relaxation. Dielectric relaxation time is the time scale for relaxation of mobile charge carriers in a material based on the dipole charges [32]. As the frequency increases, the dipoles cannot keep up with the electric field rotation speed and the dielectric constant accordingly decreases due to less polarization contribution [32, 106, 107]. However, more energy is required to follow the electric field with increasing frequency, which gives rise to increased tanδ. Both HIOKI and Agilent at 1 MHz gave very close dielectric constant values but the dielectric loss values were much lower in the latter, which was due to the different device internal impedance calibration settings. In brief, a higher relative density results in a higher ε_r and lower tanδ. Also, the change in the dielectric constant with temperature (τ_ε, ppm°C^{-1}) for the ceramic sintered at 1150°C was calculated using Equation 1.26 and measured at 5 MHz (1 MHz) as 61.8 (44.0).

Table 3.6 The dielectric properties of CeO_2-Glass samples

Sintering Temperature and Time (°C) (h)	**HIOKI ε_r, 5 MHz**	**HIOKI tanδ, 5 MHz**	**HIOKI ε_r, 1 MHz**	**HIOKI tanδ, 1 MHz**	**Agilent tanδ, 1 MHz**	**Agilent ε_r, 1 MHz**
950, 1	12.80	0.0132	12.96	0.0130	0.0047	12.83
1050, 1	21.12	0.0047	21.22	0.0021	0.0011	21.18
1100, 1	21.35	0.0044	21.43	0.0017	0.00093	21.42
1150, 1	21.36	0.0040	21.43	0.0016	0.00090	21.38
1200, 1	20.38	0.0051	20.46	0.0016	0.00071	20.53
1250, 1	19.58	0.0060	19.65	0.0017	0.00080	19.61
1300, 1	17.98	0.0081	18.09	0.0017	0.0011	18.04
1350, 1	16.75	0.0086	16.84	0.0017	0.0016	16.82

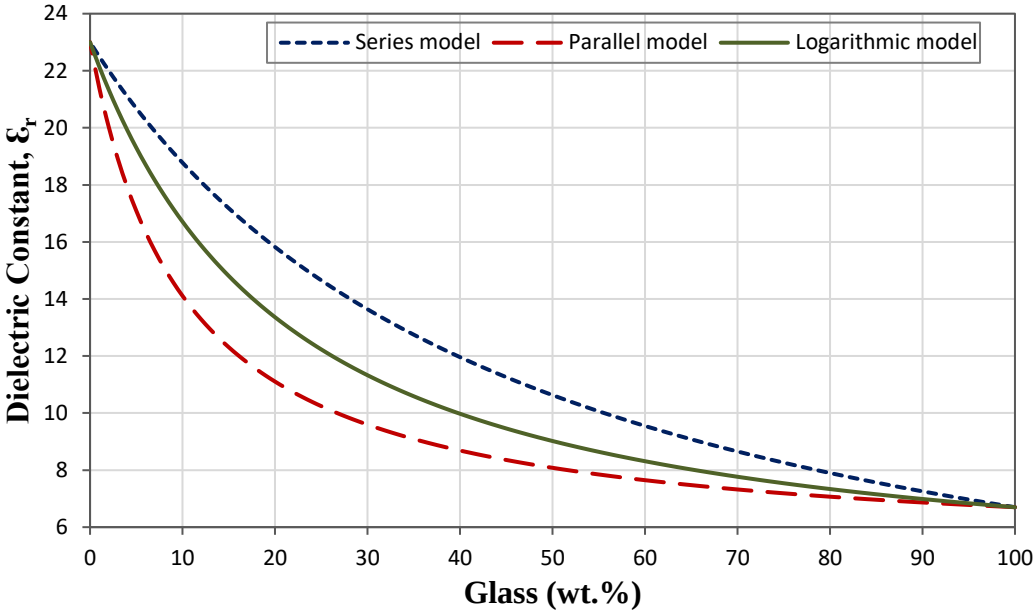

Figure 3.31 The dielectric constant of CeO_2-Glass ceramics at various glass content

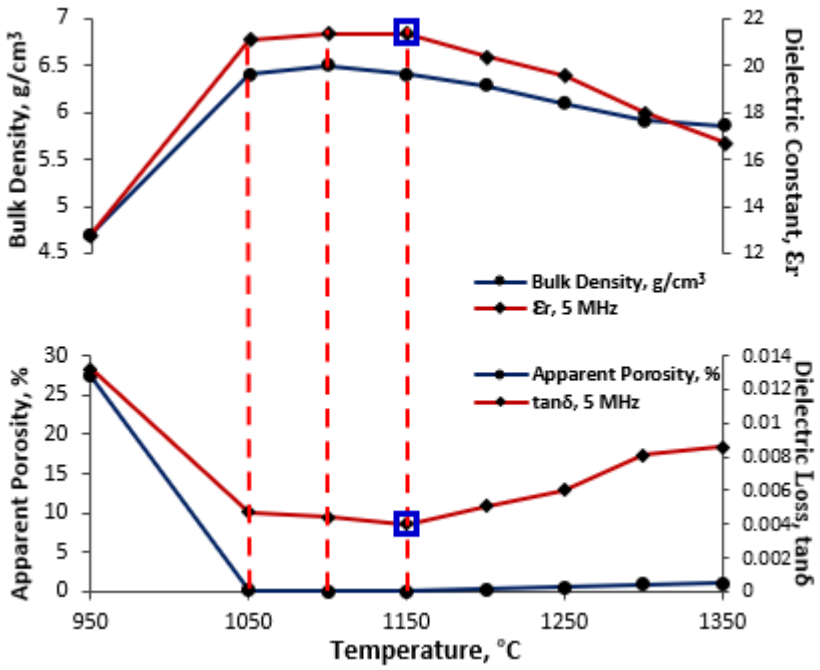

Figure 3.32 The dielectric properties versus densification of CeO_2-Glass ceramics

3.5.2 $SrNb_2O_6$ Ceramics

Table 3.7 shows the dielectric properties of $SrNb_2O_6$ ceramics sintered between 1200°C and 1325°C. Averaged ε_r (tanδ) values at 5 MHz were recorded as 28.70 (0.0056) at 1200°C, 28.87 (0.0047) at 1275°C and 27.16 (0.0051) at 1325°C (HIOKI). The dielectric properties versus densification of $SrNb_2O_6$ ceramics are given Figure 3.33. The dielectric properties are optimized (i.e., highest ε_r with lowest tanδ) when the maximum densification is attained in the ceramics. In this regard, ceramic sintered at 1275°C have the best dielectric properties among the ceramics densified between the temperature range of 1200°C-1275°C for 1 h. It is crucial to have the lowest tanδ for the microwave dielectric ceramics (e.g., Q = 1/tanδ). The dielectric properties were worsened due to the de-densification at 1325°C. Pullar at al. [86] reported that $SrNb_2O_6$ ceramic sintered at 1300°C had a ε_r = 21.7 at 6.51 GHz, which is lower than ε_r = 28.87 at 5 MHz for the ceramics sintered at 1275°C in this study. The density obtained at the maximum temperature of 1275°C (e.g. 98.14%) is much higher than reported in the literature (e.g. 94.6% at 1300°C [86]), resulting in a high ε_r. On the other hand, the ε_r decreases with increasing frequency. In this study, the dielectric properties were measured at 5 MHz and therefore affected the ε_r. Also, the change in the ε_r with temperature (τ_ε, ppm°C^{-1}) for the ceramic sintered at 1275°C was calculated using Equation 1.26 and measured at 5 MHz (1 MHz) as 280 (261).

Table 3.7 The dielectric properties of $SrNb_2O_6$ samples

Sintering Temperature and Time (°C) (h)	**HIOKI ε_r, 5 MHz**	**HIOKI tanδ, 5 MHz**	**HIOKI ε_r, 1 MHz**	**HIOKI tanδ, 1 MHz**	**Agilent tanδ, 1 MHz**	**Agilent ε_r, 1 MHz**
1200, 1	28.70	0.0056	28.82	0.0035	0.00089	25.51
1275, 1	28.87	0.0047	29.05	0.0025	0.00031	28.49
1325, 1	27.16	0.0051	27.24	0.0026	0.00066	27.01

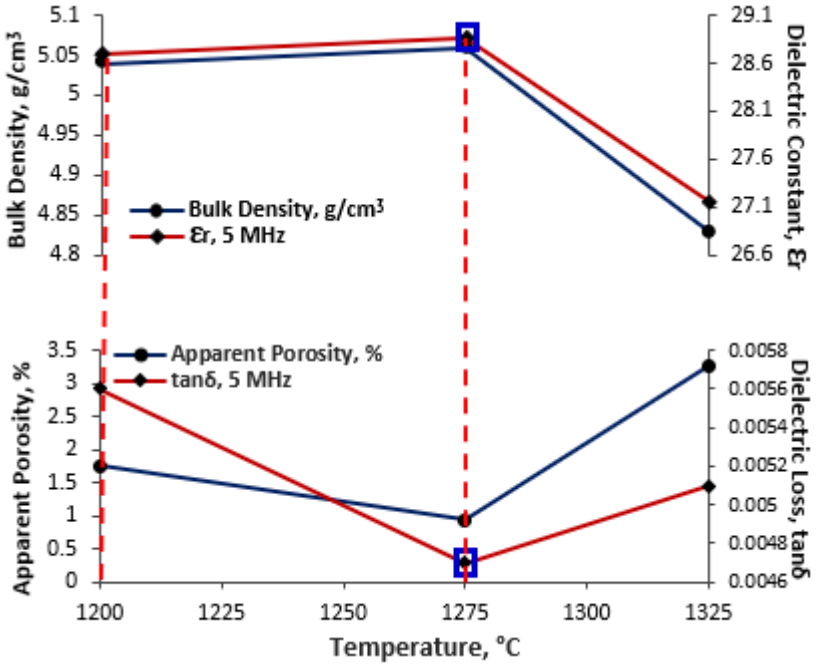

Figure 3.33 The dielectric properties versus densification of $SrNb_2O_6$ ceramics

3.5.3 $Ba_2Ti_9O_{20}$ Ceramics

Table 3.8 tabulates the dielectric properties of $Ba_2Ti_9O_{20}$ ceramics sintered between 1250°C and 1350°C. Averaged $Ɛ_r$ (tanδ) values at 5 MHz were recorded as 39.47 (0.0041) at 1250°C, 39.55 (0.0034) at 1300°C and 38.49 (0.0043) at 1350°C (HIOKI). The dielectric properties versus densification of the ceramics are given Figure 3.34. The dielectric properties are optimized (i.e., highest $Ɛ_r$ with lowest tanδ) when the maximum densification is attained in the ceramics. In this regard, ceramic sintered at 1300°C have the best dielectric properties among the ceramics densified between the temperature range of 1250°C-1300°C for 1 h. Also, the change in the $Ɛ_r$ with temperature ($\tau_ε$, ppm°C^{-1}) for the ceramic sintered at 1300°C was calculated using Equation 1.26 and measured at 5 MHz (1 MHz) as -29.8 (-23.1).

Table 3.8 The dielectric properties of $Ba_2Ti_9O_{20}$ samples

Sintering Temperature and Time (°C) (h)	**HIOKI ε_r, 5 MHz**	**HIOKI tanδ, 5 MHz**	**HIOKI ε_r, 1 MHz**	**HIOKI tanδ, 1 MHz**	**Agilent tanδ, 1 MHz**	**Agilent ε_r, 1 MHz**
1250, 3	39.47	0.0041	39.51	0.0016	0.000047	38.55
1300, 3	39.55	0.0034	39.60	0.0013	0.00034	39.66
1350, 3	38.49	0.0043	38.55	0.0018	0.00080	38.34

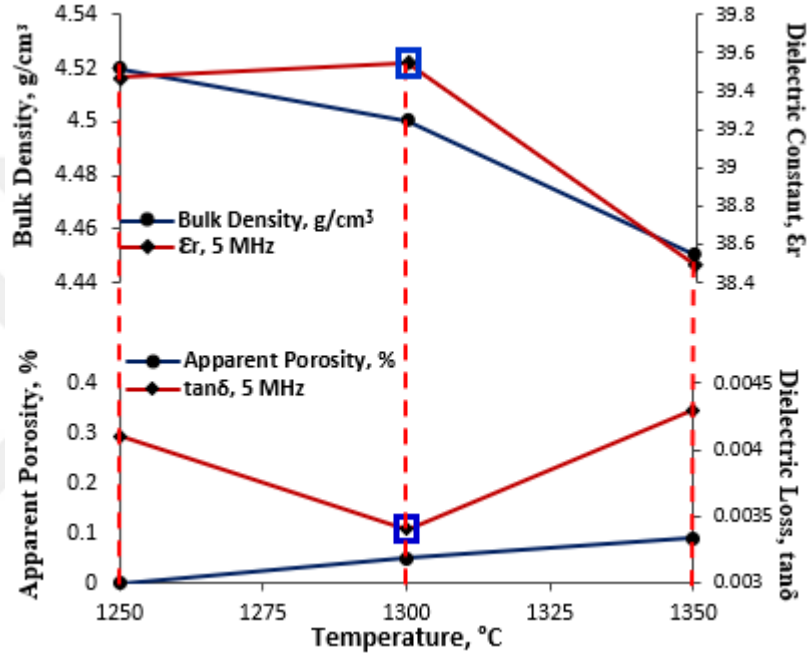

Figure 3.34 The dielectric properties versus densification of $Ba_2Ti_9O_{20}$ ceramics

3.5.4 $0.68CaTiO_3$-$0.32Ca(Zn_{1/3}Nb_{2/3})O_3$ Ceramics

Table 3.9 tabulates the dielectric properties of $0.68CaTiO_3$-$0.32Ca(Zn_{1/3}Nb_{2/3})O_3$ ceramics sintered between 1350°C and 1450°C. The dielectric properties are closely related with the densification as given in Figure 3.35 such that ε_r follows the densification path and tanδ follows the apparent porosity path. In this regard, ceramic sintered at 1400°C have the best dielectric properties among the ceramics densified between the temperature range of 1350°C-1450°C. The dielectric properties could not be measured using Agilent due to the negative values of the measuring system for the ceramics sintered at 1450°C. Also, the change in the ε_r with temperature (τ_ε,

ppm°C^{-1}) for the ceramic sintered at 1400°C was calculated using Equation 1.26 and measured at 5 MHz (1 MHz) as -312 (-316).

Table 3.9 The dielectric properties of $0.68CaTiO_3$- $0.32Ca(Zn_{1/3}Nb_{2/3})O_3$ samples

Sintering Temperature and Time (°C) (h)	**HIOKI ε_r, 5 MHz**	**HIOKI tanδ, 5 MHz**	**HIOKI ε_r, 1 MHz**	**HIOKI tanδ, 1 MHz**	**Agilent tanδ, 1 MHz**	**Agilent ε_r, 1 MHz**
1350, 4	87.68	0.0046	87.86	0.0015	0.00005	87.94
1400, 4	89.98	0.0035	90.09	0.0013	0.00061	88.97
1450, 4	86.84	0.0042	86.92	0.0013	-	-

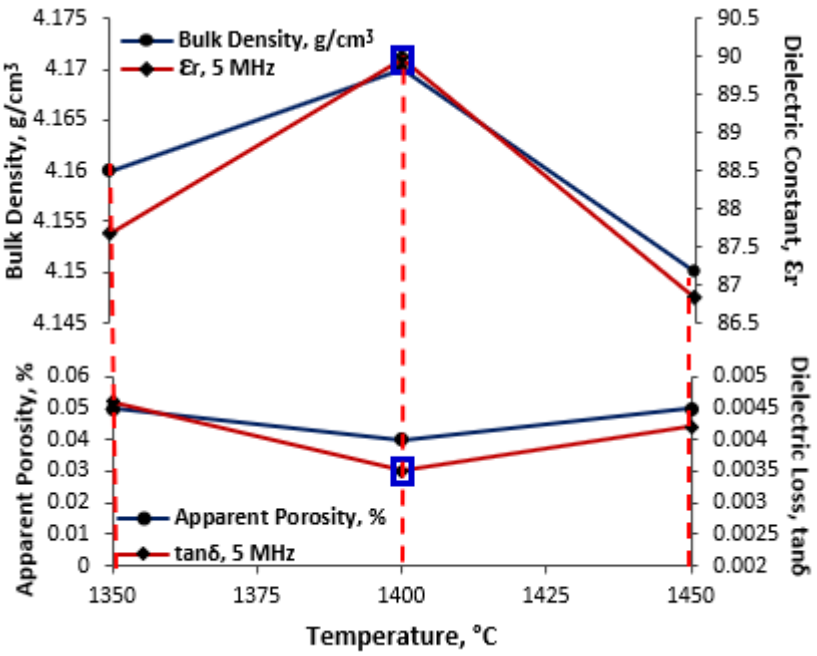

Figure 3.35 The dielectric properties versus densification of $0.68CaTiO_3$- $0.32Ca(Zn_{1/3}Nb_{2/3})O_3$ ceramics

3.5.5 $Ba_4(Nd_{0.93}Bi_{0.07})_{28/3}Ti_{18}O_{54}$ Ceramics

Table 3.10 tabulates the dielectric properties of the ceramics sintered between 1280°C and 1350°C. Averaged ε_r (tanδ) values at 5 MHz were recorded as 89.22 (0.0057) at 1280°C, 92.04 (0.0053) at 1320°C and 90.94 (0.0084) at 1350°C

(HIOKI). The dielectric properties versus densification of the ceramics are given Figure 3.36. The dielectric properties are optimized (i.e., highest Ɛr with lowest tanδ) when the maximum densification is attained in the ceramics. In this regard, ceramic sintered at 1320°C have the best dielectric properties among the ceramics densified between the temperature range of 1280°C-1350°C for 3 h. Also, the change in the $Ɛ_r$ with temperature (τ_ε, ppm°C^{-1}) for the ceramic sintered at 1320°C was calculated using Equation 1.26 and measured at 5 MHz (1 MHz) as 69.6 (79.8).

Table 3.10 The dielectric properties of $Ba_4(Nd_{0.93}Bi_{0.07})_{28/3}Ti_{18}O_{54}$ samples

Sintering Temperature and Time (°C) (h)	**HIOKI $Ɛ_r$, 5 MHz**	**HIOKI tanδ, 5 MHz**	**HIOKI $Ɛ_r$, 1 MHz**	**HIOKI tanδ, 1 MHz**	**Agilent tanδ, 1 MHz**	**Agilent $Ɛ_r$, 1 MHz**
1280, 3	89.22	0.0057	89.36	0.0017	0.00013	88.63
1320, 3	92.04	0.0053	92.18	0.0013	0.00062	92.84
1350, 3	90.94	0.0084	91.07	0.0018	0.00054	91.76

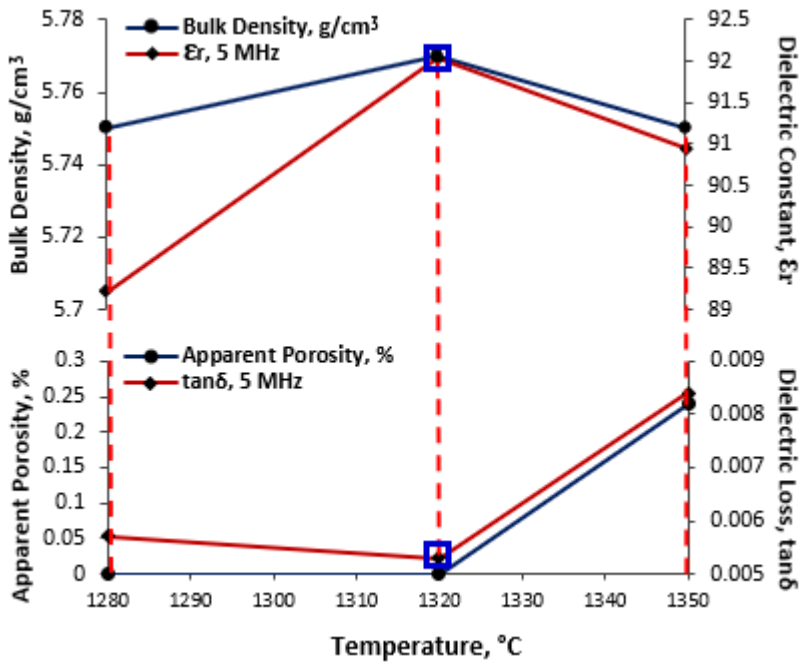

Figure 3.36 The dielectric properties versus densification of $Ba_4(Nd_{0.93}Bi_{0.07})_{28/3}Ti_{18}O_{54}$ ceramics

The maximum temperature ranges from high densification, minimum apparent porosity and high dielectric properties points of views were determined as; 1050°C-1100°C-1150°C for 1 h for CeO_2-Glass (5 wt.%), 1200°C-1275°C for 1 h for $SrNb_2O_6$, 1250°C-1300°C for 3 h for $Ba_2Ti_9O_{20}$, 1350°C-1400°C-1450°C for 4 h for $0.68CaTiO_3$-$0.32Ca(Zn_{1/3}Nb_{2/3})O_3$ and 1280°C-1320°C-1350°C for 3 h for $Ba_4(Nd_{0.93}Bi_{0.07})_{28/3}Ti_{18}O_{54}$ ceramics. The tanδ is very critical for microwave dielectric ceramics. The tanδ at 5 MHz (HIOKI) were 0.0040 for CeO_2-Glass sintered at 1150°C, 0.0047 for $SrNb_2O_6$ sintered at 1275°C, 0.0034 for $Ba_2Ti_9O_{20}$ sintered at 1300°C, 0.0035 for $0.68CaTiO_3$-$0.32Ca(Zn_{1/3}Nb_{2/3})O_3$ sintered at 1400°C and 0.0053 for $Ba_{6-3x}(Nd_{1-y}Bi_y)_{8+2x}Ti_{18}O_{54}$ x=2/3 y=0.07 sintered at 1320°C. A dielectric ceramic's loss is a function of both intrinsic and extrinsic losses [40]. Porosity, second phase, grain size, and microstructural flaws have a significant impact on extrinsic losses in low field dielectric property measurements. Overall, one of the features required for the microwave dielectric ceramics is to attain a high bulk density to control dielectric properties. It has been reported in literature that the ε_r increases (and tanδ decreases) with increasing densification by eliminating porosity [1, 68]. The relative densities ≥97% were successfully obtained for all samples at maximum temperature ranges.

3.6 Microwave Properties

As electronic devices that use frequencies in the GHz range such as cell phones, materials that have no impact on signal transmission are desirable. This is especially true for circuit materials that will transmit signals. The precise measurement and evaluation of high frequency characteristics (dielectric loss tangent, relative dielectric constant, conduction characteristics and characteristic impedance) is of utmost importance, as even the smallest changes have the potential to adversely affect signal transmission. In particular, the scattering parameters (S Parameters) are an important factor measured on circuit boards. S Parameters are the elements that determine the circuit characteristics with respect to the magnitude and phase of the incoming and outgoing transmission circuit voltage and can be measured in the MHz to GHz range using a vector network analyzer [108]. In the microwave frequency range, current (I) and voltage (V) measurements become very complex. At higher

frequency, power is measured rather than current or voltage. The power is measured at higher frequencies as opposed to current or voltage. It is challenging to execute short circuit and open circuit for AC signals over wide bandwidth at high microwave frequencies. S parameters are utilized in the microwave range to get around this issue. These S characteristics are described in terms of traveling waves that are incident and reflected [109]. In the S_{xy}, x and y subscript represent output and input port, respectively. The transmission characteristic S_{21} indicates the output power, which can be used to evaluate the degree of transmission loss, etc., while the reflection characteristic S_{11} indicates the reflected power, which can be used to evaluate the magnitude and effect of reflected waves. By measuring such S-parameters, it is possible to evaluate variations in transmission loss and determine the transmittable signal frequencies [109].

The S parameters at GHz level were measured for CeO_2-Glass, $Ba_2Ti_9O_{20}$ and $0.68CaTiO_3$-$0.32Ca(Zn_{1/3}Nb_{2/3})O_3$ ceramics at room temperature using a Vector Network Analyzer. Figure 3.37 and Figure 3.38 show the experimental setup used during the measurements and the Ag coated ceramics, respectively. One port, a control panel, an information display, and a microwave wire are all included in the test kit. Dual directional couplers and a sophisticated ratio measuring apparatus are included in each test port of the test set. Two receivers and a sweeping frequency source that powers the network under examination make up a network analyzer. The input voltage to the network is precisely measured using the first receiver. The output of the network being tested is measured using the second receiver, which is referred to as the Transmission channel. The voltage gain or loss of the network is represented as the output to input level ratio, which is shown in decibels (dB). The response plot of the network is produced after the source is swept over the desired frequency range.

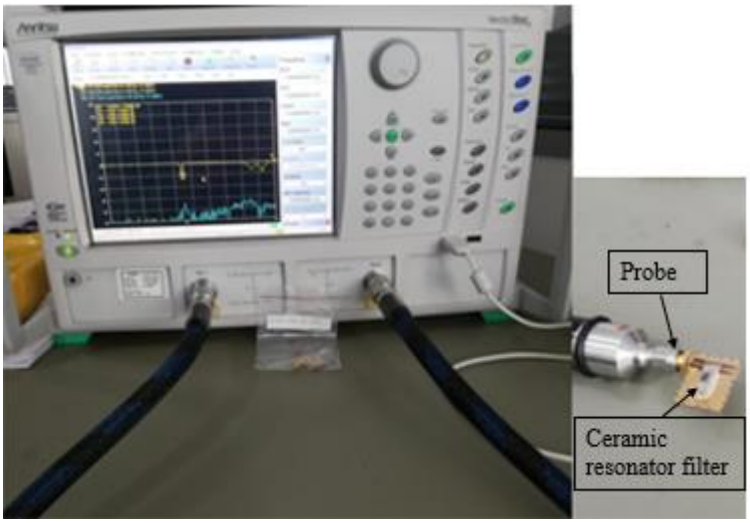

Figure 3.37 The experimental setup used during the measurements

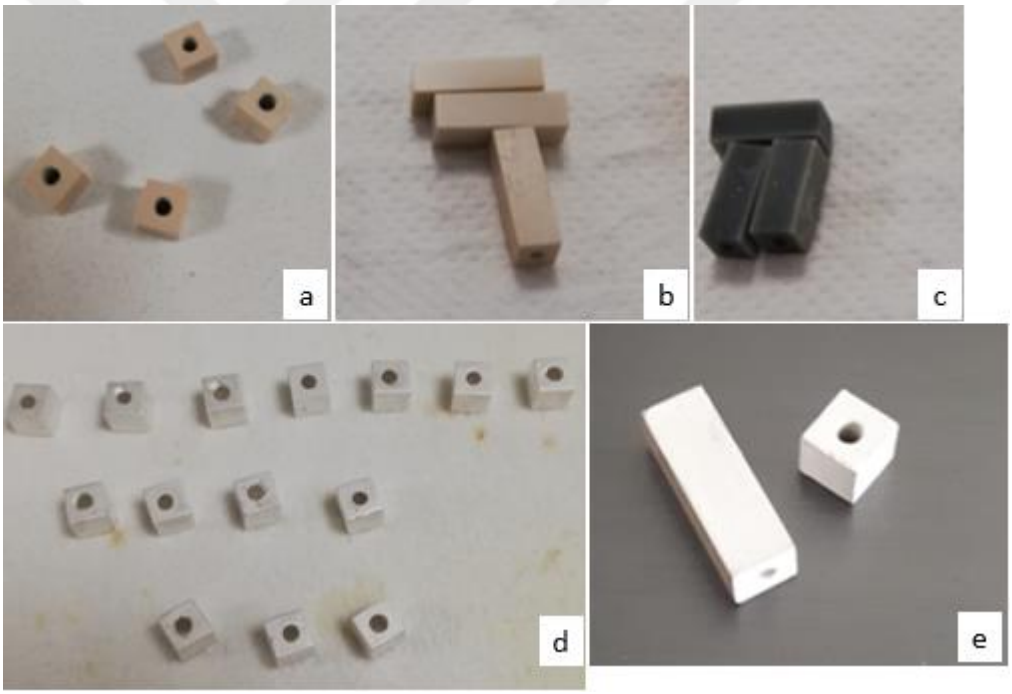

Figure 3.38 Cut and drilled ceramics at various shapes; (a) CeO_2-Glass (b) $Ba_2Ti_9O_{20}$ (c) $0.68CaTiO_3$-$0.32Ca(Zn_{1/3}Nb_{2/3})O_3$ and (d) CeO_2-Glass (e) $Ba_2Ti_9O_{20}$ (left) and $0.68CaTiO_3$-$0.32Ca(Zn_{1/3}Nb_{2/3})O_3$ (right) of silver-coated ceramics

3.6.1 CeO_2-Glass Ceramics

The microwave properties of the CeO_2-Glass ceramic sintered at 1150°C were used for the measurement. The ceramic resonator filter for microwave applications is

shown in Figure 3.39. The diameter (d) of reflection coefficient was determined from the polar chart of the ceramic resonator measurement given in Figure 3.40. The reflected parameter (S) versus the frequency of the ceramic resonator with one port measurement is shown in Figure 3.41, and the results are given in Table 3.11. The first and second subscript indicate output and input of the port in S(2,2). The resonance frequency (deep peak) was at 2.895 GHz (marked m2 point). The reflection coefficient corresponding to the deep peak was read as -18.346 dB as given in Figure 3.41. At the resonant frequency, the transmitted signal's amplitude reached a deep peak with a finite width. The breadth of the resonance curve had a -3 dB bandwidth (BG). First and second point corners frequency under -3 dB had 2890 MHz and 2903 MHz, respectively. The quality factor (Q), resonance-frequency dependent quality factor (Q.f), ε_r and tanδ were calculated as 445, 1288.3, 21 and 0.0022 at 2.895 GHz from a network analyzer. Also, the ε_r and tanδ values at 5 MHz were 21.36 and 0.004. With increasing the frequency from 5 MHz to 2.895 GHz, the ε_r decreased slightly, which is expected for the dielectric materials due to vanishing of polarization mechanisms with increasing frequency. The rotation speed of the dipoles cannot be polarized because it cannot keep up with the electric field reversal rate [32, 106, 107]. The CeO_2-Glass (5 wt.%) composition was studied for the first time in literature and its properties resulted in promising results for the microwave applications.

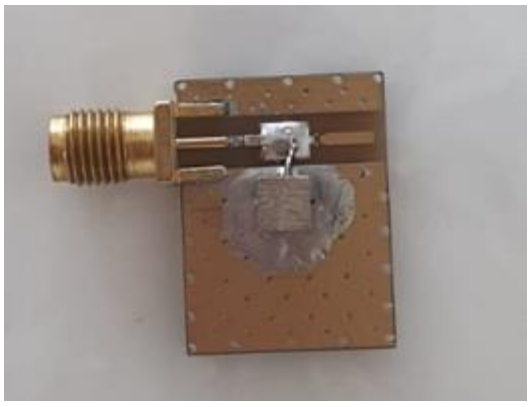

Figure 3.39 CeO_2-Glass ceramic resonator filter

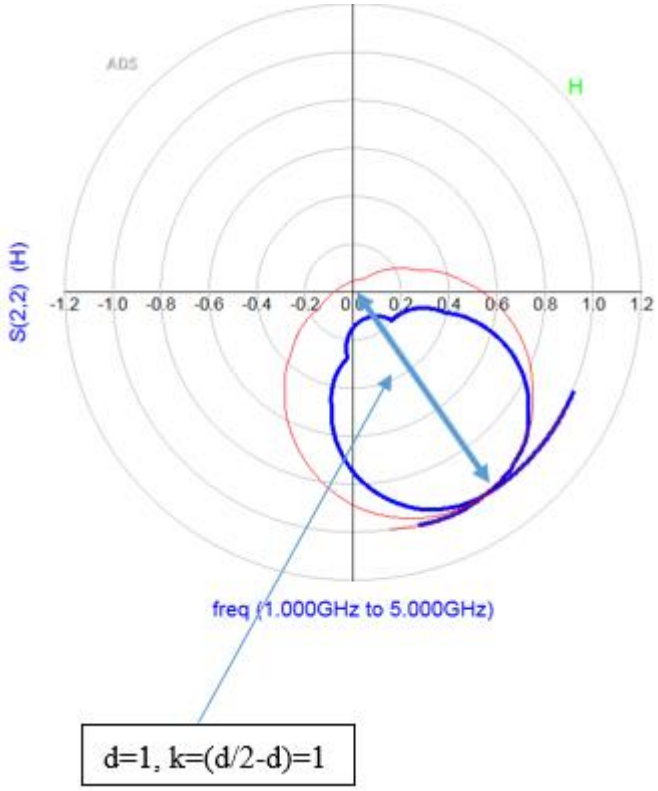

Figure 3.40 The polar chart of CeO_2-Glass ceramic resonator measurement

Table 3.11 The microwave parameters of CeO_2-Glass ceramic resonator

Resonance Frequency (MHz)	2895
3dB point -1(MHz)	2903
3dB point -2(MHz)	2890
3 dB band width (MHz)	13
d,k	1.1
Calculated dielectric constant (ε_r)	21
Calculated quality factor (Q)	445

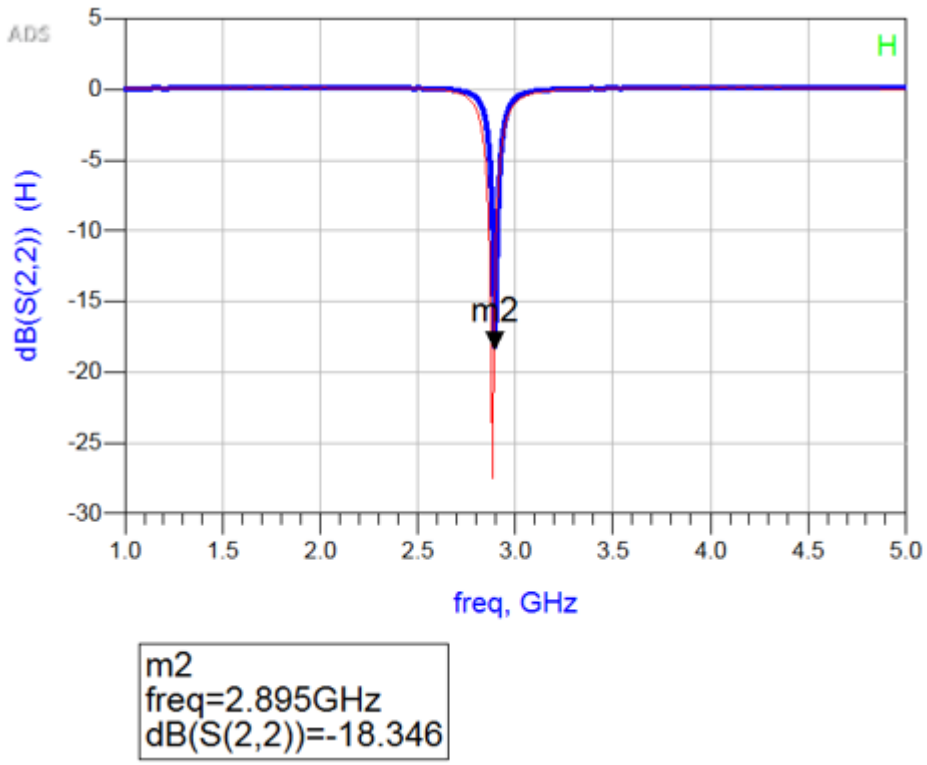

Figure 3.41 The reflected parameter versus the frequency of the ceramic resonator with one port measurement

3.6.2 $Ba_2Ti_9O_{20}$ Ceramics

The microwave properties of the $Ba_2Ti_9O_{20}$ ceramic sintered at 1300°C were used for the measurement. The ceramic resonator filter for microwave applications is shown in Figure 3.42. The diameter (d) of reflection coefficient was determined from the polar chart of the ceramic resonator measurement given in Figure 3.43. The reflected parameter (S) versus the frequency of the ceramic resonator with one port measurement is shown in Figure 3.44, and results are given in Table 3.12. The first and second subscript show output and input of the port in S(3,3). The resonance frequency (deep peak) was at 3.942 GHz. The reflection coefficient corresponding to the deep peak was read about -7.5 dB as given in Figure 3.44. At the resonant frequency, the transmitted signal's amplitude reached a deep peak with a finite width. The breadth of the resonance curve had a -3 dB bandwidth (BG). First and second point corners frequency under -3 dB had 3920 MHz and 3964 MHz, respectively. The quality factor (Q), resonance frequency dependent quality factor (Q.f), ε_r and

tanδ were calculated as 362, 1427, 36.5 and 0.0027 at 3.942 GHz from a network analyzer, respectively. Also, the ε_r (tanδ) values at 5 MHz had 39.55 (0.0034). With increasing the frequency from 5 MHz to 3.942 GHz the ε_r and loss relatively decreased due to vanishing of polarization mechanisms. Huang [80] reported that Q.f is 43200 (Q=7200) and the ε_r is 38.8 at 6 GHz measured with Hakki Coleman method. The ε_r values are very close but the Q.f is different due partly to the experimental measurement setups.

Figure 3.42 $Ba_2Ti_9O_{20}$ ceramic resonator filter

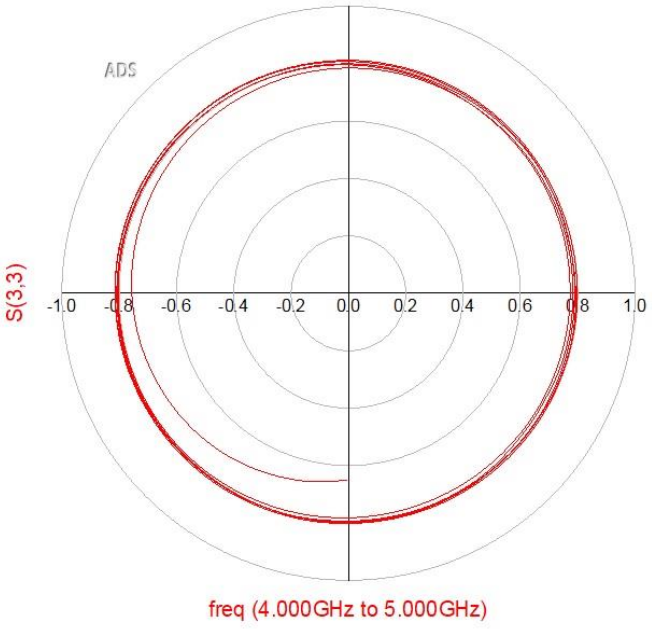

Figure 3.43 The polar chart of $Ba_2Ti_9O_{20}$ ceramic resonator measurement

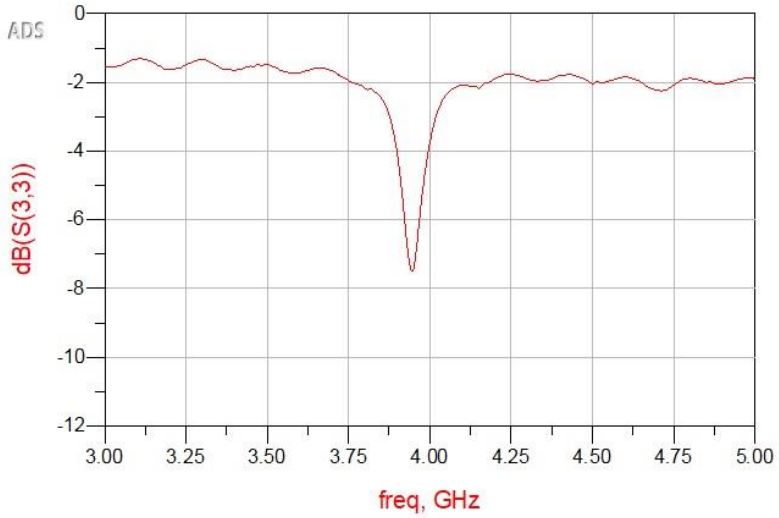

Figure 3.44 The reflected parameter versus the frequency of the ceramic resonator with one port measurement

Table 3.12 The microwave parameters of $Ba_2Ti_9O_{20}$ ceramic resonator.

Resonance Frequency (MHz)	3942
3dB point -1(MHz)	3920
3dB point -2(MHz)	3964
3 dB band width (MHz)	44
d,k	1.6
Calculated dielectric constant (ε_r)	36.5
Calculated quality factor (Q)	362

3.6.3 $0.68CaTiO_3$-$0.32Ca(Zn_{1/3}Nb_{2/3})O_3$ Ceramics

The microwave properties of the $0.68CaTiO_3$-$0.32Ca(Zn_{1/3}Nb_{2/3})O_3$ ceramic sintered at 1400°C were used for the measurement. The ceramic resonator filter for microwave applications is shown in Figure 3.45. The diameter (d) of reflection coefficient was determined from the polar chart of the ceramic resonator measurement shown in Figure 3.46. The reflected parameter versus the frequency of

the ceramic resonator with one port measurement is given in Figure 3.47, and results are given in Table 3.13. The first and second subscripts indicate output and input of the port in S(3,3). The resonance frequency (deep peak) was at 2.443 GHz. The reflection coefficient corresponding to the deep peak was read about -19 dB as given in Figure 3.47. At the resonant frequency, the transmitted signal's amplitude reached a deap peak with a finite width. The breadth of the resonance curve had a -3 dB bandwidth (BG). First and second point corners frequency under -3 dB had 2408 MHz and 2478 MHz, respectively. The quality factor (Q), resonance frequency dependent quality factor (Q.f), ε_r and tanδ were calculated as 314, 767.1, 91 and 0.0031 at 2.443 GHz from a network analyzer, respectively. Also, ε_r (tanδ) values at 5 MHz had 89.98 (0.0035). With increasing the frequency from 5 MHz to 2.443 GHz the ε_r slightly increased, and loss decreased. The reason for the increase in the ε_r may be due to the experimental setup and copper connection. There is no composition studied for the value of x=0.32 in the (1-x)$CaTiO_3$-x$Ca(Zn_{1/3}Nb_{2/3})O_3$ composition in the literature. However, the properties for x=0.2 (ε_r=115, Q.f =5030 and Q=1397) and x=0.4 (ε_r=76, Q.f=7530 and Q=1615) have been reported [77]. The ε_r=91 found for the x=0.32 is in between the literature values but Q.f value is lower due partly to the experimental measurement setups.

Figure 3.45 0.68$CaTiO_3$-0.32$Ca(Zn_{1/3}Nb_{2/3})O_3$ ceramic resonator filter

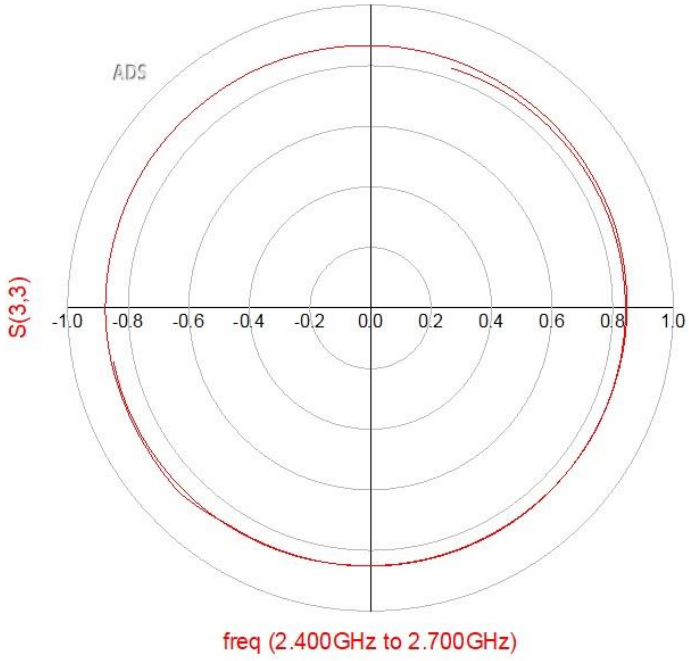

Figure 3.46 The polar chart of $0.68CaTiO_3$-$0.32Ca(Zn_{1/3}Nb_{2/3})O_3$ ceramic resonator measurement

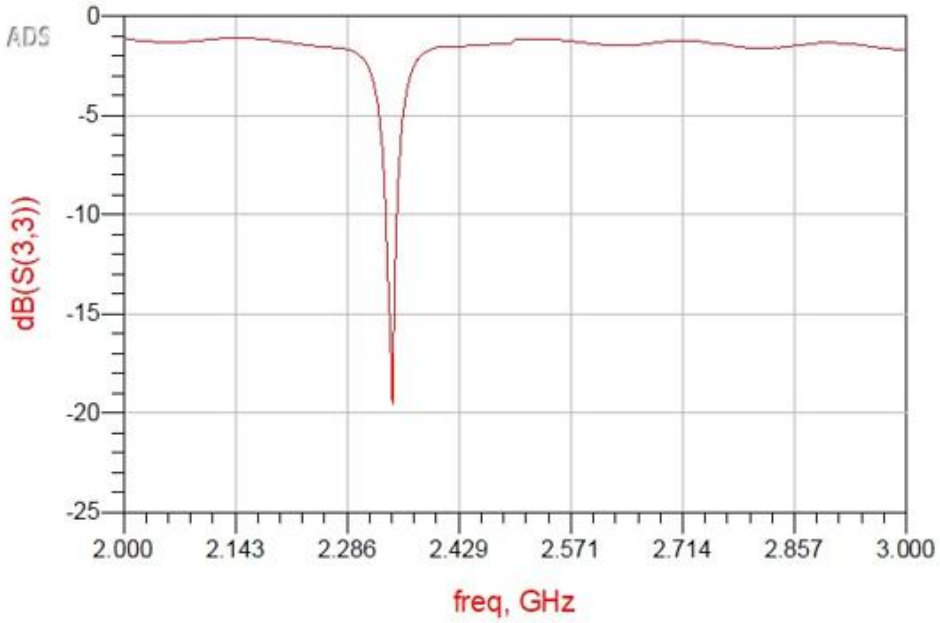

Figure 3.47 The reflected parameter versus the frequency of the ceramic resonator with one port measurement

Table 3.13 The microwave parameters of $0.68CaTiO_3$-$0.32Ca(Zn_{1/3}Nb_{2/3})O_3$ ceramic resonator

Resonance Frequency (MHz)	2443
3dB point -1(MHz)	2408
3dB point -2(MHz)	2478
3 dB band width (MHz)	70
d,k	1.8
Calculated dielectric constant (ε_r)	91
Calculated quality factor (Q)	314

Table 3.14 compiles densification, dielectric and microwave properties for each composition. The maximum densification ranges and best condition were determined based on the highest ε_r and lowest tanδ. The relative densities ≥97.35% were successfully obtained for all samples. The microwave properties were measured for $0.68CaTiO_3$- $0.32Ca(Zn_{1/3}Nb_{2/3})O_3$ sintered at 1400°C, for $Ba_2Ti_9O_{20}$ sintered at 1300°C, and for CeO_2-Glass (5 wt.%) sintered at 1150°C.

Table 3.14 Densification, dielectric and microwave properties for each composition.

Composition (Densification range – best condition)	Density, g/cm^3	Relative Density, %	Apparent Porosity, %	ε_r, 5 MHz (1 MHz)	tanδ, 5 MHz (1 MHz)	Resonance Frequency, GHz	Q factor (Q.f)	ε_r (tanδ)
CeO_2-Glass (5 wt.%) (1050-1100-1150°C)	6.40	98.50	0.06	21.36 (21.43)	0.0040 (0.0016)	2.895	445 (1288)	21 (0.0022)
$SrNb_2O_6$ (1200-1275°C)	5.06	98.14	0.94	28.87 (29.05)	0.0047 (0.0025)	-	-	-
$Ba_2Ti_9O_{20}$ (1250-1300°C)	4.50	97.60	0.05	39.55 (39.60)	0.0034 (0.0013)	3.942	362 (1427)	36.5 (0.0027)
$0.68CaTiO_3$-$0.32Ca(Zn_{1/3}Nb_{2/3})O_3$ (1350-1400-1450°C)	4.17	97.35	0.04	89.98 (90.09)	0.0035 (0.0013)	2.443	314 (767)	91 (0.0031)
$Ba_4(Nd_{0.93}Bi_{0.07})_{28/3}Ti_{18}O_{54}$ (1280-1320-1350°C)	5.77	98.60	0.00	92.04 (92.18)	0.0053 (0.0013)	-	-	-

CHAPTER 4

CONCLUSIONS

New research and developments on microwave communication result in a rising demand for dielectric resonators. Dielectric oxide ceramics are used as filters, oscillators in a variety of applications from mobile phones to global positioning systems. It has also played an important role in the microwave wireless communications industry by reducing the size and cost of the antenna components.

In this study, dielectric ceramic compositions (i.e., CeO_2-Glass (5 wt.%, Al_2O_3-SiO_2-CaO based), $SrNb_2O_6$, $Ba_2Ti_9O_{20}$, $0.68CaTiO_3$-$0.32Ca(Zn_{1/3}Nb_{2/3})O_3$ and $Ba_{6-3x}(Nd_{1-y}Bi_y)_{8+2x}Ti_{18}O_{54}$ x=2/3 and y=0.07) with various dielectric constants between 20 and 100 were synthesized by solid state method and successfully fabricated by dry pressing. The ceramics were then characterized for densification, phase formation, microstructure evolution, dielectric and microwave properties. XRD proved the desired phase formation after calcination and sintering for all compositions. Maximum densification temperature range was first determined based on a high bulk density with a near zero apparent porosity but the best sintering temperature was determined based on the highest dielectric constant with the lowest dielectric loss. The best conditions were: 1150°C for CeO_2-Glass (5 wt.%) with a relative density of 98.50% and apparent porosity of 0.06%, 1275°C for $SrNb_2O_6$ with a relative density of 98.14% and apparent porosity of 0.94%, 1300°C for $Ba_2Ti_9O_{20}$ with a relative density of 97.60% and apparent porosity of 0.05%, 1400°C for $0.68CaTiO_3$-$0.32Ca(Zn_{1/3}Nb_{2/3})O_3$ with a relative density of 97.35% and apparent porosity of 0.04%, and 1320°C for $Ba_4(Nd_{0.93}Bi_{0.07})_{28/3}Ti_{18}O_{54}$ with a relative density of 98.60% and apparent porosity of 0.00%. SEM studies indicated that CeO_2-glass ceramics were densified by liquid phase sintering, and the other ceramics were densified by solid state sintering.

The dielectric properties followed the densification paths. The ε_r (tanδ) values at 5 MHz were 21.36 (0.0040) for the CeO_2-Glass (5 wt.%) sintered at 1150°C, 28.87 (0.0047) for $SrNb_2O_6$ sintered at 1275°C, 39.55 (0.0034) for $Ba_2Ti_9O_{20}$ sintered at

1300°C, 89.98 (0.0035) for $0.68CaTiO_3$-$0.32Ca(Zn_{1/3}Nb_{2/3})O_3$ sintered at 1400°C and 92.04 (0.0053) for $Ba_4(Nd_{0.93}Bi_{0.07})_{28/3}Ti_{18}O_{54}$ sintered at 1320°C. A near-full densification is important for the microwave properties because a low dielectric loss (or, high quality factor) is required for low noise and power loss in the signal. The microwave properties of the ceramics CeO_2-Glass sintered at 1150°C, $Ba_2Ti_9O_{20}$ sintered at 1300°C and $0.68CaTiO_3$-$0.32Ca(Zn_{1/3}Nb_{2/3})O_3$ sintered at 1400°C were measured using the network analyzer. The Q.f values of CeO_2-Glass, $Ba_2Ti_9O_{20}$ and $0.68CaTiO_3$-$0.32Ca(Zn_{1/3}Nb_{2/3})O_3$ ceramic resonator filters were 1288.3 at 2.895 GHz, 1427 at 3.942 GHz and 767.1 at 2.443 GHz, respectively.

The ceramic compositions to obtain dielectric constants between 20 and 100 were determined and successful densified to ≥97.35% relative density. A near-full densification was required to eliminate porosity from the microstructures to obtain high dielectric constant and low dielectric loss, which is critical for the microwave applications. The CeO_2-Glass (5 wt.%) composition was studied for the first time in literature and their properties resulted in promising results for the microwave applications.

REFERENCES

[1] Sebastian, M. T., “CHAPTER ONE- INTRODUCTION,” in Dielectric Materials for Wireless Communication, Elsevier, ISBN: 9780080453309, pp. 1–10, 2008.

[2] Narang, S. B. & Bahel, S., “Low loss dielectric ceramics for microwave applications: A review,” Journal of Ceramic Processing Research, vol. 11, no. 3, pp. 316–321, 2010.

[3] Moulson, A. J. & Herbert, J. M., “Chapter 5: Dielectrics and Insulators,” in Electroceramics: Materials, Properties, Applications, ISBN: 9780470867969, pp. 243–333, 2003.

[4] Basu, J. & Bhattacharyya, T. K., “Microelectromechanical resonators for radio frequency communication applications,” Microsystem Technologies, vol. 17. pp. 1557–1580, 2011.

[5] Ingram, D. J. E. & King, C. v, “Spectroscopy at Radio and Microwave Frequencies,” J Electrochem Soc, vol. 103, no. 5, 1956.

[6] Napoli, L. S. & Hughes, J. J., “A Simple Technique for the Accurate Determination of the Microwave Dielectric Constant for Microwave Integrated Circuit Substrates,” IEEE Trans Microw Theory Tech, vol. 19, no. 7, pp. 664–665, 1971.

[7] Bonetti, R. R. & Atia, A. E., “Analysis of Microstrip Circuits Coupled to Dielectric Resonators,” IEEE Trans Microw Theory Tech, vol. 29, no. 12, pp. 1333–1337, 1981.

[8] Plourde, J. K. & Ren, C. L., “Application of Dielectric Resonators in Microwave Components,” IEEE Trans Microw Theory Tech, vol. 29, no. 8, pp. 754–770, 1981.

[9] Ohsato, H., “Research and development of microwave dielectric ceramics for wireless communications,” Journal of the Ceramic Society of Japan, vol. 113, no. 1323, pp. 703–711, 2005.

[10] Lewiner, J., “Evolution of experimental techniques for the study of the electrical properties of insulating materials,” IEEE Transactions on Electrical Insulation, vol. EI-21, no. 3, pp. 351–360, 1986.

[11] Raju, G. G., “Chapter 1: Introductory Concepts,” in Dielectrics in Electric Fields, Marcel Dekker., ISBN: 9780429223068, pp. 1–26, 2003.

[12] Eckertová, L., Physics of Thin Films. Springer Science & Business Media, ISBN: 13: 978-1-4615-7591-7, 1977.

[13] Gurov, V. A., Solid-state electronics. Moscow: Tekhnosfera, 2008.

[14] Johnson, W. C., “Electronic transport in insulating films,” IEEE Trans Nucl Sci, vol. 19, no. 6, pp. 33–40, 1972.

[15] “What are Energy Bands?” https://byjus.com/physics/what-are-energy-bands/ (retrieved Oct. 24, 2022).

[16] von Hippel, A., “Chapter Two: Molecular Approach,” in Dielectrics and Waves, ISBN: 9780262720038, pp. 93–234, 1954.

[17] Chełkowski, August., Dielectric Physics. Elsevier Scientific Pub. Co., ISBN: 9780444416995, 1980.

[18] Smyth, C. P. & Sundheim, B. R., “Dielectric Behavior and Structure,” J Electrochem Soc, vol. 103, no. 10, pp. 1–70, 1956.

[19] Harrop, P. J., Dielectrics. Butterworths, ISBN: 0408703873, 1972.

[20] Khan, A. S. & Mukerji, S. K., Electromagnetic Fields: Theory and Applications, vol. 1. CRC Press, ISBN: 9781003046134, 2020.

[21] Brodie, Graham, Mohan V. Jacob, & Peter Farrell, Microwave and Radio-Frequency Technologies in Agriculture. Walter de Gruyter GmbH & Co KG, ISBN: 978-3110455397, 2015.

[22] “Electric dipole - Electrostatics.” Retrieved: Oct. 20, 2022. [Online]. Available: https://www.brainkart.com/article/Electric-dipole_38365/

[23] von Hippel, A., “Chapter One: Macroscopic Approach,” in Dielectrics and Waves, New York, ISBN: 9780262720038, pp. 1–86, 1954.

[24] Carter, C. B. & Norton, M. G., “Chapter 31: Locally Redistributing Charge,” in Ceramic Materials: Science and Engineering, Springer Science,Business Media, ISBN: 978-1-4614-3522-8, pp. 573–591, 2013.

[25] Martinez-Vega, J., “Chapter 1. Physics of Dielectrics,” in Dielectric Materials for Electrical Engineering, John Wiley & Sons - ISTE,. ISBN: 978-1-84821-165-0, pp. 1–16, 2013.

[26] Zhang, L., “Fundamental Study and Development of 0-3 Dielectric Composites with High Dielectric Constant,” Auburn University, 2013.

[27] Li, B. & Zhong, W. H., “Theoretical Analysis of Dielectric Relaxation in Polymer Nanocomposites,” in Polymer Nanocomposites for Dielectrics, Springer New York, ISBN: 978-1-4419-1590-0, pp. 17–28, 2010.

[28] Martinez-Vega, J., “Chapter 4. Dielectric Relaxation in Polymeric Materials,” in Dielectric Materials for Electrical Engineering, John Wiley & Sons - ISTE, ISBN: 978-1-84821-165-0, pp. 79–99, 2013.

[29] Kao & Kwan Chi, “2. Electric Polarization and Relaxation,” Dielectric Phenomena in Solids. Elsevier, ISBN: 978-0-12-396561-5, pp. 41–112, 2004.

[30] “Section 6 Dielectric Materials.” http://www.mse.ntu.edu.tw/~cwc/course_files/Section%206_2010.pdf (retrieved Oct. 24, 2022).

[31] Raju, G. G., “Chapter 2: Polarization and Static Dielectric Constant,” in Dielectrics in Electric Fields, CRC press, ISBN: 9780429223068, pp. 29–80, 2003.

[32] Raju, G. G., “Chapter 3: Dielectric Loss and Relaxation-I,” in Dielectrics in Electric Fields, New York: CRC press, ISBN: 9780429223068, pp. 83–134, 2003.

[33] “Engineering Physics II, Chapter Physics, Dielectric Materials.” https://www.brainkart.com/article/Dielectric-Materials_6813 (retrieved Oct. 10, 2022).

[34] Silaghi M.A., & Golubeva, I., “Chapter 1: Polymeric Dielectric Materials,” in DIELECTRIC MATERIAL, Marius Alexandru Silaghi, Ed., ISBN: 9789535107644, pp. 1–26, 2012.

[35] Raju, G. G., “Chapter 4: Dielectric Loss and Relaxation-II,” in Dielectrics in Electric Fields, New York: CRC Press, ISBN: 9780429223068, pp. 137–139, 2003.

[36] Placidi, P., & Gasperini, L., & Grassi, A., & Cecconi, M., & Scorzoni, A., “Characterization of low-cost capacitive soil moisture sensors for IoT networks,” Sensors (Switzerland), vol. 20, no. 12, 2020.

[37] “Types of polarisation and Frequency dependence - Science Key.” http://sciencekey.weebly.com/types-of-polarisation-and-frequency-dependence.html (retrieved Oct. 10, 2022).

[38] Ejaz, T., “Optimization of Spit-Ring and Split-Ball Resonators for Effective Permittivity and Volume Fraction Extraction,” 2017.

[39] “Clausius Mossotti Equation | Static relative Permittivity | Polarization of Dielectric Materials .” http://physics-ref.blogspot.com/2012/12/clausius-mossotti-equation-static.html (retrieved Oct. 16, 2022).

[40] Sebastian, M. T., “Chapter 2- Measurement of Microwave Dielectric Properties and Factors Affecting them,” in Dielectric Materials for Wireless Communication, Elsevier., Amsterdam, ISBN: 978-0-08-045330-9, pp. 11–47, 2008.

[41] Chen, L. F., & Ong, C. K., & Neo, C. P., & Varadan, V. v, & Varadan, V. K., “Chapter 1: Eleectromagnetic Properties of Materials,” in Microwave Electronics: Measurement and Materials Characterization, John Wiley & Sons, ISBN: 978-0-470-84492-2, pp. 1–34, 2004.

[42] Buchanan, R. C., “Chapter 1: Ceramic Insulators,” in Ceramic materials for electronics, CRC press, ISBN: 13: 978-0-8247-4028-3, pp. 1–86, 2018.

[43] Akhtaruzzaman, Md., “Dielectric studies of some oxide materials, nitride ceramics and glasses,” 1989.

[44] Keyrouz, S. & Caratelli, D., “Dielectric Resonator Antennas: Basic Concepts, Design Guidelines, and Recent Developments at Millimeter-Wave Frequencies,” Int J Antennas Propag, vol. 2016, 2016.

[45] Kajfez, D. & Guillon, P., “Chapter 2: Microwave resonators,” in Dielectric Resonators, Georgia: Noble Publishing Corporation, ISBN: 9781884932052, 1998.

[46] Moulson AJ & Herbert JM, “Chapter 2: Elementary Solid State Science,” in Electroceramics: Materials, Properties, Applications, John Wiley & Sons, ISBN: 9780470867969, pp. 5–90, 2003.

[47] “Dielectric Materials.” https://www.brainkart.com/article/Dielectric-Materials_6827/ (retrieved Jan. 06, 2023).

[48] “Dielectric Strength | Constant | Loss | Definition - Your Electrical Guide.” https://www.yourelectricalguide.com/2018/06/dielectric-strength-dielectric-constant-dielectric-loss.html (retrieved Dec. 18, 2022).

[49] Wing, Z. N. & Halloran, J. W., “Dielectric loss in porous TiO2,” Ceram Int, vol. 43, no. 5, pp. 4618–4621, 2017.

[50] Surendran K, “Investigations on low loss dielectric ceramic materials for wireless communication,” Kerala University, 2004.

[51] I. J. Bahl & P. Bhartia, “Chapter 3: Resonators,” in Microwave Solid State Circuit Design, vol. 26, no. 02, New York: Wiley, pp. 79–128, 1988.

[52] Burfoot, J. C., Ferroelectrics: An introduction to the physical principles. D. Van Nostrand Company, ISBN: 9780442311612, 1967.

[53] Krupka, J., “Frequency domain complex permittivity measurements at microwave frequencies,” in Measurement Science and Technology, vol. 17, no. 6, pp. R1–R16, 2006.

[54] Wersing, W., “Microwave ceramics for resonators and filters,” Curr Opin Solid State Mater Sci, vol. 1, no. 5, pp. 715–731, 1996.

[55] Gurevich, V. L. & Tagantsev, A. K., “Intrinsic dielectric loss in crystals,” Adv Phys, vol. 40, no. 6, pp. 719–767, 1991.

[56] Gurevich, V. L. & Tagantsev, A. K., “Intrinsic dielectric loss in crystals: Low temperature,” Sov. Phys. JETP, vol. 64, no. 6, pp. 142–151, 1986.

[57] Braginsky, V. B., & Ilchenko, V. S., & Bagdassarov, K. S., “Experimental observation of fundamental microwave absorption in high-quality dielectric crystals,” Phys Lett A, vol. 120, no. 6, pp. 300–305, 1987,

[58] Shirey, H. M., “Low Temperature Synthesis of the Microwave Dielectric Material, Barium Magnesium Tantalate (BMT),” University of Pittsburgh, 2003.

[59] Korkmaz, E., “Effects of Different Dopants on the Sintering Behaviour and Dielectric Properties of Ba (Zn 1/3 NB 2/3) O 3 Microwave Dielectric Ceramics,” Marmara Universitesi (Turkey), 2010.

[60] Chen, Y. C., & Tsao, S. M., & Lin, C. S., & Wang, S. C., & Chien, Y. H., "Microwave dielectric properties of 0.95MgTiO3-0.05CaTiO3 for application in dielectric resonator antenna," J Alloys Compd, vol. 471, no. 1–2, pp. 347–351, 2009.

[61] Buchanan, R. C., Ceramic Materials for Electronics, Marcel Dekker. New York, ISBN: 9780367394134, 2004.

[62] Jones, S. B. & Friedman, S. P., "Particle shape effects on the effective permittivity of anisotropic or isotropic media consisting of aligned or randomly oriented ellipsoidal particles," Water Resour Res, vol. 36, no. 10, pp. 2821–2833, Oct. 2000.

[63] Budenstein, P. P., "On the mechanism of dielectric breakdown of solids," IEEE Transactions on Electrical Insulation, vol. EI-15, no. 3, pp. 225–240, 1980.

[64] Zhit, D. H., & Sunt, Z. H., & Santt, X. X., "Dynamic aspects of linear elastic fracture mechanics applied to dielectricbreakdown," J Phys D Appl Phys, vol. 26, no. 5, pp. 829–836, 1993.

[65] Cohn, S. B., "Microwave bandpass filters containing high-Q dielectric resonators," IEEE Trans Microw Theory Tech, vol. 16, no. 4, pp. 218–227, 1968.

[66] Inder Bahl & Prakash Bhartia, "Chapter 1: Introduction," in Microwave Solid State Circuit Design, New York: Wiley, ISBN: 978-0-471-20755-9, pp. 1–23, 1988.

[67] "TE MODE-This Co., Ltd." http://thisdr.com/en/product/dielectric-resonator-te-mode/ (retrieved Dec. 22, 2022).

[68] Freer, R. & Azough, F., "Microstructural engineering of microwave dielectric ceramics," J Eur Ceram Soc, vol. 28, no. 7, pp. 1433–1441, 2008.

[69] Ohsato, H., “Microwave materials with high Q and low dielectric constant for wireless communications,” in Materials Research Society Symposium Proceedings, vol. 833, 2005.

[70] Ohsato, H., Kagomiya, I., & Chae, K.-W., “Microwave dielectric ceramics with rare-earth elements (I),” Journal of the Korean Physical Society, vol. 61, no. 6, pp. 971–979, 2012.

[71] Ohsato, H., Tsunooka, T., Sugiyama, T., Kakimoto, K. I., & Ogawa, H., “Forsterite ceramics for millimeterwave dielectrics,” in Journal of Electroceramics, vol. 17, no. 2–4, pp. 445–450, 2006.

[72] Ohsato, H., Tsunooka, T., Kan, A., Kakimoto, K. I., & Ogawa, H., “Microwave-millimeterwave dielectric materials,” in Key Engineering Materials vol. 269, 2004.

[73] Ohsato, H., “Science of tungstenbronze-type like Ba6–3xR8+ 2xTi18O54 (R= rare earth) microwave dielectric solid solutions,” J Eur Ceram Soc, vol. 21, no. 15, pp. 2703–2711, 2001.

[74] Ohsato, H., & Kato, H. K. H., & Mizuta, M. M. M., & Nishigaki, S. N. S., & Okuda, T. O. T., “Microwave Dielectric Properties of the Ba6-3x (Sm 1-y,\mbRy) 8+ 2xTi 18O 54 (\mbR= Nd and La) Solid Solutions with Zero Temperature Coefficient of the Resonant Frequency,” Jpn J Appl Phys, vol. 34, no. 9S, p. 5413, 1995.

[75] Wu, Y. J. & Chen, X. M., “Structures and microwave dielectric properties of Ba6- 3x (Nd, Biy) 8+ 2xTi18O54 (x= 2/3) solid solution,” J Mater Res, vol. 16, no. 6, pp. 1734–1738, 2001.

[76] Valant, M. & Suvorov, D., “Dielectric Properties of the Fluorite-Like Bi2O3–Nb2O5 Solid Solution and the Tetragonal Bi3NbO7,” Journal of the American Ceramic Society, vol. 86, no. 6, pp. 939–944, 2003.

[77] Liu, H., & Wu, Z., & Ouyang, S., “Dielectric properties of (1- x) CaTiO3–xCa (Zn1/3Nb2/3) O3 ceramic system at microwave frequency,” Journal of the American Ceramic Society, vol. 88, no. 2, pp. 453–455, 2005.

[78] Ota, Y., & Kakimoto, K., & Ohsato, H., & Okawa, T., “Low-temperature sintering of Ba6- 3xSm8+ 2xTi18O54 microwave dielectric ceramics by B2O3 and GeO2 addition,” J Eur Ceram Soc, vol. 24, no. 6, pp. 1755–1760, 2004.

[79] Chen, X. M., & Liu, D., & Hou, R. Z., & Hu, X., & Liu, X. Q., “Microstructures and microwave dielectric characteristics of Ca (Zn1/3Nb2/3) O3 complex perovskite ceramics,” Journal of the American Ceramic Society, vol. 87, no. 12, pp. 2208–2212, 2004.

[80] Huang, C.-L., & Weng, M.-H., & Lion, C.-T., & Wu, C.-C., “Low temperature sintering and microwave dielectric properties of Ba2Ti9O20 ceramics using glass additions,” Mater Res Bull, vol. 35, no. 14–15, pp. 2445–2456, 2000.

[81] Jawahar, I. N., & Mohanan, P., & Sebastian, M. T., “A5B4O15 (A= Ba, Sr, Mg, Ca, Zn; B= Nb, Ta) microwave dielectric ceramics,” Mater Lett, vol. 57, no. 24–25, pp. 4043–4048, 2003.

[82] Tsunooka, T., & Sugiyama, H., & Kakimoto, K., & Ohsato, H., & Ogawa, H., “Zero temperature coefficient τf and sinterability of forsterite ceramics by rutile addition,” in Journal of the Ceramic Society of Japan, Supplement Journal of the Ceramic Society of Japan, Supplement 112-1, PacRim5 Special Issue, pp. S1637–S1640, 2004.

[83] Mori, N., & Sugimoto, Y., & Harada, J., & Higuchi, Y., “Dielectric properties of new glass-ceramics for LTCC applied to microwave or millimeter-wave frequencies,” J Eur Ceram Soc, vol. 26, no. 10–11, pp. 1925–1928, 2006.

[84] Surendran, K. P., & Santha, N., & Mohanan, P., & Sebastian, M. T., “Temperature stable low loss ceramic dielectrics in (1-x) ZnAl2O4 -xTiO

system for microwave substrate applications," The European Physical Journal B-Condensed Matter and Complex Systems, vol. 41, no. 3, pp. 301–306, 2004.

[85] Lee, H.-J., & Kim, I.-T., & Hong, K. S. H. K. S., "Dielectric properties of AB2O6 compounds at microwave frequencies (a= Ca, Mg, Mn, Co, Ni, Zn, and b= Nb, Ta)," Jpn J Appl Phys, vol. 36, no. 10A, p. L1318, 1997.

[86] Pullar, R. C., & Breeze, J. D., & Alford, N. M., "Characterization and microwave dielectric properties of M2+ Nb2O6 ceramics," Journal of the American Ceramic Society, vol. 88, no. 9, pp. 2466–2471, 2005.

[87] Richtmyer, R. D., "Dielectric resonators," J Appl Phys, vol. 10, no. 6, pp. 391–398, 1939.

[88] Schlicke, H. M., "Quasi-Degenerated Modes in High εr Dielectric Cavities," J Appl Phys, vol. 24, no. 2, pp. 187–191, 1953.

[89] Okaya, A. & Barash, L. F., "The dielectric microwave resonator," Proceedings of the IRE, vol. 50, no. 10, pp. 2081–2092, 1962.

[90] Masse, D. J., & Pucel, R. A., & Readey, D. W., & Maguire, E. A., & Hartwig, C. P., "A new low-loss high-k temperature-compensated dielectric for microwave applications," Proceedings of the IEEE, vol. 59, no. 11, pp. 1628–1629, 1971.

[91] Plourde, J. K., & Linn, D. F., & O'Bryan Jr, H. M., & Thomson Jr, J., "Ba2Ti9O20 as a microwave dielectric resonator," Journal of the American Ceramic Society, vol. 58, no. 9–10, pp. 418–420, 1975.

[92] Wakino, K., & Nishikawa, T., & Tamura, S., & Ishikawa, Y., & Katsume, M., "Microwave dielectric materials," 1977 IEEE-Four Joint Cov. Rec., 1977.

[93] Wakino, K., & Nishikawa, T., & Tamura, S., & Ishikawa, Y., "Microwave bandpass filters containing dielectric resonators with improved temperature stability and spurious response," in 1975 IEEE-MTT-S International Microwave Symposium, pp. 63–66, 1975.

[94] “Ceramic Resonators, Coaxial TEM Resonators.” https://www.tect-electronics.com/uploads/files/IMC/Ceramics%20Resonators.pdf (retrieved Jan. 06, 2023).

[95] Duran, C., & Trolier-McKinstry, S., & Messing, G. L., “Fabrication and electrical properties of textured Sr0. 53Ba0. 47Nb2O6 ceramics by templated grain growth,” Journal of the American Ceramic Society, vol. 83, no. 9, pp. 2203–2213, 2000.

[96] Dursun, G. M., “Alumina/glass composites for low temperature co-fired ceramics (LTCC) and radome applications,” Ankara Yıldırım Beyazıt Üniversitesi Fen Bilimleri Enstitüsü, 2018.

[97] Raheem, Z., “Standard Test Methods for Apparent Porosity, Water Absorption, Apparent Specific Gravity , and Bulk Density of Burned Refractory Brick and Shapes by Boiling Water,” American Society for Testing and Materials, vol. 00, no. Reapproved 2019.

[98] Lo, C.-L., & Duh, J.-G., & Chiou, B.-S., & Lee, W.-H., “Low-temperature sintering and microwave dielectric properties of anorthite-based glass-ceramics,” Journal of the American Ceramic Society, vol. 85, no. 9, pp. 2230–2235, 2002.

[99] “The dielectric constant.” http://physics.bu.edu/~duffy/semester2/c08_dielectric_constant.html (retrieved Oct. 23, 2022).

[100] Dursun, G. M. & Duran, C., “Glass alumina composites for functional and structural applications,” Ceram Int, vol. 45, no. 9, pp. 12550–12557, 2019.

[101] Kingery, W. D., & Bowen, H. K., & Uhlmann, D. R., Introduction to Ceramics, vol. 17. John wiley & sons, ISBN: 978-0-471-47860-7, 1976.

[102] Santha, N. I., & Petzelt, J., “Effect of doping on the Dielectric properties of Cerium Oxide in the Microwave and Far-Infrared Frequency Range,” Journal of the American Ceramic Society, vol. 87, no. 7, pp. 1233–1237, 2004.

[103] Prof. Dr. Cihangir DURAN, “MSE 517 Sintering Theory.”

[104] German, R. M., & Suri, P., & Park, S. J., “Liquid phase sintering,” J Mater Sci, vol. 44, no. 1, pp. 1–39, 2009.

[105] Penn, S. J., & Schrapel, K., “Effect of porosity and grain size on the microwave dielectric properties of sintered alumina,” Journal of the American Ceramic Society, vol. 80, no. 7, pp. 1885–1888, 1997.

[106] Li, H.-M., & Ra, C., & Zhang, G., & Kim, J.-D., “Frequency and temperature dependence of the dielectric properties of a PCB substrate for advanced packaging applications,” Journal of the Korean Physical Society, vol. 54, no. 3, pp. 1096–1099, 2009.

[107] Tataroğlu, A., “METAL-OKSIT-YARI ILETKEN (MOS) KAPASITÖRÜN DIELEKTRIK PARAMETRELERININ FREKANS VE SICAKLIK BAĞIMLILIĞI,” Gazi University Journal of Science Part C: Design and Technology, vol. 4, no. 2, pp. 65–70, 2016.

[108] “Electric / Electronic Property Evaluation Technology | Nitto in Türkiye.” https://www.nitto.com/tr/tr/rd/base/analyze/electric/ (retrieved Jan. 13, 2023).

[109] “S parameters | Scattering parameters | S11, S22,S12,S21.” https://www.rfwireless-world.com/Terminology/S-Parameters-Scattering-parameter.html (retrieved Jan. 13, 2023).

APPENDICES

Appendix A: The density of CeO_2-Glass ceramics at various glass content (theoretical density of 2.43 g/cm^3 for the glass and 7.65 g/cm^3 for CeO_2).

Appendix B: The dielectric constant of CeO_2-Glass ceramics at various glass content (the dielectric constant of 6.37 for the glass and 23 for CeO_2).

Appendix A - The density of CeO_2-Glass ceramics at various glass content

Table A.1 The density of CeO_2-Glass ceramics at various glass content (theoretical density of 2.43 g/cm^3 for the glass and 7.65 g/cm^3 for CeO_2).

CeO_2, wt.%	Glass wt.%	CeO_2 vol	Glass vol	CeO_2 volume fraction	Glass volume fraction	Series model	Parallel model	Logarithmic model
0	100	0	41.152	0	1	2.43	2.43	2.43
76	24	9.935	9.877	0.501	0.499	5.048	3.694	4.319
77	23	10.065	9.465	0.515	0.485	5.120	3.748	4.388
78	22	10.196	9.053	0.530	0.470	5.195	3.805	4.461
79	21	10.327	8.642	0.544	0.456	5.272	3.866	4.537
80	20	10.458	8.230	0.560	0.440	5.351	3.931	4.616
81	19	10.588	7.819	0.575	0.425	5.433	4.000	4.700
82	18	10.719	7.407	0.591	0.409	5.517	4.074	4.788
83	17	10.850	6.996	0.608	0.392	5.604	4.153	4.880
84	16	10.980	6.584	0.625	0.375	5.693	4.238	4.977
85	15	11.111	6.173	0.643	0.357	5.786	4.329	5.079
86	14	11.242	5.761	0.661	0.339	5.881	4.427	5.187
87	13	11.373	5.350	0.680	0.320	5.980	4.534	5.301
88	12	11.503	4.938	0.700	0.300	6.082	4.650	5.421
89	11	11.634	4.527	0.720	0.280	6.188	4.776	5.548
90	10	11.765	4.115	0.741	0.259	6.297	4.914	5.683
91	9	11.895	3.704	0.763	0.237	6.411	5.066	5.827
92	8	12.026	3.292	0.785	0.215	6.528	5.234	5.979
93	7	12.157	2.881	0.808	0.192	6.650	5.420	6.141
94	6	12.288	2.469	0.833	0.167	6.777	5.627	6.314
95	5	12.418	2.058	0.858	0.142	6.908	5.861	6.499
96	4	12.549	1.646	0.884	0.116	7.045	6.124	6.697
97	3	12.680	1.235	0.911	0.089	7.187	6.425	6.910
98	2	12.810	0.823	0.940	0.060	7.335	6.772	7.138
99	1	12.941	0.412	0.969	0.031	7.489	7.175	7.384
100	0	13.0719	0	1	0	7.65	7.65	7.65

Appendix B - The dielectric constant of CeO_2-Glass ceramics at various glass content

Table B.1 The dielectric constant of CeO_2-Glass ceramics at various glass content (the dielectric constant of 6.37 for the glass and 23 for CeO_2).

CeO_2, wt.%	Glass wt. %	CeO_2 vol	Glass vol	CeO_2 volume fraction	Glass volume fraction	Series model	Parallel model	Logarithmic model
0	100	0	41.152	0	1	6.37	6.37	6.37
76	24	9.935	9.877	0.501	0.499	14.709	9.993	12.127
77	23	10.065	9.465	0.515	0.485	14.941	10.154	12.345
78	22	10.196	9.053	0.530	0.470	15.179	10.324	12.574
79	21	10.327	8.642	0.544	0.456	15.424	10.505	12.814
80	20	10.458	8.230	0.560	0.440	15.676	10.699	13.066
81	19	10.588	7.819	0.575	0.425	15.936	10.906	13.331
82	18	10.719	7.407	0.591	0.409	16.204	11.128	13.610
83	17	10.850	6.996	0.608	0.392	16.481	11.367	13.904
84	16	10.980	6.584	0.625	0.375	16.766	11.624	14.214
85	15	11.111	6.173	0.643	0.357	17.061	11.902	14.541
86	14	11.242	5.761	0.661	0.339	17.365	12.204	14.887
87	13	11.373	5.350	0.680	0.320	17.680	12.533	15.253
88	12	11.503	4.938	0.700	0.300	18.005	12.891	15.641
89	11	11.634	4.527	0.720	0.280	18.342	13.285	16.053
90	10	11.765	4.115	0.741	0.259	18.690	13.719	16.490
91	9	11.895	3.704	0.763	0.237	19.052	14.199	16.957
92	8	12.026	3.292	0.785	0.215	19.426	14.733	17.454
93	7	12.157	2.881	0.808	0.192	19.814	15.332	17.985
94	6	12.288	2.469	0.833	0.167	20.217	16.008	18.554
95	5	12.418	2.058	0.858	0.142	20.636	16.775	19.163
96	4	12.549	1.646	0.884	0.116	21.072	17.655	19.818
97	3	12.680	1.235	0.911	0.089	21.524	18.674	20.524
98	2	12.810	0.823	0.940	0.060	21.996	19.869	21.285
99	1	12.941	0.412	0.969	0.031	22.487	21.287	22.108
100	0	13.0719	0	1	0	23	23	23